2023

PAEK- AND PES-LIKE PERARYLATED PHOSPHONIUM IONENES: SYNTHESIS, THERMAL PROPERTIES, AND CONDUCTIVITY

Samantha Sims

PAEK- AND PES-LIKE PERARYLATED PHOSPHONIUM IONENES: SYNTHESIS, THERMAL PROPERTIES, AND CONDUCTIVITY

A Thesis

Presented to

the Faculty of the Department of Chemistry

Murray State University

Murray, Kentucky

In Partial Fulfillment

of the Requirements for the Degree

of Master of Science in Chemistry

Samantha M. Sims

November 20, 2023

Acknowledgements

This project and my master's degree as a whole could not have been accomplished without the immense support I have received from my family. As a student also working full time to teach my own students, I often struggled to split time and finish all the classwork, homework, grading, parent phone calls, and basic chores of living. I want to thank my mom, dad, and sister for always supporting me, listening to me vent, and helping to pick up the slack on days when there was just too much to do. My parents, James and Christy Sims, have both shown me what it looks like to work hard and persevere. Whether it be through working to become a "Dr. Nurse" or putting in overtime hours at work, they both exhibit the resiliency and dedication that I hope to one day achieve. My sister, Ella Sims, has been my emotional support and personal therapist along the way. I can't wait to see what she achieves as she continues to grow and move towards life after high school. I also would like to thank my grandparents, Charlotte Moyers and Ross E. Calvin Moyers Jr. Saturday evenings playing games at "Meme and Papa's house" gave me the boost I needed to keep working and will continue to be the best part of my week.

I also want to thank my research advisor Dr. Kevin Miller, who has helped me to grow as a chemist and has been responsible for much of the improvement in my lab and data recording techniques. I also want to thank him for advocating for me and ensuring that I got the courses and support I needed to meet my educational goals. With this, I

want to extend my gratitude to the rest of the Murray State Chemistry Department for being flexible with my teaching schedule. Thank you to all the professors that have gotten creative with recorded classes, night classes, and Zoom.

Additionally, thanks are also owed to the donors to the American Chemical Society Petroleum Research Fund (ACS PRF# 60862-UR7) that provided funds for this project and the Murray State University Polymer and Materials Science Laboratory, where a majority of the characterization methods took place.

Abstract

Ionic liquids (ILs) are useful for many applications due to the tunability of their characteristic properties making these salts ideal for many applications. To further increase possible areas of application for these materials, some ILs can be incorporated into polymer structures to form poly ionic liquids (PILs) or ionenes. The specific ions used within the material will determine the thermal, mechanical, and chemical stability properties exhibited by the polymer. Adjustments can be made to the ion structures during the synthetic process to influence these observed properties.

Fuel cells, batteries, solar cells, and capacitors all require materials that can withstand high temperatures. With this, phosphonium ionenes are of interest, as these polymers typically display enhanced thermal stabilities when compared to other cations commonly used in ionene structures. The thermal stability of the ionene can be further improved via adjusting the functionality of the phosphonium ion. Perarylation of the phosphonium often leads to the enhanced thermal stability desired for the aforementioned applications. In applications such as the fuel cell, alkaline stability is desired alongside thermal stability. Perarylated phosphonium ions commonly also display the desired chemical stability for this application.

In this project, polyaryletherketone (PAEK)- and polyethersulfone (PES)- like phosphonium ionenes were synthesized. Initially, bromide monomers were produced via P-C coupling. Anion exchange to $[NTf_2]^-$ was then completed. These monomers were

characterized via DSC, TGA. ^{1}H NMR spectroscopy, ^{13}C NMR spectroscopy, ^{31}P NMR spectroscopy and elemental analysis.

Nickel catalyzed polymerization was then completed to form four different ionenes. Ionene structures varied based upon substituent positioning (*m*- or *p*-) and use of either a carbonyl or sulfone linker between the phosphorus atoms. The ionenes were characterized via DSC, TGA, ^{1}H NMR spectroscopy, ^{13}C NMR spectroscopy, ^{31}P NMR spectroscopy, elemental analysis, alkaline stability testing, solubility testing, and DRS.

The desired ionenes were successfully synthesized and the desired thermal and alkaline stabilities were observed. The ion conductivity was lower than desired. Based on the collected data, future research will focus on manipulations of the perarylated phosphonium structure to lower the T_g and increase ionic conductivity, without losing the thermal and alkaline stabilities.

Table of Contents

List of Figures

List of Schemes

List of Tables

Permission to Reprint

Chapter 1: Introduction

1.1 Ionic Liquid Containing Polymers

Ionic liquids (ILs) exist in the liquid state at relatively low temperatures due to the loosely coordinated ions that comprise them. These salts have melting points at temperatures of 100°C and lower.[1-4] ILs have characteristic properties that make them ideal for many various applications. Some of these properties include high thermal stability and conductivity, low volatility, and typically low flammability.[2-4] Fine tuning of the cation and anion structures allow for IL properties to be tailored to best fit the desired application.[1,3]

Cations used in ILs are typically bulky and poorly coordinating organic molecules. Some general classes of cations commonly used are imidazoliums, pyridiniums, ammoniums, and phosphoniums.[2,5,6] Figure 1.1 below shows the basic structure of each of these commonly used cations.

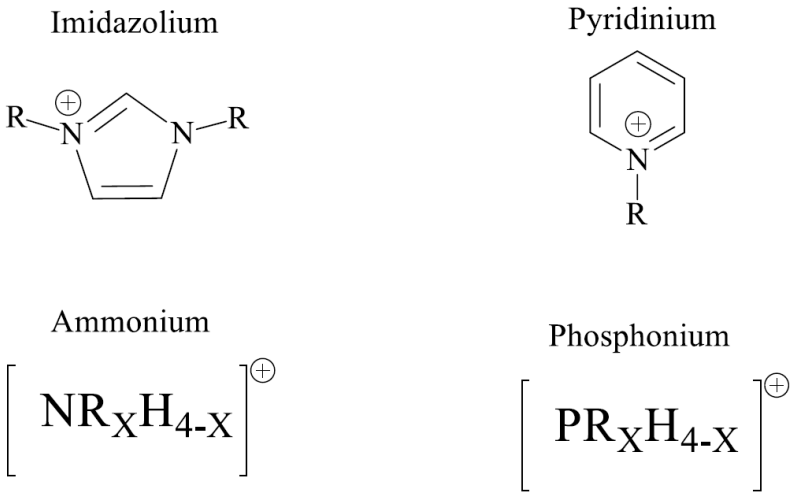

Figure 1.1: Common cation structures.

The anions used are also varied to meet the needs of multiple applications. Some commonly used anions are bulky fluorinated molecules such as bis(trifluoromethylsulfonyl) imide, ditriflamide ($[NTf_2]^-$), hexafluorophosphate, tosylate, or tetrafluoroborate.[1] Figure 1.2 illustrates these fluorinated anionic structures. When the application requires more highly coordinating ions, smaller inorganic anions, such as Cl^-, Br^-, or I^- are used.

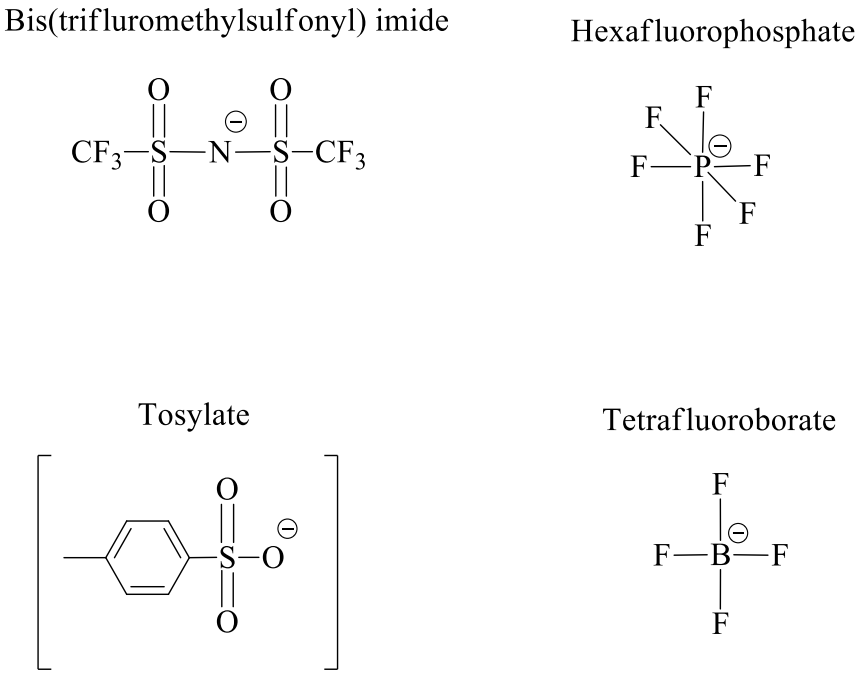

Figure 1.2: Common anion structures.

When ionic liquids are linked into polymer structures, they are referred to as poly(ionic liquid)s (PILs). Not all ionic liquids are able to become PILs, as a polymerizable functional group must be present within the molecule in order for these to act as monomer units for such polymers.[6] As one of the ionic species within the IL becomes linked in repeating units, the resulting PIL is formed.[7] PILs are of particular interest due to the combination of ionic liquid and macromolecular structure properties

that they possess.[7,8] Like the monomers they are made from, PILs are versatile and can be tuned for specific applications. PILs have the advantage of improved mechanical stability and reduced issues with leaching over their IL counterparts.[8] PILs can also act as single ion conductors due to the immobilization of one of the ions within the polymer structure. Though this trait is often seen as advantageous, the drawback to this is reduced conductivity caused by a restriction of ion and polymer chain mobility.[8] The observed characteristics for a particular PIL, such as the thermal stability, ionic conductivity, and morphology, can be fine-tuned to the application by varying the selected bound ion, counterion, and alkyl substituent length of the monomer components.[6] Based on this fine-tuning process, ionic liquids are incorporated into a polymer in different orientations as shown in Figure 1.3. The ionic liquid group can be "pendant" to the main polymer chain. The IL group may instead be directly bound into the "backbone" or main chain of the PIL. When specifically the cationic portion of the ionic liquid is incorporated in a "backbone" manner, the polymer is more appropriately called an ionene.[9,10,11] In addition, if the IL or another monomer component have a functionality over two, a covalently crosslinked network can be formed.

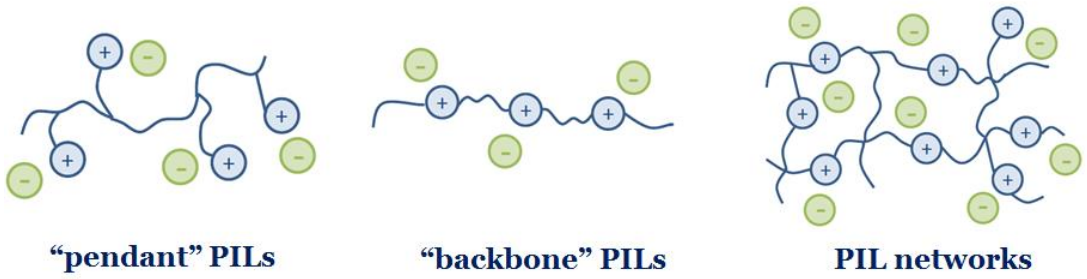

Figure 1.3: Common PIL structures

Throughout the research concerned with ILs and their corresponding PILs, nitrogen containing cations such as imidazoliums and ammoniums are commonly used. Though currently less explored in many application areas, phosphonium containing ionic liquids have become of interest in recent years. This interest is being garnered due to the unique properties these ILs possess. Phosphonium ILs are typically less dense than water. They also have high thermal and electrochemical stabilities, properties that are of high priority for many processes.[2] This makes them ideal candidates in processes that operate at temperatures higher than 100°C.[1] Phosphonium ILs are being investigated for possible applications in many areas such as electrolytes in batteries, solar cells, and capacitors, as well as agents to prevent corrosion and as reaction media.[1] Frackowiak et al. explored phosphonium ILs for use in super-capacitors and found a widened electrochemical window for the tested phosphonium containing ILs over ammonium counterparts.[12] Green et al. applied phosphonium ILs as a recyclable and therefore more "green" reaction media. In this context, the phosphonium ILs reaction media demonstrated higher efficiency and reactivity for Diels-Alder cycloadditions, Grignard reactions, Michael additions, and aryl halide oxidation reactions.[2]

Previous research concerning PILs has also primarily focused on nitrogen containing structures (ammonium, imidazolium, triazolium), however, phosphonium poly(ionic liquid)s, like the IL monomers that comprise them, also show unique properties compared to their nitrogen containing counterparts. Hemp et al.[6,13] compared PIL homopolymers prepared from styrenyl-substituted phosphonium and ammonium monomers. As displayed in Figure 1.4, higher thermal stability regardless of the length of the alkyl substituent (methyl, ethyl, propyl, butyl, etc.) and ionic conductivities for the phoshonium

PILs was observed. Likely due to weaker coordination between the ions, the phosphonium PILs also displayed a depressed glass transition temperature (T_g) and a less complex degradation profile in comparison to the ammonium counterparts. In addition, phosphonium PILs have an advantage over other nitrogen containing PILs due to phosphoniums' lowered susceptibility to degradation, their flame retardancy, and biocompatibility.[13,14]

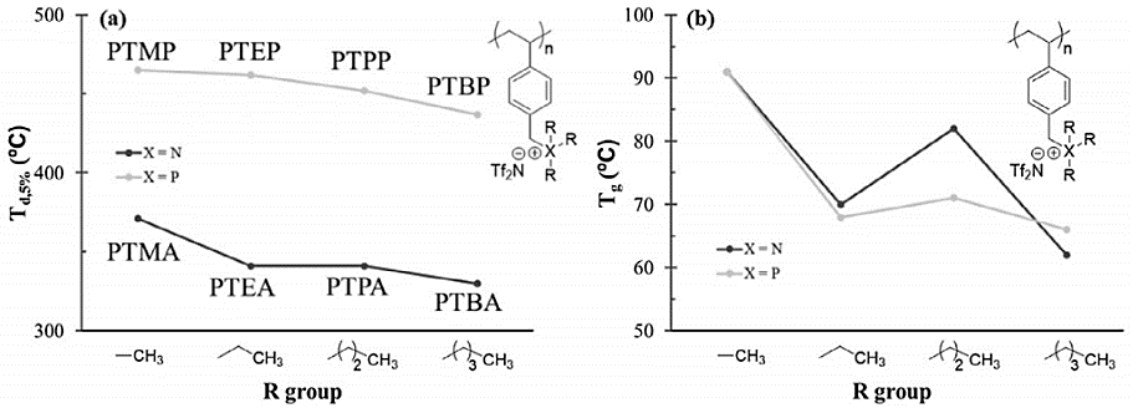

Figure 1.4: Comparison of thermal stability (a) and glass transition temperature (T_g) (b) of P-based and N-based PILs.[13]

1.2 Applications of Phosphonium Poly(ionic liquid)s and Ionenes

In the literature, phosphonium containing PILs and the backbone specific phosphonium "ionenes" have been tailored for their desired application, synthesized, and characterized. For example, Hemp et. al. synthesized polymers with phosphonium ionic liquid groups pendant to the main polymer chain with the goal of using the polymer in the context of non-viral nucleic acid transport and delivery. Though ammonium based PILs had been explored previously, phosphonium PILs were of interest due to reduced cytotoxicity and improved solution stability. In this work, the researchers explored the

effects that alkyl chain length as well as type of IL monomer used had nucleic acid transport effectiveness. Ammonium equivalents of each phosphonium PIL were utilized for comparison. The variations of polymers synthesized are displayed in Figure 1.5.[14] They found that the triethyl variants were unable to deliver the DNA effectively to HeLa cells, and the tributyl-based vectors, were successful in effective delivery to the HeLa cells as these samples displayed the expected induced protein expression. This was true for both the ammonium and phosphonium variants.

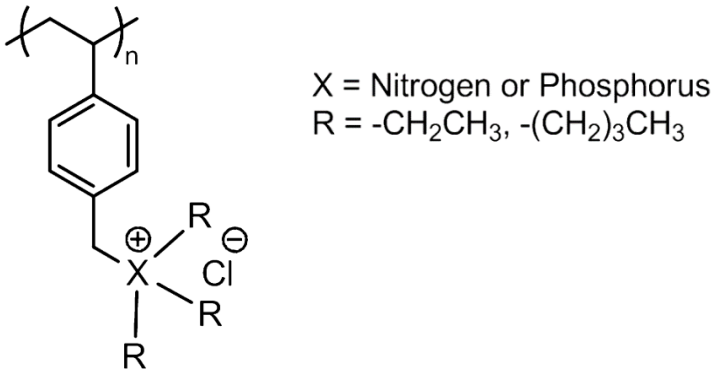

Figure 1.5: Hemp et. al. synthesized polymer variants.

In another article worked on by many of the same researchers, Hemp et al. reported on a similar application of nucleic acid binding and delivery by synthesizing block copolymers containing poly(ethylene oxide) and phosphonium PIL pendant chains using reversible addition fragmentation transfer (RAFT) polymerization.[15] More work by this research group explored not only the cation and alkyl chain length, but the effects of the counter anion as well. In this study, it was found that bulkier and less basic anions, such as $[NTf_2]^-$, improved thermal stabilities and reduced T_g values. The phosphonium PILs

displayed overall higher thermal stabilities and conductivities versus the ammonium equivalents.[6]

Phosphonium ionenes have also been synthesized. In order for an ionene to be constructed, the phosphonium IL monomers used must have at minimum dual functionality. While more functionalities in the IL can still result in incorporation of the monomer in the backbone, functionalities more than two typically result in formation of a crosslinked network. One possible application of these ionenes is in the context of alkaline fuel cells. With this in mind, the researchers in one study characterized their synthesized ionenes for both thermal and pH stabilities, both of which are requirements in alkaline fuel cells. The researchers also examined the influence of charge density on thermal properties and melt flow. In the same study, further investigation of possible nucleic acid transport applications was included by performing DNA gel shift arrays. The polymerization process utilized in this study is displayed in Scheme 1.1 below.[9]

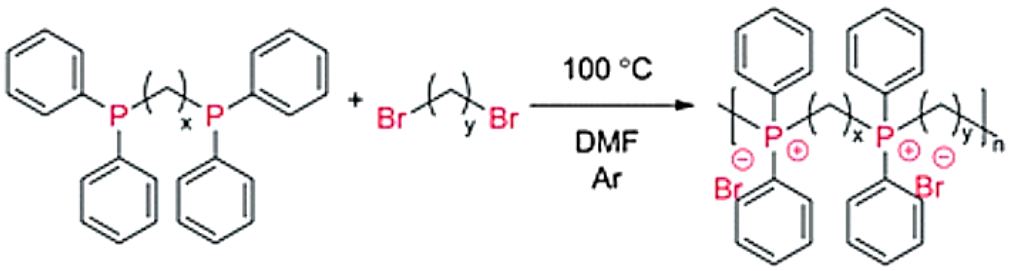

Scheme 1.1: Hemp et. al. step growth polymerization used to build phosphonium ionenes.[9]

As an undergraduate research student at Murray State, I have been a part of synthesizing and characterizing phosphonium ionenes. In our 2019 article, we discuss the

synthesis and characterization of the bis(phosphonium)-containing ‘ene’ monomers. From these monomers PIL films were made utilizing thiol-ene photopolymerization and were further characterized. See Scheme 1.2 for the polymerization process. The mole ratio of the phosphonium and PTMP monomers was varied to adjust the extent of crosslinking in the network.[16]

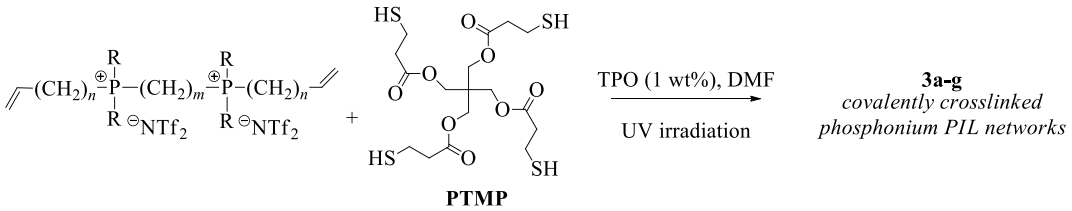

2a: R = Ph, *m* = 4, *n* = 1
2b: R = Ph, *m* = 4, *n* = 4
2c: R = Ph, *m* = 12, *n* = 1
2d: R = *i*-Pr, *m* = 4, *n* = 1
2e: R = *i*-Pr, *m* = 12, *n* = 1

Scheme 1.2: Photopolymerization of phosphonium monomers.

In addition to varying the extent of crosslinking, the overall rigidity, and, as a result, thermal, ion conductivity, and mechanical properties were explored by varying alkyl spacer chain length, side chain R group, and counterion used. In general, more rigid structures led to higher *Tg* values and lower ion conductivities (10^{-7} S/cm at 30°C). With this, phenyl side chains, shorter alkyl spacing chains, and more extensive crosslinking created the higher rigidity that exhibited these properties. The more flexible polymer structures created with isopropyl side chains, longer alkyl spacing chains, and less crosslinking, displayed the opposite properties with lower *Tg* values and slightly higher conductivities (10^{-5} S/cm at 30°C). All the PILs displayed relatively high thermal stabilities with $T_{d5\%} > 350$°C.[16]

1.3 Perarylated Phosphonium Ionic liquids and Ionenes

Beyond just having a phosphonium IL or ionene, these structures can be synthesized to be perarylated. Due to the bulky nature of the perarylated phosphonium ions, these "ionic liquids" don't always fit into the classical IL definition of having a melting point of less than 100°C. As such, sometimes these ionic substances are instead referred to as mesothermal ILs. Though they may melt above 100°C, the IL general term is often still used, as the melting points for these salts are still several hundred degrees lower than what is typically seen for inorganic salts. Perarylated phosphonium salts are still able to be fine-tuned to meet the desired application like the otherwise substituted PILs with lower melting points. [17] Perarylated versions of phosphonium PILs and ionenes have the distinct advantage of having further enhanced thermal stability. While other phosphonium PILs and ionenes have relatively high thermal stabilities, this stability is limited by decomposition via anion-involved retro-S_N2 or E2 pathways. PILs built upon the tetraphenylphosphonium (PPh_4^+) ion are not limited by these decomposition pathways.[18] This superior thermal stability has been demonstrated in the literature in multiple studies.[17,18, 19]

In their 2020 article, Rabideau et. al. sought to explore ILs and mesothermal ILs for use as heat transfer fluids, extreme condition lubricants, biomass pretreatment solvents, and catalysts in high temperature reaction systems.[17] For these applications, long-term thermal stability is among the desired properties in a suitable for the application material. Previously published research suggested that peraryl phosphonium and sulfonium salts would be ideal candidates for these applications as they have been shown to display the desired thermal stability.[20] One drawback of these materials, however, is the higher

melting point than what is seen in many ILs. To combat this, modifications of the ion structure are often made with the goal of lowering the melting point of the material. One published way to achieve this is based upon adding asymmetric moieties and adjusting the identity and location of substituents.[18] Based upon this, the researchers hypothesized that replacing hydrogen with the considerably more electronegative fluorine at select points in the cations would be able to significantly aid in lowering the melting point of the ILs. The fluorine would create a strong and directional dipole within the ion that was not previously seen when the hydrogen was positioned at the same location(s). The authors synthesized perarylphosphonium, perarylsulfonium, piperidinium, and imidazolium salts with bistriflimide counterions and varied the location of the substituted fluorine (Figure 1.6.)[17]

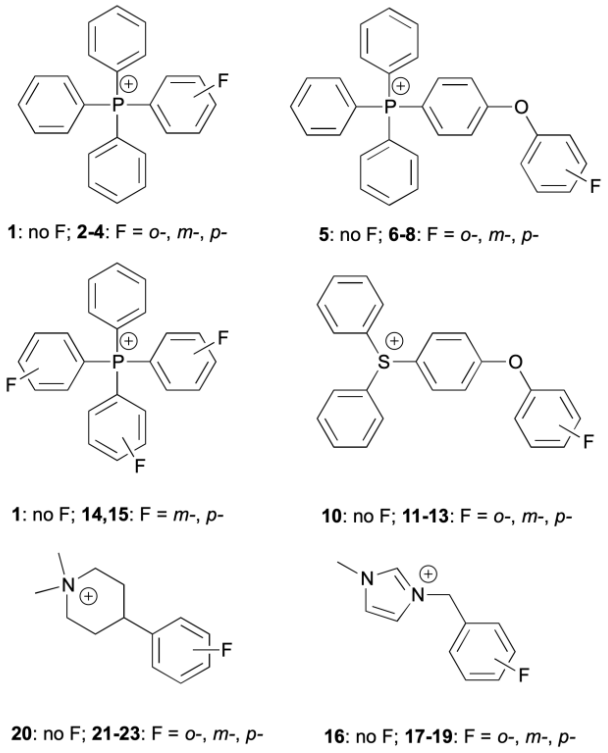

Figure 1.6: Rabideau et. al. structures of the IL cations with variable fluorine position.[17]

They then calculated the dipole moments of the cations using quantum-based calculations and found melting points via differential scanning calorimetry (DSC). The results showed that increasing the dipole moment of the cation with the directional forces introduced via fluorine substitution did, in general, decrease the melting point of the salt. The exception to this was when the directional forces were overly strong and instead formed a glassy material. The authors noted that further research is needed to better understand this concept and its applicability across other IL materials.[17]

Cassity et. al. also investigated the effects of structure on the melting points of ILs. However, this group exclusively focused their study on perarylated phosphonium salts. Specifically, the researchers wanted to synthesize PPH_4^+ derivatives with structural variations such as phenoxy, diarylketone, and sulfone groups to better understand how the cation structure correlated to the thermal stability and melting point of the salts.

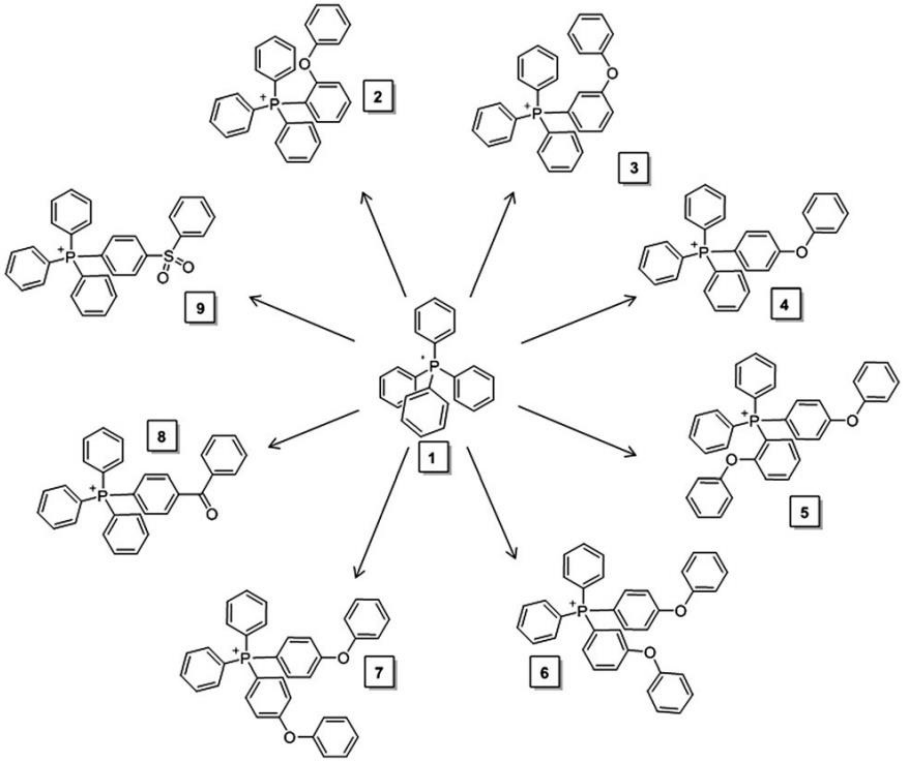

Figure 1.7: Cassity et. al. synthesized PPH_4^+ derivative cations.[18]

Once synthesized, the materials underwent 90 days of thermal stressing in open to the air and 300°C conditions. With this applied stress, the salts were assessed for loss of mass and for any changes that may have occurred in the ion structure. The thermal stress testing yielded that the structures of all tested phosphonium ILs remained unchanged after the 90-day heat exposure. Melting point data revealed that a lowering of melting point is observed when the dipole moment of the cation is increased due to an increased cation alignment that stabilizes the liquid state of the IL.[18] As was observed with Rabideau et. al., this is interrupted when the dipoles and resulting forces become too strong and add thermodynamic complications to the melting process.[17,18]

The effects of a perarylated phosphonium cation structure have also been studied once the ion has been incorporated into a polymer ionene system. There are multiple routes of achieving the desired perarylated phosphonium PIL and the exact method chosen will depend on the substituents incorporated into the structure, available materials, cost, etc. Wan et. al. presents one possible mode of synthesis. In their method, P-C coupling is performed from commercially available arylphosphines (or alkylphosphines depending on the desired end structure) and commercially available aryl dihalides.

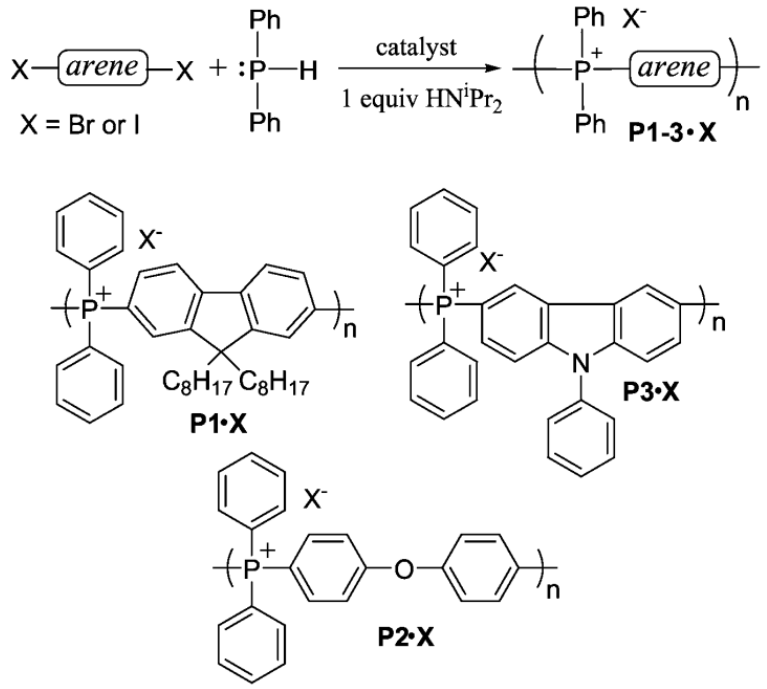

Scheme 1.3: Wan et. al. Ionene synthesis via coupling of arylphosphine and aryl dihalide.[19]

This process on its own has a relatively poor yield due to the double deprotonation needed to form the ionene chain. To improve the yield for this process, the authors added one molar equivalent of diisopropylamine to act as a base and aid in the deprotonation process. In addition, a catalyst was used to aid in the reaction. Specifically, the authors found that $NiBr_2$ and $Pd_2(dba)_3$, where dba is dibenzylideneacetone, were both effective in catalyzing the polymerization reactions. The resulting PILs were analyzed for thermal stability. While the polymers with bromide counterions had relatively high thermal stabilities, the authors sought to increase stability further by changing the counterion. Anion exchange to $[NTf_2]$ and the resulting polymers did display a significant increase in thermal stability. Alkaline stability of each $[NTf_2]^-$ polymer variation was also analyzed, and a high stability was seen for all of the three $[NTf_2]^-$ polymers.[19]

Perarylated phosphoium PILs were explored in the context of optoelectronic applications by Bedford et. al. The group was interested in the perarylated polymer due to the added thermal stability created by the resistance that these structures have to decomposition via S_N2 nucleophilic attack. The researchers chose to derive the desired perarylated polymers from chromophore parent structures. To achieve this, they catalyzed a P-C bond formation with a $NiBr_2$. Though literature had also supported a palladium catalyst as a possibility, the nickel catalyst was chosen due to cost. The catalyzed reaction resulted in a coupling of a triarylphosphine and an alkyl bromide.

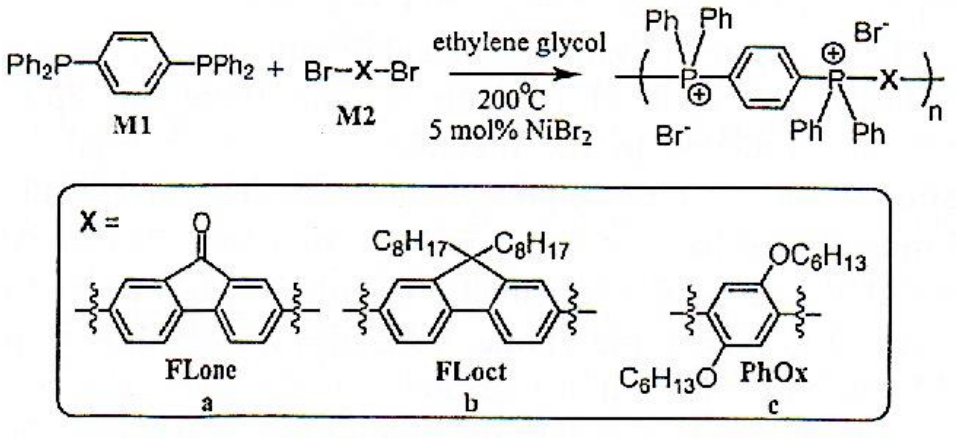

Scheme 1.4: Bedford et. al. $NiBr_2$ catalyzed P-C coupling.[21]

Polymerization was completed using fluorene-derived comonomers due to the desired optical application of the materials. Thermal and chemical stability testing was completed on the resulting polymers. The thermal stability was lower than what has been previously observed for perarylated phosphonium PILs; however, the researchers attributed this to the fluorene-derived comonomers. The polymers did not degrade with exposure to the strong base KO^tBu when exposed over a one-hour period at room temperature. However, complete decomposition was seen with 24-hour exposure to 6 M NaOH at 60°C. This

observed degradation couldn't have occurred via an SN2 pathway due to the lack of sp^3 carbon leaving groups on the phosphonium. The authors propose that the degradation is instead due to a nucleophilic aromatic substitution pathway.[21]

While Wan et. al. and Bedford et. al. constructed ionene style polymers with the phosphonium monomers, researchers Yang and Smith instead chose to synthesize a crosslinked polymer network in their 2018 work. This pair wished to explore the perarylated phosphonium polymers for an alkaline fuel cell application. Within some fuel cells, a PIL based membrane can be utilized to separate the cathode and anode compartments. This membrane is permeable and allows for OH^- ions to pass through. Due to the nature of alkaline fuel cells, the PIL used must have both high thermal and alkaline stability. While these features are observed in the ionene version of the perarylated phosphonium PILs that the researchers explored, the mechanical strength to form a membrane was not able to be achieved. Thus, the researchers hypothesized that the formation of cross-linkages to form a polymer network would add the necessary mechanical strength without losing the other desired properties. They synthesized the network with different molar ratios of monomer components to vary the extent of observed cross-linkage. Figure 1.8 shows an example portion of the 1:1 molar ratio polymer. The resulting polymers displayed high thermal stability, high alkaline stability, and resistance to swelling due to water exposure. In addition, the polymers were highly porous in nature, as would also be a desired property for alkaline fuel cell membrane applications.

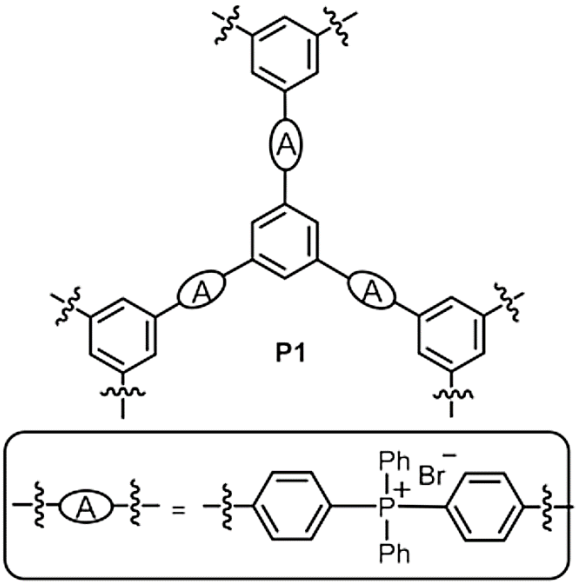

Figure 1.8: Portion of crosslinked polymer created by Yang and Smith.[22]

1.4 Project Purpose

As discussed previously, phosphonium ILs, PILs, and ionenes have been shown in the literature to display high thermal stability and alkaline stability. Due to these properties, these materials are promising in many applications, such as in fuel cells. In the literature, ionenes such as polyaryletherketone (PAEK) and polyethersulfone (PES) with aryl groups also display relatively high thermal stability.[23,24]

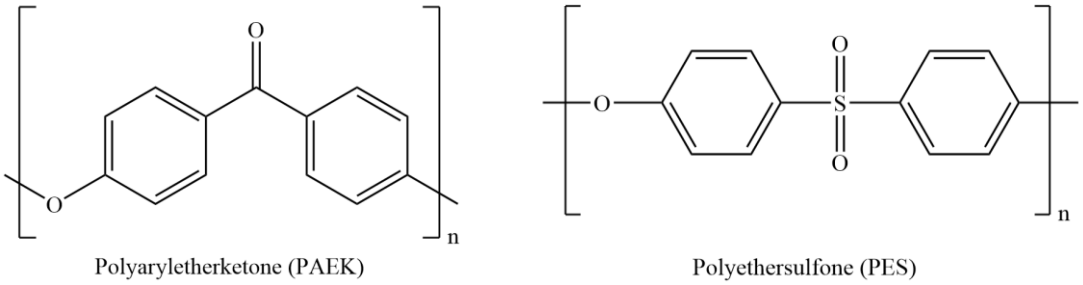

Figure 1.9: PAEK and PES structures

With these ideas in mind, this project focused on the synthesis and characterization of phosphonium PAEK and PES style ionene polymers using a nucleophilic aromatic substitution strategy. Ionenes were successfully made and evaluated for their thermal and conductive properties, as well as their chemical resistivity under alkaline conditions. The four [NTf_2] paired ionene variations synthesized are shown in Figure 1.10.

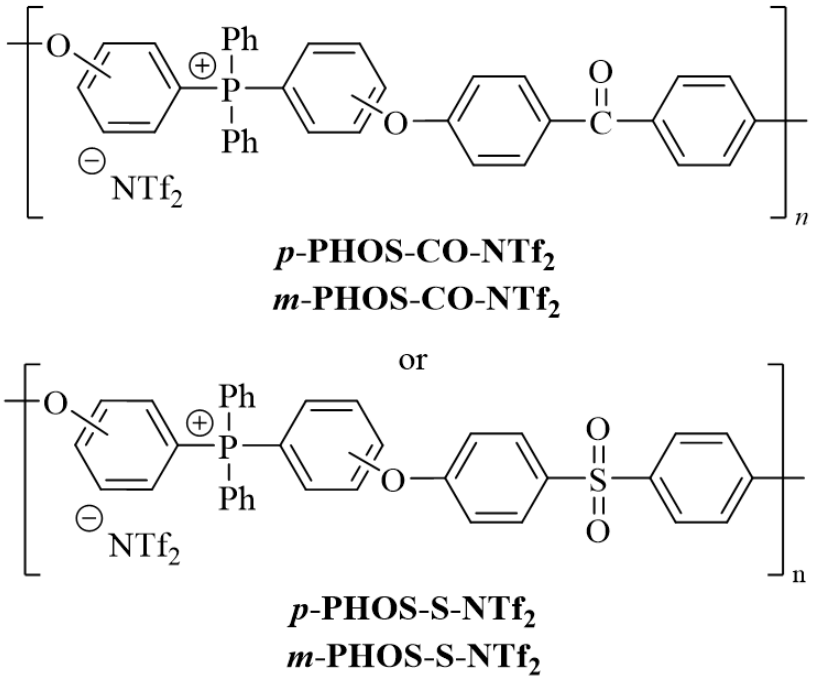

Figure 1.10: The four synthesized and characterized $[NTf_2]^-$ ionene variations for this project.

Chapter 2: Results and Discussion

2.1 Synthesis and Characterization of Phosphonium Monomers

The bis(hydroxyphenyl)diphenyl phosphonium bromide monomers were synthesized via two different methods. Approach A was completed with the aid of a *tert*-butyldimethylsilyl chloride (TBDMSCl) protecting group as shown in Scheme 2.1. Once the *p*- or *m*-bromophenol was protected (structure **1**), a lithium-halogen exchange was completed by reaction with *n*-BuLi, followed by chlorodiphenylphosphine to produce a TBDMS-protected hydroxyphenyldiphenylphosphine (Structure **2**). The protecting group was then removed with tetrabutylammonium fluoride (TBAF) to produce a *p*- or *m*-hydroxyphenyldiphenyl phosphine (structure **3**). Though this approach was successful and resulted in an overall yield of 65-70%, the protection-deprotection strategy was a relatively lengthy and cumbersome process.

As a result, the one-step Approach B was attempted based upon the method used by García-Márquez.[25] In this approach, diphenylphosphine was reacted with *p*- or *m*-iodophenol using Pd-catalyzed cross-coupling conditions to directly produce structure **3** with yields of 75-85%. This approach was more time efficient; however, it did have to be completed under dry argon as diphenylphosphine is highly air sensitive.

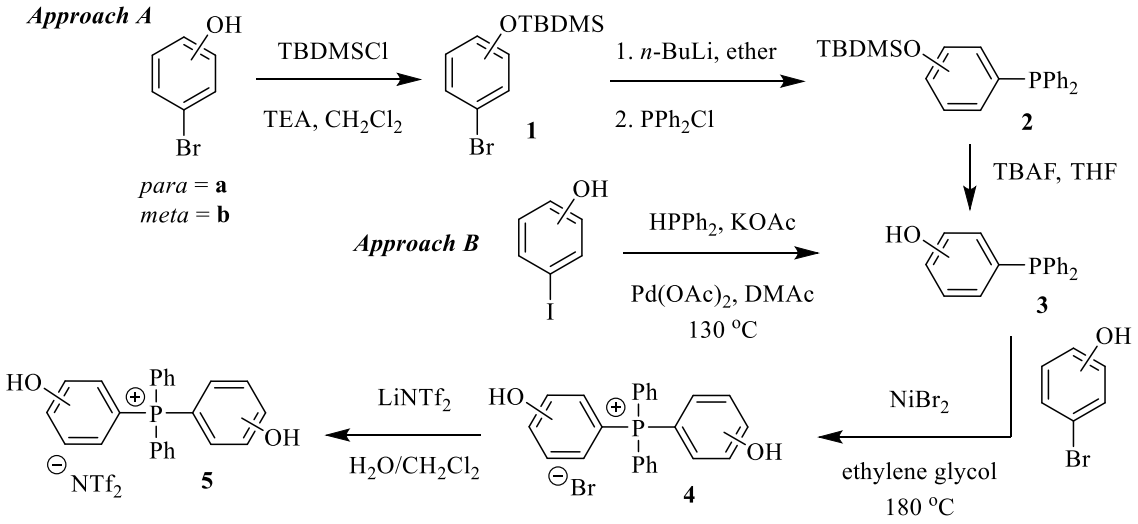

Scheme 2.1: Preparation of *p*- and *m*-bis(hydroxyphenyl)diphenylphosphonium salts.

Regardless of the method used to produce structure **3**, the next step was nickel-catalyzed coupling of this structure with either *p*- or *m*-bromophenol, a method described previously in the literature.[18] This resulted in the formation of a *p*- or *m*-bis(hydroxyphenyl)diphenyl phosphonium bromide salt (structure **4**). The final step in the monomer formation was an anion exchange in which the Br^- was replaced by $[NTf_2]^-$ via reaction of structure **4** with $LiNTf_2$ to yield structure **5**.

The bis(hydroxyphenyl)diphenyl phosphonium Br^- and $[NTf_2]^-$ monomers (structures **4** and **5**) were analyzed for purity via ^1H, ^{13}C, and ^{31}P NMR spectroscopy as well as elemental analysis. NMR spectroscopy and elemental analysis data are included in the appendix. The thermal properties of the monomers were analyzed via differential scanning calorimetry (DSC) and thermogravimetric analysis (TGA). Table 2.1 depicts both sets of data.

Table 2.1: Thermal properties of the *p*- and *m*-bis(hydroxyphenyl)diphenylphosphonium salts.

Monomer		**DSC T_m (°C)**	**TGA $T_{d5\%}$ (°C)**
p-PHOS-OH-Br	**4a**	318	353
p-PHOS-OH-NTf_2	**5a**	183	409
m-PHOS-OH-Br	**4b**	249	340
m-PHOS-OH-NTf_2	**5b**	5.6 (T_g)	405

Both the Br^- and $[NTf_2]^-$ *p*-substituted phosphonium salts (monomers **4a** and **5a**) displayed a melting transition (T_m), with the bulkier $[NTf_2]$ salt exhibiting a significantly lower value at 183°C versus the 318°C displayed by the Br^- analog. The *m*-substituted version of the Br^- salt (monomer **4b**) exhibited a further decreased T_m value. The *m*-substituted $[NTf_2]$ analog (compound **5b**) exhibited a glass transition temperature (T_g) rather than a T_m. This indicates that the solid-phase packing in these perarylated phosphonium salts can be disrupted by altering the substitution location (*meta* vs. *para*) and/or the counteranion used ($[NTf_2]$ vs. [Br]). This observation is not novel as it has also been observed for other perarylated phosphonium salts in past literature.[18,26] Relatively high thermal stabilities were observed for all of the salts, with the $T_{d5\%}$ values for the $[NTf_2]$ analogs exhibiting values in excess of 400°C. A comparison of the four monomers can be seen in the graphed DSC (Figure 2.1) and TGA (Figure 2.2) data.

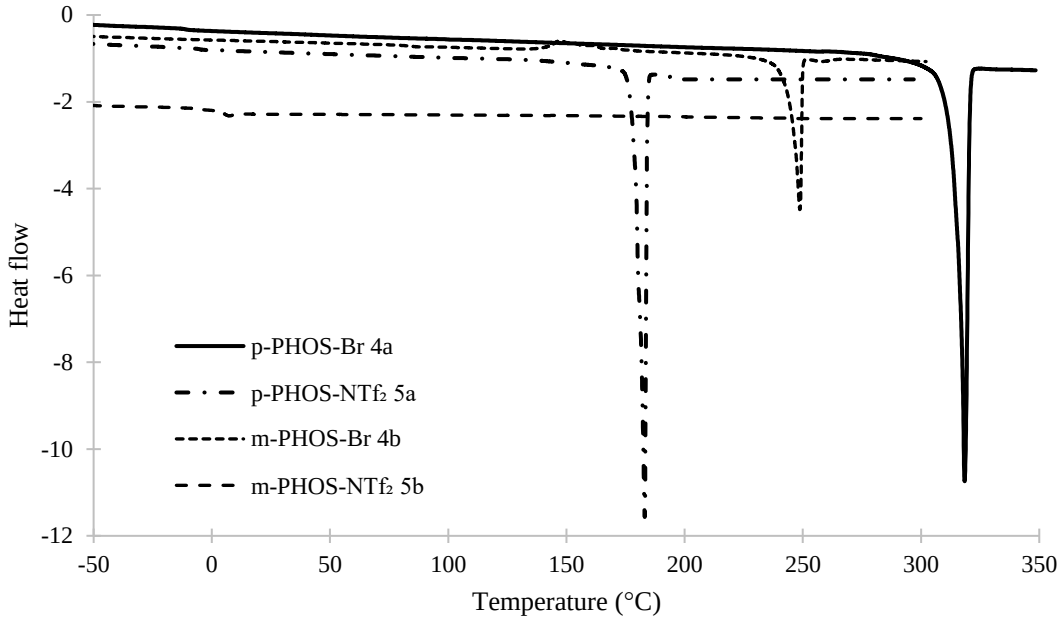

Figure 2.1: Overlay of DSC thermograms for dihydroxy-terminated phosphonium monomers.

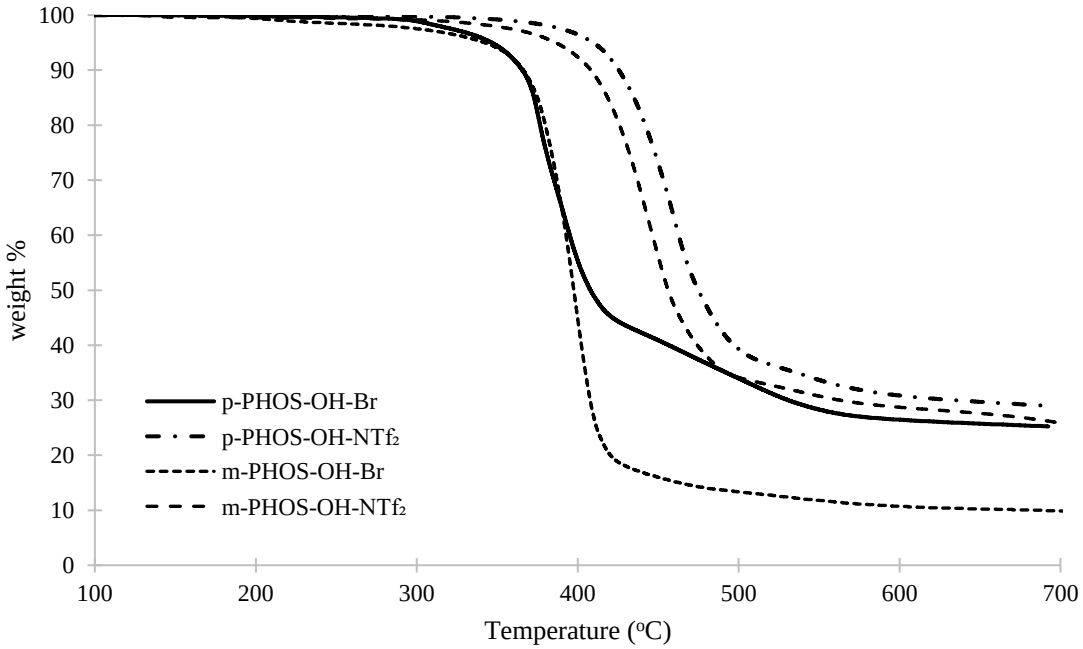

Figure 2.2: Overlay of TGA traces for dihydroxy-terminated phosphonium monomers.

2.2 Polymerization and Ionene Characterization

Polymerization was carried out with the bis(hydroxyphenyl)diphenyl phosophonium [NTf_2] monomers (monomers **5a** and **5b**) via nucleophilic aromatic substitution. The monomer was reacted with a stoichiometric amount of either 4,4′-difluorobenzophenone or 4,4′-difluorodiphenyl sulfone under basic conditions as displayed in Scheme 2.2. ^{1}H and ^{31}P NMR spectroscopy was used to confirm completion of the polymerization reaction, as the disappearance of the respective monomeric signals was observed. The resulting product was an off-white solid for all four perarylated phosphonium ionenes.

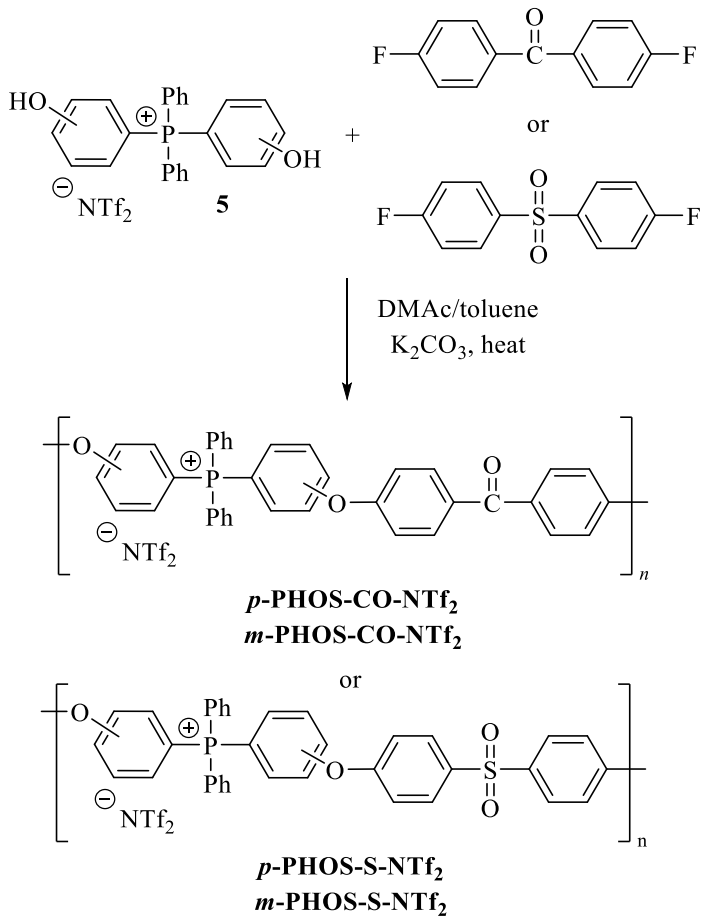

Scheme 2.2: Preparation of perarylated phosphonium ionenes.

Solubility testing of each ionene was completed in several common laboratory solvents at concentrations of 100 mg/mL. Solubility data collected is displayed in Table 2.2, where a result of "Y" indicates complete solubility, and a result of "N" indicates insolubility and/or cloudiness at this concentration.

Table 2.2: Solubility table of perarylated phosphonium ionenes.

Ionene	**water**	**methanol**	**acetone**	**acetonitrile**	**chloroform**	**THF**	**toluene**	**DMF**	**DMSO**
p-PHOS-CO-NTf_2	N	N	Y	N	Y	Y	N	Y	Y
m-PHOS-CO-NTf_2	N	N	Y	Y	Y	Y	N	Y	Y
p-PHOS-S- NTf_2	N	N	Y	N	Y	Y	N	Y	Y
m-PHOS-S-NTf_2	N	N	Y	Y	Y	Y	N	Y	Y

^{31}P NMR spectroscopy was used to determine ionene molecular weights via the traditional end-group integral analysis strategy. With this method, the signal for the end group phosphorus atom displays a slightly different chemical shift value (~26.7 ppm) than the phosphorus atoms within the internal repeating units of the polymer (~27.2 ppm). Analogous polymerizations were conducted with an excess of either 4,4′-difluorobenzophenone or 4,4′-difluorodiphenyl sulfone added at the end of the polymerization to ensure both ends were capped by an aryl fluoride rather than a phosphonium group. The resulting ^{31}P NMR spectroscopy data yielded significantly decreased or completely disappeared signal at 26.7 ppm, supporting that the ~26.7 ppm signal observed with other ionenes was an end group phosphorus as predicted. With this

data, the molecular weights of the ionenes were determined to be between 9.9-13.6 kg/mol as displayed in table 2.3.

Table 2.3: Molecular weights and thermal properties of perarylated phosphonium ionenes.

Ionene	**^{31}P NMR MW (kg/mol)**	**DSC T_g (°C)**	**TGA $T_{d5\%}$ (°C)**
p-PHOS-CO-NTf_2	9.9	101	383
m-PHOS-CO-NTf_2	13.6	54.5	368
p-PHOS-S- NTf_2	10.5	99.5	388
m-PHOS-S-NTf_2	13.4	55.8	381

DSC and TGA were utilized to analyze the thermal properties of the ionenes. All four of the perarylated phosphonium ionenes displayed a T_g value and no T_m transition. Little impact on T_g was observed when changing between carbonyl and sulfone linkers. A ~40-45°C decrease in T_g was observed when changing from *para* to *meta* ionenes. As with the monomer DSC data, the decrease in T_g observed with the *meta* ionenes is attributed to solid-state packing between polymer chains being disrupted in these structures. The thermal stability for each ionene was found to be reduced in comparison to the corresponding phosphonium monomeric precursors. These stabilities were, however, comparable to or improvements on that seen for other phosphonium ionenes and perarylated phosphonium ionenes previously reported in the literature. [6,13,16,19,21,22,27,28] A summary of the obtained thermal data is included in Table 2.3 as well as in Figures 2.3 and 2.4. These results indicate that subtle changes in the ionene structure can result in a significant decrease in T_g value, whilst still maintaining thermal stability.

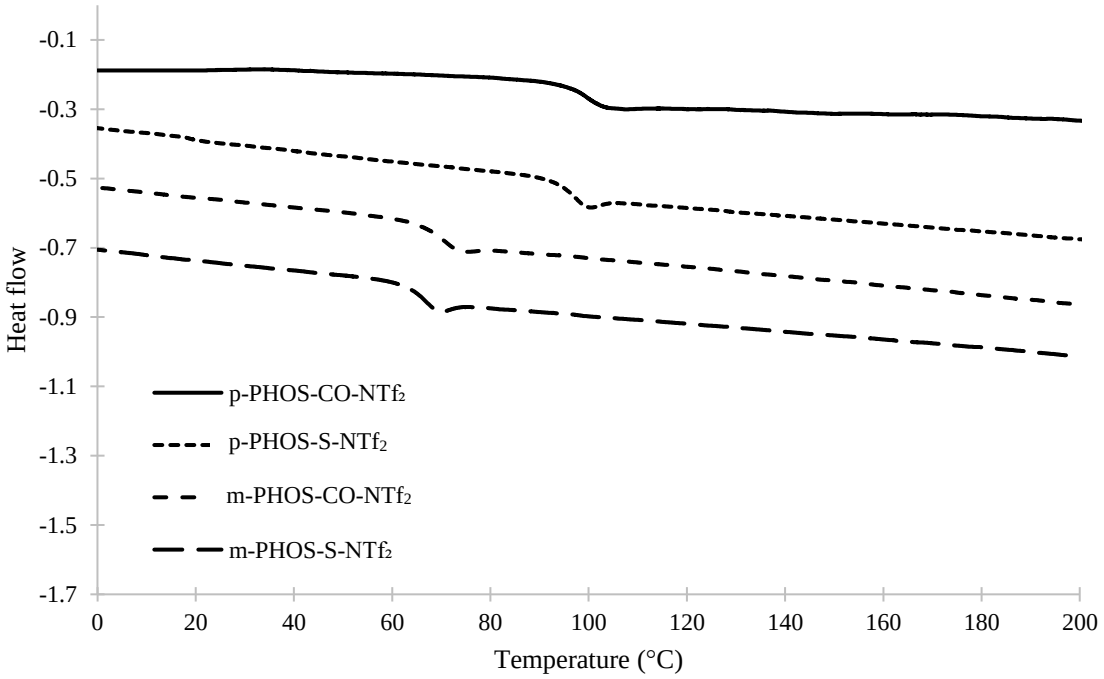

Figure 2.3: Overlay of DSC thermograms for phosphonium ionenes.

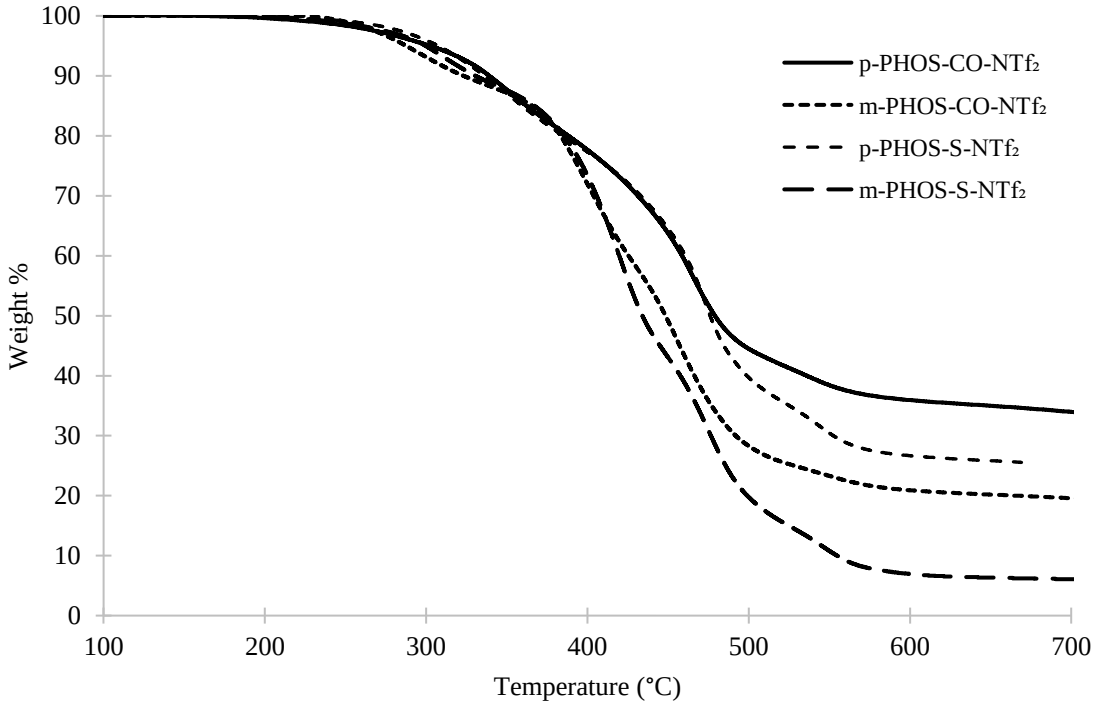

Figure 2.4: Overlay of TGA traces for phosphonium ionenes.

Clear films with varying yellow tint of the ionenes were successfully made with use of acetonitrile and DMF solvents and a PTFE mold. These worked well for conductivity studies; however, mechanical properties could not be determined as the films were too brittle to acquire any useful stress-strain or modulus data.

2.3 Alkaline Stability

In addition to thermal stability, chemical stability was also examined. Each ionene was exposed to 1M and 6M NaOH solutions at room temperature for 72 hours and at 65°C for 48 hours. ^{1}H and ^{31}P NMR spectroscopy was used to monitor the structure. No degradation was observed for any of the ionenes under any of these conditions. Prior work on perarylated phosphonium ionenes has shown that decomposition due to a retro-S_NAr mechanism is possible if one of the aryl rings bound to the phosphonium atom is activated with an electron-withdrawing substitutent; however, the present are resistant to this as the substituent attached to the phosphonium center is electron-donating (phenoxy), leading to stabilization.[2,21]

2.4 Conductivity

Dielectric relaxation spectroscopy (DRS) was used to determine temperature-dependent ionic conductivities for each of the phosphonium ionenes. Complex dielectric permittivity values $\sigma^*(\omega,T)$ were measured isothermally at 30% RH in 10°C steps from 30 °C below the T_g to 60°C above the T_g of each ionene over a frequency range of 0.1-10^7 Hz. From this data, the DC-conductivity (σ) was determined from the plateau value observed in the spectral dependence of the real conductivity, a method that has been

previously used in the literature.[16,29] Figure 2.5 shows the measured log σ values as a function of temperature. None of the ionenes were particularly conductive, with conductivities to the order of ~10^{-7} S/cm at 120 °C. These are lower than previously reported phosphonium PILs and ionenes; however, the comparison is not a perfect one, as none of these previously reported polymers were perarylated.[13,16,30,31] This is likely attributed to the high degree of π-π interactions creating glassy, high T_g polymers where ion mobility and conductivity is restricted.

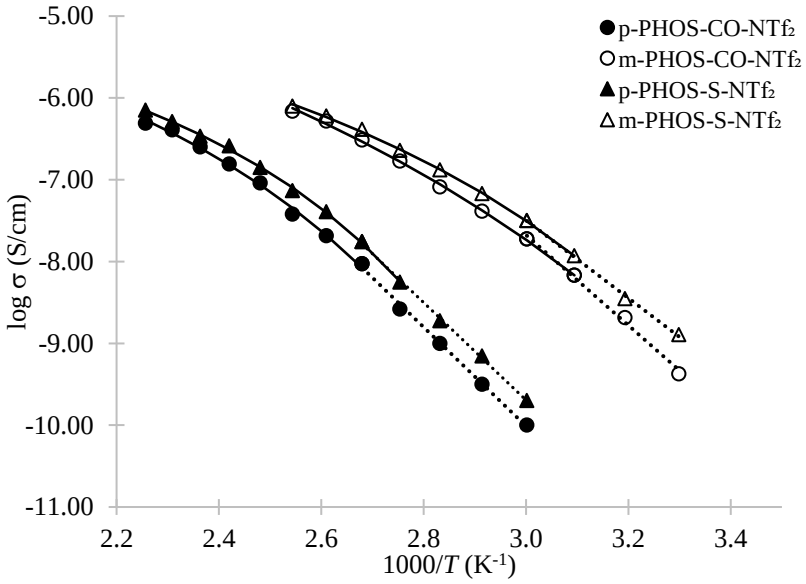

Figure 2.5: Overlay of log conductivity (S/cm) versus 1000/T at 30% RH for the perarylated phosphonium ionenes. Note: Dashed lines are Arrhenius fits for data at or below the T_g while the solid curves are VFT fits for data at or above the T_g.

Meta-analogs exhibited higher conductivities at 1-to-2 orders-of-magnitude higher than the *para*-analogs when comparing the same temperature range. As changes in polymer segmental motion, (observed in the data as T_g changes) directly affect ionic

conductivity, this observation was in line with what was expected. This data supports that ionic conductivity is T_g- dependent, as depicted in the T_g-normalized ionic conductivity plot (Figure 2.6). This plot shows a near-complete collapse of the ionic conductivities when polymer segmental motion (T_g) is accounted for. Between the ionenes with the same substitution structure (both *para*- or both *meta*-), the sulfone derivative resulted in a slightly higher conductivity than their carbonyl counterparts. This is likely due to the stronger electron-withdrawing nature of the sulfone that could aid ion transport through stronger localized dipole moments.[32]

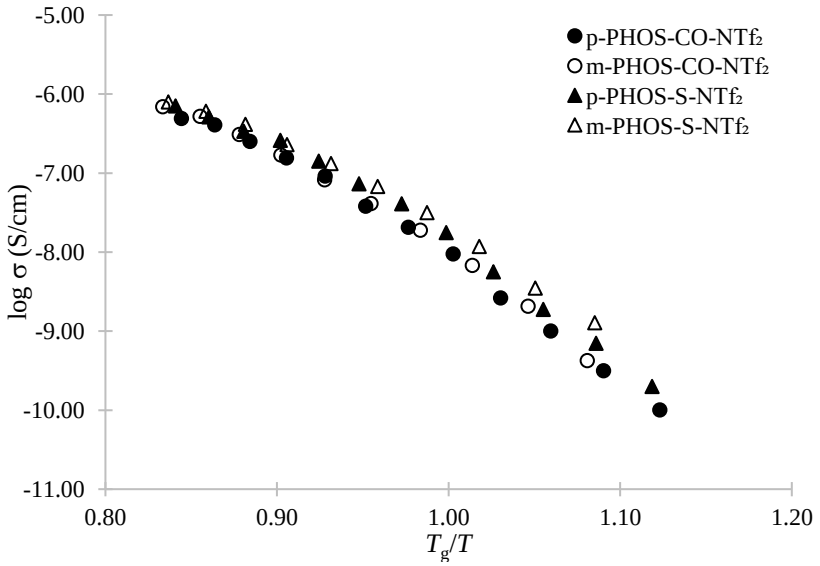

Figure 2.6: T_g-normalized overlay of log conductivity (S/cm) versus 1000/T at 30% RH for the perarylated phosphonium ionenes.

Ionenes and other ionic-liquid containing polymers can exhibit both Arrhenius and VFT (Vogel-Fulcher-Tamman) behavior with respect to their ionic conductivities.[29,33,34] Arrhenius-like behavior in the ionic conductivity data is typically seen at temperatures close to and below the T_g, reflecting the thermal hopping frequency of ions. The dashed

lines for each ionene data set in Figure 2.5 represent linear, Arrhenius fits with activation energy (E_a) values as shown in Table 2.4. Ionic conductivities exhibit VFT behavior, when at temperature close to and above the T_g. This is attributed to additional contributions from segmental motion of the polymer and/or relaxation events due to the applied potential. The solid, curved fits shown for each data set in Figure 2.5 represent the VFT fits according to the following expression:

$$\sigma = \sigma_\infty x \exp\left(-DT_o/(T-T_o)\right)$$

where σ_∞ is the infinite conductivity, T_o is the Vogel temperature (where ion motion stops), and D is the strength parameter. Table 2.4. displays each of these fitting parameters for each ionene. Significantly low infinite conductivity and D values were observed, indicating poor ion mobility.

Table 2.4: Activation energies and VFT fitting parameters for perarylated phosphonium ionenes.

Ionene	E_a (kJ/mol)	σ_∞(S/cm)	T_o (K)	D
p-PHOS-CO-NTf_2	115.8	7.44×10^{-5}	233	2.6
m-PHOS-CO-NTf_2	105.8	2.04×10^{-4}	286	3.9
p-PHOS-S- NTf_2	114.1	2.05×10^{-4}	273	3.7
m-PHOS-S-NTf_2	91.0	2.13×10^{-3}	303	7.3

The large amount of π-π interactions between polymer chains is likely to severely restrict the ability of anion hopping, creating this poor conductivity; however, more work would need to be done to better describe the ion mobility in these systems. A slight

increase in ion mobility is observed *meta*-analogs used, though this does not create significantly conductive systems when compared to other phosphonium ionenes with alkyl components in their structure.[13,35]

2.5 Summary and Future Research

Four bis(hydroxyphenyl)diphenyl phosphonium bromide monomers were synthesized, followed by anion exchange to $[NTf_2]^-$. The monomers were checked for purity and then characterized for their thermal properties via DSC and TGA.

These monomers were then used individually to synthesize four phosphonium PAEK/PES style ionene polymers via nucleophilic aromatic substitution. Ionenes were successfully made and evaluated for their solubilities in various organic solvents, molar masses, thermal stabilities, alkaline stabilities, and conductive properties.

Regardless of the poor ionic conductivities observed, these perarylated phosphonium ionene systems serve as a baseline set of materials where ion mobility and conductivity could be further improved through structural changes in the backbone. The results of this project indicate that minor changes in ionene structure can result in significant decreases in T_g values, and, as a result, can possibly lead to improved ion mobility and conductivity. Future research will focus on planning possible structural modifications, synthesizing the new ionenes, and completing characterization for comparison. With this, the challenge will be to find modifications that will allow for a reduced T_g value while maintaining high thermal and alkaline stabilities.

Chapter 3: Experimental

3.1 Materials and General Notes

All reagents and solvents utilized in this study were purchased and were used as received unless otherwise noted below. The tetrahydrofuran (THF) (99.99%), diethyl ether (99.9 %), and N,N-dimethylacetamide (99.5%) were purchased as anhydrous materials and used in a manner to maintain this state. The 4,4-difluorobenzophenone (99%) and the 4,4'-difluorodiphenyl sulfone (99%) were purchased from Sigma Aldrich. The ACS grade ethylene glycol used was further purified before use via distillation over magnesium sulfate and was then stored in a glass desiccator. Ultrapure water with a resistivity of 18 MΩ-cm was produced using an ELGA Purelab® Ultra filtration device.

3.2 Monomer Characterization Methods

^{1}H and ^{13}C NMR spectra were obtained on a 400 MHz JEOL-ECS spectrometer and chemical shift values for the observed peaks were referenced to residual solvent signals ($CDCl_3$: ^{1}H, 7.26 ppm; ^{13}C, 77.16 ppm; DMSO-d_6: ^{1}H, 2.50 ppm; ^{13}C, 39.52 ppm). The NMR spectra of Br^- and the $[NTf_2]^-$ monomers, as well as intermediates and ionenes are included in the Appendix.

A Perkin-Elmer 2400 CHNS/O Series II elemental analyzer was used to complete elemental analysis on all Br^- and the $[NTf_2]^-$ monomer materials. In preparation for elemental analysis and thermal testing, samples were placed in a vacuum oven set to

40°C and < 0.01 mmHg for 48 hours prior to analysis. This ensured the removal of any moisture and/or remaining residual solvent.

Residual Br^- monomer in monomers **5a** and **5b** was determined using ion chromatography (IC; ICS-110, Dionex) with an eluent concentration of 4.5 mM carbonate/1.4 mM bicarbonate, a flow rate of 1.2 mL/min, and a suppressor current of 31 mA. Aqueous standards prepared by serial dilution of a 1000 ppm bromide stock solution (sodium bromide, > 99.9 %) were used to complete calibration of the instrument. For each phosphonium, 10-15 mg of the salt was dissolved in 1 mL of acetone and injected. Residual bromide in monomers **5** was found to be less than 0.01% w/w.

A TA Instruments Q200 differential scanning calorimeter was used to complete differential scanning calorimetry (DSC), with a heating rate of 2°C/min on 4-8 mg samples. Glass transition temperatures (T_g) were determined by the inflection point of the curve observed from the second heating cycle. Melting temperatures (T_m) were determined at the maximum point of the endothermic transition. DSC experiments were performed in duplicate with an error of ±1.5°C and values reported from the second heating cycle.

A TA Instruments Q550 thermogravimetric analyzer (TGA) was used to analyze the thermal stabilities of the monomers under constant dry nitrogen flow and a heating rate of 10°C/min. $T_{d5\%}$ is defined as the temperature at which 5% weight loss was observed. All TGA Td5% experiments were performed in duplicate with an error of ±1.0°C.

3.3 Preparation of *p*/*m*-hydroxyphenyldiphenylphosphine (Approach A)

*Synthesis of TBDMS-protected p-bromophenol **1a***. In a 500-mL round-bottomed flask equipped with magnetic stir bar, *p*-bromophenol (10.00 g, 0.0578 mol) was dissolved 120 mL of dichloromethane. To this, tert-butyldimethylsilyl chloride (TBDMSCl, 10.89 g, 0.0723 mol) and triethylamine (6.43 g, 0.0636 mol) were added sequentially. The round bottom flask was capped, wrapped in aluminum foil, and the reaction solution was stirred at room temperature overnight. The reaction was then transferred to a 250 mL separatory funnel where it was washed with DI water (75 mL). The organic phase was isolated, the solvent was removed under reduced pressure, and the residue was dissolved in hexanes (150 mL). The solution was subsequently washed in separatory funnel with DI water (2 x 75 mL) and brine (75 mL). The organic layer was then dried over Na_2SO_4/$MgSO_4$, filtered, and the solvent removed under reduced pressure. This resulted in a crude, light yellow oil that was then purified by high vacuum distillation at 93-95°C and 0.1 mm Hg. This yielded 15.79 g (95% yield) of **1a,** a clear, colorless oil. ^{1}H NMR ($CDCl_3$): δ 7.31 (d, 2 H, *J* = 9.2 Hz), 6.71 (d, 2 H, *J* = 9.2 Hz), 0.97 (s, 9 H), 0.18 (s, 6 H). ^{13}C NMR ($CDCl_3$): δ 154.82, 132.27, 121.89, 113.61, 25.62, 18.17, -4.50. Anal. Calcd. For $C_{12}H_{19}BrOSi$: C 50.17, H 6.67. Found: C 51.55, H 6.64.

*Synthesis of TBDMS-protected p-Ph2PPhOH **2a***. To a 100-mL Schlenk flask under dry argon TBDMS-protected p-bromophenol (2.50 g, 8.67 mmol) was added and dissolved in 20 mL of anhydrous diethyl ether. This solution was stirred in a salted ice bath to reduce the temperature to 0°C. While at this lowered temperature, n-butyllithium (5.2 mL, 13.0 mmol, 2.5 M in hexanes) was added dropwise over a 15-minute period via addition funnel. The resulting solution was then stirred at room temperature for 90

minutes. The reaction mixture was then again cooled to 0°C and chlorodiphenylphosphine (3.15 g, 13.9 mmol) was added dropwise over a 15-minute period via addition funnel. The mixture was then allowed to stir at room temperature overnight. The reaction was then filtered through a silica gel plug with diethyl ether and the solvent was removed under reduced pressure to give 2.92 g (86% yield) of an off-white solid. ^{1}H NMR ($CDCl_3$): δ 7.25-7.33 (m, 10 H), 7.21 (d, 2 H, *J* = 8.8 Hz), 6.81 (d, 2 H, *J* = 8.8 Hz), 0.97 (s, 9 H), 0.19 (s, 6 H). ^{13}C NMR ($CDCl_3$): δ 156.60, 135.57, 135.36, 133.60, 133.55, 133.36, 128.49, 128.42, 128.35, 120.35, 120.27, 25.60, 18.15, -4.41. ^{31}P NMR ($CDCl_3$): δ -3.23. Anal. Calcd. For $C_{24}H_{29}OPSi$: C 73.43, H 7.45. Found: C 73.84, H 7.39.

*Synthesis of p-hydroxyphenyldiphenyl phosphine **3a***. In a 300-mL Schlenk flask under dry argon **2a** (13.00 g, 33.1 mmol) was dissolved in 130 mL of anhydrous diethyl ether. The stirred solution was cooled to 0°C and tetrabutylammonium fluoride (TBAF, 66.2 mL, 66.2 mmol) was added dropwise via an addition funnel over 45 minutes. The resulting solution was then warmed to room temperature and stirred overnight. The reaction was again cooled to 0°C and 3mL of concentrated HCl was added dropwise by pipette over the course of 10 minutes. The resulting reaction mixture was then stirred at room temperature for 4 hours. Once this time had passed, volatiles were removed under reduced pressure and the remaining residue was partitioned between anhydrous diethyl ether (150 mL) and DI water (100 mL) via separatory funnel. The organic phase was washed with additional portions of DI water (2 x 75 mL) and then dried over Na_2SO_4/$MgSO_4$. This was then filtered and solvent removed under reduced pressure to yield a viscous yellow oil. 150 mL of hexanes were added, and the mixture was

vigorously stirred for 60 minutes, followed by isolation via filtration and washing with cold hexanes. After drying under reduced pressure, a white solid (7.56 g, 82% yield) was obtained. ^{1}H NMR ($CDCl_3$): δ 7.28-7.35 (m, 10 H), 7.21 (d, 2 H, *J* = 8.8 Hz), 6.83 (d, 2 H, *J* = 8.8 Hz). ^{13}C NMR ($CDCl_3$): δ 156.59, 137.76, 137.66, 135.91, 135.70, 133.48, 133.29, 128.49, 128.45, 128.37, 127.55, 127.48, 115.82, 115.74. ^{31}P NMR ($CDCl_3$): δ –3.20 Anal. Calcd. For $C_{18}H_{15}OP$: C 77.69, H 5.43. Found: C 77.29, H 5.03.

Synthesis of TBDMS-protected m-bromophenol ***1b***. In a 500-mL round-bottomed flask equipped with magnetic stir bar, *m*-bromophenol (10.00 g, 0.0578 mol) was dissolved in 120 mL of dichloromethane. TBDMSCl (10.89 g, 0.0723 mol) and triethylamine (6.43 g, 0.0636 mol) were added sequentially, and the resulting solution was stirred at room temperature overnight. The reaction was then transferred to a separatory funnel with DI water (75 mL). The organic phase was isolated, and the solvent was removed under reduced pressure. The remaining residue was dissolved in 150 mL of hexanes. This solution was then washed with DI water (2 x 75 mL), brine (75 mL), dried over Na2SO4/MgSO4, filtered, and the solvent removed under reduced pressure. This yielded a crude, light yellow oil. Purification of the oil was completed via high vacuum distillation at 92-95°C and 0.1 mm Hg. The result was 15.52 g (93% yield) of **1b**, a clear, colorless oil. ^{1}H NMR ($CDCl_3$): δ 7.08 (m, 2 H), 7.01 (m, 1 H), 6.77 (m, 1 H), 0.98 (s, 9 H), 0.20 (s, 6 H). ^{13}C NMR ($CDCl_3$): δ 156.50, 130.39, 124.44, 123.49, 122.44, 118.79, 25.58, 18.14, -4.49. Anal. Calcd. For $C_{12}H_{19}BrOSi$: C 50.17, H 6.67. Found: C 50.48, H 6.54.

Synthesis of TBDMS-protected m-Ph2PPhOH ***2b***. In a 200-mL Schlenk flask under dry argon, **1b** (5.00 g, 17.3 mmol) was dissolved in 70 mL of anhydrous diethyl ether.

This solution was stirred at 0°C and n-butyllithium (10.4 mL, 26.0 mmol, 2.5 M in hexanes) was added dropwise via addition funnel over a 20-minute period. The solution was then stirred at room temperature for 90 minutes. The reaction mixture was then cooled again to 0°C and chlorodiphenylphosphine (6.29 g, 27.7 mmol) was added dropwise via addition funnel over a 20-minute period. The mixture was allowed to stir at room temperature overnight and was then filtered through a silica gel plug with diethyl ether. The solvent was removed under reduced pressure to give 5.92 g (87% yield) of a light yellow oil. ^{1}H NMR ($CDCl_3$): δ 7.26-7.34 (m, 10 H), 7.20 (t, 1 H, *J* = 7.8 Hz), 6.93 (t, 1 H, *J* = 7.8 Hz), 6.81 (d, 1 H, *J* = 6.8 Hz), 6.68 (d, 1 H, *J* = 7.6 Hz), 0.89 (s, 9 H), 0.05 (s, 6 H). ^{13}C NMR ($CDCl_3$): δ 156.63, 137.77, 137.67, 135.60, 135.39, 134.05, 133.95, 133.58, 133.39, 132.12, 132.03, 128.52, 128.44, 128.37, 128.14, 128.06, 120.38, 120.30, 25.60, 18.19, -4.39. ^{31}P NMR ($CDCl_3$): δ –3.23. Anal. Calcd. For $C_{24}H_{29}OPSi$: C 73.43, H 7.45. Found: C 73.22, H 7.51.

Synthesis of m-hydroxyphenyldiphenyl phosphine ***3b***. In a 200-mL Schlenk flask under dry argon, **2b** (8.00 g, 20.4 mmol) was dissolved in 80 mL of anhydrous diethyl ether. The stirred solution was cooled to 0°C and TBAF (41.0 mL, 41.0 mmol) was added dropwise via an addition funnel over 30 minutes. The resulting solution was then warmed to room temperature and stirred overnight. After this, the reaction was again cooled to 0°C and 2 mL of concentrated HCl was added dropwise via pipette over a 10-minute period. The resulting reaction mixture stirred at room temperature for 4 hours, then the volatiles were removed under reduced pressure. The resulting residue was then partitioned between anhydrous diethyl ether (80 mL) and DI water (50 mL) in a separatory funnel. The organic phase was washed with two additional portions of DI

water (2 x 50 mL), dried over $Na_2SO_4/MgSO_4$, filtered and solvent removed to give a light yellow oil. 100 mL of hexanes were added, and the resulting mixture was vigorously stirred for 60 minutes, followed by isolation, filtration and washing with cold hexanes. After drying under reduced pressure, a white solid (4.72 g, 83% yield) was obtained. ^{1}H NMR ($CDCl_3$): δ 7.28-7.36 (m, 10 H), 7.20 (t, 1 H, *J* = 8.4 Hz), 6.89 (t, 1 H, *J* = 7.6 Hz), 6.82 (d, 1 H, *J* = 8.0 Hz), 6.72 (d, 1 H, *J* = 7.2 Hz). ^{13}C NMR ($CDCl_3$): δ 155.61, 155.54, 138.85, 138.75, 136.76, 136.66, 133.82, 133.62, 129.76, 129.68, 128.77, 128.52, 128.43, 126.19, 125.99, 120.10, 119.92, 115.87. ^{31}P NMR ($CDCl_3$): δ –3.20. Anal. Calcd. For $C_{18}H_{15}OP$: C 77.69, H 5.43. Found: C 77.45, H 5.38.

3.4 Preparation of *p/m*-hydroxyphenyldiphenylphosphine (Approach B)

Synthesis of p-hydroxyphenyldiphenylphosphine ***3a***. A procedure reported by García-Márquez et al. was followed.[25] In a 50-mL Schlenck flask equipped with a magnetic stir bar, *p*-iodophenol (4.00 g, 0.0182 mol), potassium acetate (2.68 g, 0.0273 mol), palladium acetate (40 mg), and anhydrous DMAc (20 mL) were added. The flask was then purged with argon and diphenylphosphine (4.06 g, 0.0218 mol) was added dropwise via a double-ended needle into the reactor over a 15-minute period. During the addition, the mixture turned a light purple color, then to a yellow color after completion. The vessel was purged once more with argon, then warmed to 130°C. This temperature was held, and the reaction mixture was allowed to stir for 3 hours. A dark purple color developed over this stirring period. The mixture was removed from heat and allowed to cool to room temperature. Once cooled, the reaction was poured into a separatory funnel with 250 mL of brine. Extraction was completed via washing with ethyl ether (3 x 150

mL). Organic layers were combined, dried over Na_2SO_4, filtered, and the solvent was removed under reduced pressure. This yielded a viscous purple oil. The crude oil was purified by gradient elution column chromatography on silica gel (0-20 % ethyl acetate in hexanes), resulting in 4.12 g (81% yield) of a clear, colorless oil, which solidified upon standing. NMR (^{1}H, ^{13}C, ^{31}P) spectra matched that of the **3a** synthesized from Approach A.

*Synthesis of m-hydroxyphenyldiphenylphosphine **3b***. In a two-necked, 100-mL Schlenck flask equipped with a magnetic stir bar *m*-iodophenol (4.00 g, 0.0182 mol), potassium acetate (2.68 g, 0.0273 mol), palladium acetate (40 mg), and anhydrous DMAc (20 mL) were added. The flask was then purged with argon and diphenylphosphine (4.06 g, 0.0218 mol) was added dropwise via a double-ended needle into the reactor over a 15-minute period. During the addition, the mixture turned a light purple color, then to a yellow color after completion. The vessel was purged once more with argon, then warmed to 130°C, the temperature held, and the reaction mixture stirred for 3 hours. A dark purple color developed. After cooling to room temperature, the reaction was poured into a separatory funnel with 300 mL of brine. The contents were extracted with ethyl ether (3 x 200 mL), the organic layers were combined, dried over Na_2SO_4, filtered, and the solvent was removed with reduced pressure to give a viscous purple oil. The crude oil was purified by gradient elution column chromatography on silica gel (0-15% ethyl acetate in hexanes), resulting in 4.37 g (86% yield) of a clear, colorless oil, which solidified upon standing. NMR (^{1}H, ^{13}C, ^{31}P) spectra matched that of the **3b** synthesized from Approach A.

3.5 Preparation of *p*-bis(hydroxyphenyl)diphenylphosphonium monomeric salts

*Synthesis of p-bis(hydroxyphenyl)diphenylphosphonium bromide **4a***. To a 100-mL, PTFE screw-capped pressure vessel, *p*-hydroxyphenyldiphenyl phosphine **3a** (3.40 g, 0.0122 mol), *p*-bromophenol (2.21 g, 0.0128 mol), nickel (II) bromide (84 mg) and freshly distilled ethylene glycol (8.5 mL) were added. The mixture was heated to 180°C and stirred for 4 hours. The reaction was then cooled to room temperature and poured onto 100 mL of DI water. The resulting precipitate was isolated and then washed with DI water (2 x 25 mL) and dichloromethane (3 x 25 mL). The white solid was then dried in a vacuum oven, affording 4.32 g (78% yield). ^{1}H NMR (DMSO-d_6): δ 10.5 (bs, 2 H), 7.89 (dt, 2 H, J = 9.4, 2 Hz), 7.73-7.80 (m, 4 H), 7.62-7.69 (m, 4 H), 7.48 (d, 2 H, J = 8.8 Hz), 7.45 (d, 2 H, J = 8.8 Hz), 7.11 (d, 2 H, J = 8.8 Hz), 7.10 (d, 2 H, J = 8.8 Hz). ^{13}C NMR (DMSO-d_6): δ 163.45, 163.43, 136.70, 136.58, 134.82, 134.80, 134.22, 134.11, 130.33, 130.11, 120.09, 119.19, 117.57, 117.43, 106.22, 105.25. ^{31}P NMR (DMSO-d_6): δ 21.79. Anal. Calcd. For $C_{24}H_{20}BrO_2P$: C 63.87, H 4.47. Found: C 64.45, H 4.28.

*Synthesis of m-bis(hydroxyphenyl)diphenylphosphonium bromide **4b***. In a 100-mL, PTFE screw-capped pressure vessel equipped with a magnetic stir bar, *m*-hydroxyphenyldiphenylphosphine **3b** (4.37 g, 0.0157 mol), *m*-bromophenol (2.86 g, 0.0165 mol), nickel (II) bromide (0.11 g), and anhydrous ethylene glycol (20 mL) were added. The contents were flushed with argon, heated to 180°C and held stirring at that temperature for 24 hours. The contents were then cooled to room temperature and poured into a separatory funnel with 150 mL dichloromethane. The reaction was washed with DI water (3 x 75 mL) and the solvent was removed under reduced pressure. This resulted in an off-white solid (5.19 g, 73% yield). ^{1}H NMR (DMSO-d_6): δ 10.5 (bs, 2 H), 6.96 (dt, 2

H, *J* = 14.4, 2 Hz), 7.11 (dd, 2 H, *J* = 8.4, 12.2 Hz), 7.28 (d, 2 H, *J* = 8.4 Hz), 7.61 (m, 2 H), 7.68-7.75 (m, 4 H), 7.76-7.84 (m, 4 H), 7.94 (t, 2 H, *J* = 6.8, 2 Hz). ^{13}C NMR (DMSO-d_6): δ 158.7, 158.5, 135.3, 135.2, 134.5, 134.4, 132.0, 131.8, 130.5, 130.4, 125.0, 124.9, 122.4, 122.4, 120.5, 120.4, 119.0, 118.2, 118.1, 117.4. ^{31}P NMR (DMSO-d_6): δ 24.58. Anal. Calcd. For $C_{24}H_{20}BrO_2P$: C 63.87, H 4.47. Found: C 63.95, H 4.31.

Synthesis of p-bis(hydroxyphenyl)diphenylphosphonium bis(trifluoromethylsulfonyl)imide ***5a***. In a 250-mL round-bottomed flask, *p*-bis(hydroxyphenyl)diphenylphosphonium bromide **4a** (4.60 g, 10.2 mmol) was dissolved in 80 mL of a 20:1 CH_2Cl_2:CH_3OH solution. To this stirred solution, a solution of lithium bis(trifluoromethylsulfonylimide) (3.07 g, 10.7 mmol) in DI water (20 mL) was added. The mixture was stirred at room temperature for 48 hours. The organic phase was then separated in a separatory funnel, washed with DI water (3 x 30 mL), and the solvent was removed under reduced pressure to afford a white solid (6.43 g, 97% yield). A negative, qualitative silver nitrate test (acetone/DI water) was observed. ^{1}H NMR (DMSO-d_6): δ 11.05 (bs, 2 H), 7.88 (dt, 2 H, *J* = 9.2, 2 Hz), 7.73-7.80 (m, 4 H), 7.65-7.71 (m, 4 H), 7.45-7.51 (m, 4 H), 7.14 (d, 2 H, *J* = 8.5 Hz), 7.10 (d, 2 H, *J* = 8.5 Hz). ^{13}C NMR (DMSO-d_6): δ 163.54, 163.51, 136.71, 136.58, 134.82, 134.81, 130.32, 130.19, 120.12, 119.4 (q, *J* = 320 Hz, -CF_3), 119.2, 117.6, 117.4, 106.2, 105.2. ^{31}P NMR (DMSO-d_6): δ 24.58. Anal. Calcd. For $C_{26}H_{20}F_6NO_6PS_2$: C 47.93, H 3.09, N 2.15, S 9.85. Found: C 48.15, H 2.88, N 1.99, S 9.77.

Synthesis of m-bis(hydroxyphenyl)diphenylphosphonium bis(trifluoromethylsulfonyl)imide ***5b***. *m*-Bis(hydroxyphenyl)diphenylphosphonium bromide **4b** (3.65 g, 8.09 mmol) was dissolved in 80 mL of dichloromethane and a

solution of lithium bis(trifluoromethylsulfonyl)imide (2.44 g, 8.49 mmol) in DI water (50 mL) was added. The resulting mixture was stirred vigorously for 24 hours. The organic phase was then removed via separatory funnel, washed with DI water (3 x 40 mL), and the solvent was removed under reduced pressure to yield an off-white solid (5.15 g, 98% yield). A negative, qualitative silver nitrate test (acetone/DI water) was observed. ^{1}H NMR (DMSO-d_6): δ 10.5 (bs, 2 H), 6.95 (dt, 2 H, J = 14.8, 1.8 Hz), 7.12 (dd, 2 H, J = 8.1, 12.3 Hz), 7.28 (d, 2 H, J = 8.4 Hz), 7.62 (m, 2 H), 7.69-7.75 (m, 4 H), 7.77-7.84 (m, 4 H), 7.95 (t, 2 H, J = 6.8, 1.6 Hz). ^{13}C NMR (DMSO-d_6): δ 158.7, 158.6, 135.3, 135.3, 134.6, 134.5, 131.9, 130.5, 130.4, 125.0, 124.9, 122.5, 122.4, 120.5, 120.4, 119.5 (q, J = 320 Hz, -CF_3), 119.0, 118.3, 118.1, 117.4. ^{31}P NMR (DMSO-d_6): δ 24.58. Anal. Calcd. For $C_{26}H_{20}F_6NO_6PS_2$: C 47.93, H 3.09, N 2.15, S 9.85. Found: C 47.77, H 3.11, N 2.01, S 9.62.

3.6 Polymerization

In a 50-mL, two-necked round-bottomed flask with magnetic stir bar the dihydroxy-terminated phosphonium bis(trifluoromethylsulfonyl)imide monomer (2.00 g, 3.07 mmol), either 4,4′-difluorobenzophenone or 4,4′-difluorosulfone (3.07 mmol), potassium carbonate (1.61 g, 11.6 mmol) and 15 mL of a 4:1 solution of DMAc:toluene were added. A short path distillation head was attached to the flask along with an argon inlet. The mixture was flushed with dry argon and heated to 145°C resulting in a toluene:water azeotrope beginning to distill over. The temperature was gradually increased (5°C/hr) until a maximum temperature of 165°C was achieved. The distillation head was then removed, the reaction mixture was purged again with dry argon, and the flask was

capped. The mixture was allowed to continue stirring at 165°C for an additional 16 hours. The reaction was cooled to room temperature and poured onto 100 mL of DI water with stirring. A tan precipitate formed as a result. The solid was then isolated, washed while stirring with DI water (2 x 100 mL), then dried in a vacuum oven for 48 hours (60°C, < 0.01 mm Hg). The process resulted in a series of light tan powders. ^{31}P NMR spectra of the corresponding ionene polymers can be found in the Appendix.

3.7 Polymer Thermal Characterization

Differential scanning calorimetry (DSC), at a heating rate of 2°C/min on 4-8 mg samples, was utilized to determine any thermal transitions of the polymers. Glass transition temperatures (T_g) were determined by the inflection point of the curve observed from the second heating cycle. Melting transitions (T_m) were determined at the maximum of the endothermic peak observed from the second heating cycle. DSC *Tg* experiments were performed in duplicate with an error of ±2.0°C. A TA instruments Q550 TGA was used to study $T_{d5\%}$ values under a constant nitrogen flow at a heating rate of 10°C/min.

3.8 Chemical Stability Studies

A procedure by Smith et al. was followed to perform alkaline stability testing. 20 mg of an ionene was dissolved in 2 mL of chloroform in a 25 mL round-bottomed flask.[28] The chloroform was allowed to slowly evaporate under ambient conditions, forming a thin film of the ionene around the bottom of the flask. Next, 4 mL of either 1M or 6M NaOH solution was added and the system was allowed to set for a predetermined amount of time, either at room temperature or at 65°C. Chloroform was then added to the round-

bottomed flask, mixed for 30-min with a stir bar, the organic phase was isolated, and the solvent was removed under reduced pressure. The resulting ionene was then analyzed via ^{1}H and ^{31}P NMR spectroscopy for any changes in chemical shift values as well as relative integrations.

3.9 Conductivity

The ionene to be tested (0.25 g) was dissolved in acetonitrile (0.25 g) with gentle heating. The resulting solution was then poured into a circular PTFE mold (d = 30 mm), attached to a glass microscope slide with binder clips. The solvent was allowed to slowly evaporate (24 hours at room temperature, 24 hours in 60°C oven, and then 48 hours in 60°C vacuum oven), resulting in a series of light tan films with a thickness on the order of 0.30 ± 0.02 mm as shown below in Figure 3.1.

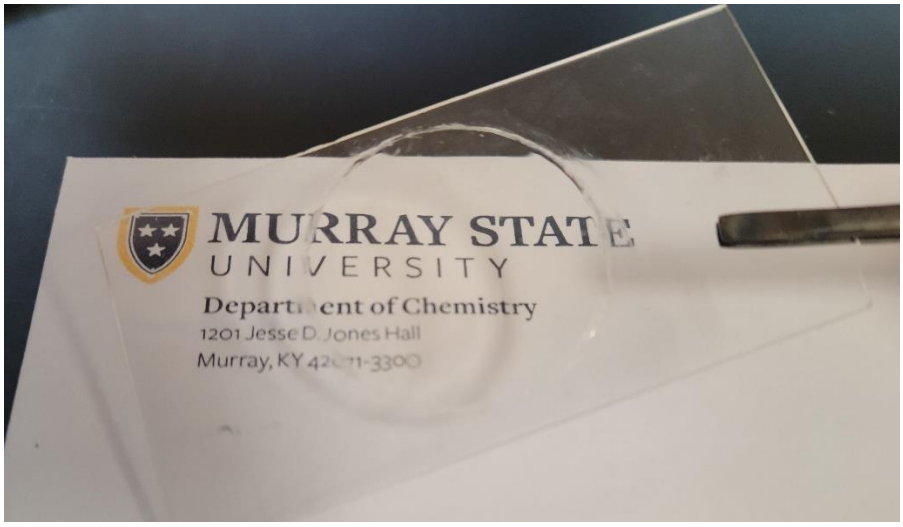

Figure 3.1: Photo of an ionene film prepared (from acetonitrile) of *p*-PHOS-CO-NTf_2.

The PTFE circular mold was then removed and replaced with a circular PTFE film with the same thickness as the polymer film. This was then inverted onto a second glass slide where two parallel copper strips were attached, 1.3 mm apart. The apparatus, held together by binder clips, (shown in Figure 3.2) was placed into an Espec BTL-433 benchtop temperature/humidity oven (30 % RH) for 1 hour at a temperature 40°C higher than the *Tg* of the polymer in order to ensure good contact between the film and the electrodes.

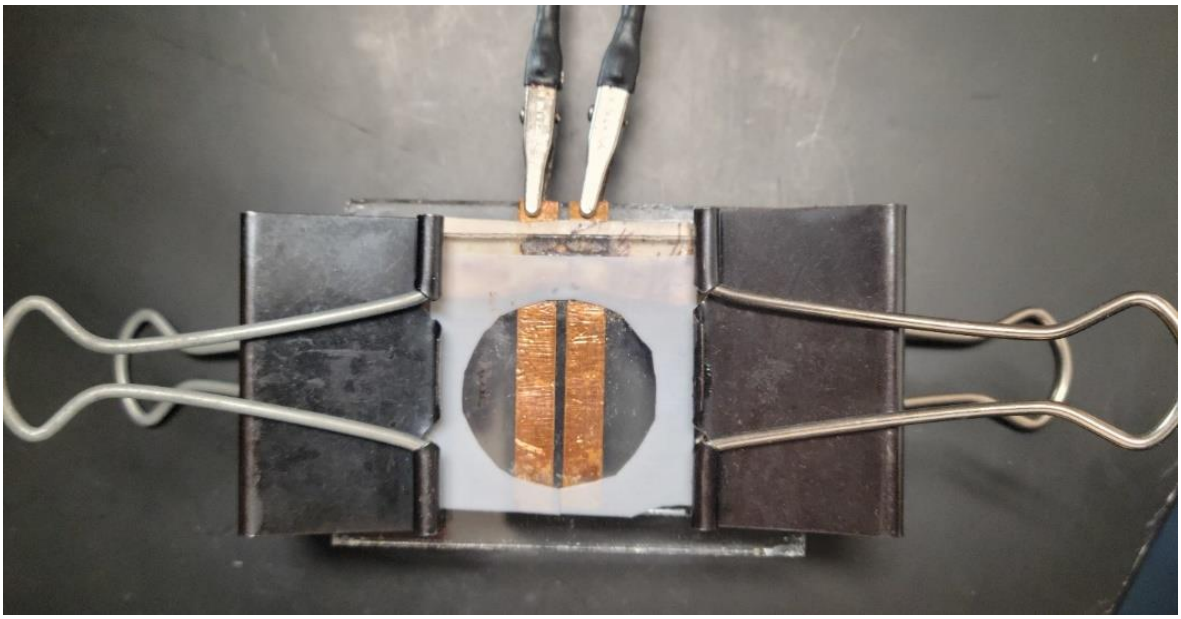

Figure 3.2: Ionene film from Figure 3.1 loaded into conductivity apparatus.

The oven was then cooled to 30°C (30 % RH) and held for 24-hr prior to the start of the experiment. A Metrohm Autolab 302N potentiostat was used to perform the electrochemical impedance spectroscopy (EIS).[29] This device did not allow for humidity control at temperatures above 100°C; however, the humidity remained between 20-30% at the elevated temperatures. The alternating voltage setpoint was ±0.01 V and the

frequency was varied from 0.1 Hz to 1.0 MHz. After each measurement, the oven temperature was increased 10 °C and the sample was allowed to equilibrate for approximately 45 minutes to ensure a constant resistivity (< 1% relative standard deviation) was observed. The experiment was stopped once the sample was observed to visibly flow around the PTFE spacer. Open and closed "blank" calibration experiments were completed on the system to correct for any impendence values for residual or strong impedances in the measurement of all cables.

3.10 Polymer Molecular Weight Determination

20 mg of ionene sample and 3 mg of triphenylphosphine were dissolved in 0.75 mL of DMSO-d_6. This solution was then transferred via pipette to an NMR tube and a ^{31}P NMR experiment was conducted. A relaxation delay of 10 seconds was used over the 1000 scans collected. The triphenylphosphine signal was set as the standard to -4.7 ppm. Molecular weights were determined by assigning the ^{31}P NMR signal from the end group an integration value of one. Since polymerizations were done stoichiometrically, the single phosphorus represented by the end group at ~26.7 ppm plus the integration at ~27.3 ppm, the ^{31}P signal assigned to the phosphorus atoms the repeating unit, indicated the average number of repeating units per polymer chain. The molecular weight was then determined by taking this value and multiplying by the molecular weight of the repeating unit. ^{31}P NMR spectroscopy experiments were completed in duplicate for each sample and the signals were integrated three times, resulting in values which were $\pm$ 2% of those reported in this project.

References

1. Fraser, K. J.; MacFarland D. R. Phosphonium-Based Ionic Liquids: An Overview. *Aust. J. Chem*. **2009**, 63, 309-321.
2. Green, M. D.; Schreiner, C.; Long, T. E. Thermal, Rheological, and Ion-Transport Properties of Phosphonium-Based Ionic Liquids. *J. Phys. Chem. A.* **2011**, 115, 13829-13835.
3. Plechkova, N. V.; Seddon, K. R. Applications of Ionic Liquids in the Chemical Industry. *Chem. Soc. Rev*. **2008**, 37, 123-150.
4. Rogers, R. D.; Seddon, K. R. Ionic Liquids: Solvents of the Future? *Science* **2003**, 302, 792-793.
5. Visser, A. E.; Swatloski, R. P.; Rwichert, W. M.; Mayton, R.; Sheff, S.; Wierzbicki, A.; Davis, J. H.; Rogers, R. D. Task-Specific Ionic Liquids Incorporating Novel Cations for the Coordination and Extraction of Hg^{2+} and Cd^{2+}: Synthesis, Characterization, and Extraction Studies. *Environ. Sci. Technol.* **2002**, 36, 2523-2529
6. Hemp, S. T.; Zhang, M; Allen, M. H.; Cheng, S.; Moore, R. B.; Long, T. E. Comparing Ammonium and Phosphonium Polymerized Ionic Liquids: Thermal Analysis, Conductivity, and Morphology. *Macromol. Chem. Phys.* **2013**, 214, 2099-2107.

7. Taghavikish, M.; Subianto, S.; Dutta, N. K.; Choudhury, N. R. Facile Fabrication of Polymerizable Ionic Liquid Based-Gel Beads via Thiol-ene Chemistry. *ACS Appl. Mater. Interfaces* **2015**, 7, 17298-17306.
8. Rhoades, T. C.; Wistrom, J. C.; Johnson, R. D.; Miller, K. M. Thermal, Mechanical, and Conductive Properties of Imidizolium-containing Thiol-ene Poly(Ionic Liquid) Networks. *Polymer* **2016**, 100, 1-9.
9. Hemp, S. T.; Zhang, M; Allen, Tamami, M.; Long, T. E. Phosphonium Ionenes from Well-Defined Step-Growth Polymerization: Thermal and Melt Rheological Properties. *Polym. Chem*. **2013**, 4, 3582-3590.
10. Kammakakam, I.; O'Harra, K. E.; Bara, J. E.; Jackson, E. M. Design and Synthesis of Imidazolium-Mediated Tröger's Base-Containing Ionene Polymers for Advanced CO_2 Separation Membranes. *ACS Omega* **2019**, 4, 3439−3448.
11. Liu, Y.; Sheri, M.; Cole, M. D.; Yu, D. M.; Emrick, T.; Russell, T. P. Transforming Ionene Polymers into Efficient Cathode Interlayers with Pendent Fullerenes. *Angew. Chem. Int. Ed.* **2019**, 58, 17, 5677-5681.
12. Frackowiak, E; Lota, G; Pernak, J. Room-Temperature Phosphonium Ionic Liquids for Supercapacitor Application. *Appl. Phys. Lett.* **2005**, 86, 164104.
13. Chen, M; White, B. T.; Kasprzak, C. R.; Long, T. E. Advances in Phosphonium-based Ionic Liquids and Poly(Ionic Liquid)s as Conductive Materials. *European Polymer Journal* **2018**, 108, 28-37.
14. Hemp, S. T.; Allen Jr, M. H.; Green, M. D.; Long, T. E. Phosphonium-Containing Polyelectrolytes for Nonviral Gene Delivery. *Biomacromolecules* **2012**, 13, 231−238.

15. Hemp, S. T.; Smith, A. E.; Bryson, J. M.; Allen, M. H.; Long, T. E. Phosphonium-Containing Diblock Copolymers for Enhanced Colloidal Stability and Efficient Nucleic Acid Delivery. *Biomacromolecules* **2012,** *13*, 2439-2445.
16. Sims, S. M.; Bontrager, N. C.; Whittaker, R. E.; Miller, K. M.; Correlating Structure with Ionic Conductivity in Bis(Phosphonium)-Containing [NTf_2] Thiol–ene Networks. *Polym. Int.* **2019**, 68, 1557–1565.
17. Rabideau, B. D.; Soltani, M.; Parker, R. A.; Siu, B.; Salter, E. A.; Wierzbicki, A.; West, K. N.; Davis Jr, J. H. Tuning the Melting Point of Selected Ionic Liquids Through Adjustment of the Cation's Dipole Moment. *Phys. Chem. Chem. Phys*. **2020**, 22, 12301-12311.
18. Cassity, C. A.; Siu, B.; Soltani, M.; McGeehee, J. L.; Strickland, K. J.; Vo, M.; Salter, E. A.; Stenson, A. C.; Wierzbicki, A.; West, K. N.; Rabideau, B. D.; Davis Jr, J. H. The Effect of Structural Modifications on the Thermal Stability, Melting Points, and Ion Interactions for a Series of Tetraaryl-Phosphonium-Based Mesothermal Ionic Liquids. *Phys. Chem. Chem. Phys*. **2017**, 19, 31560-31571.
19. Wan, W.; Yang, X.; Smith, R. C. Convenient Route to Tetraarylphosphonium Polyelectrolytes *via* Metal-Catalyzed P-C Coupling Polymerization of Aryl Dihalides and Diphenylphosphine. *Chem. Commun.* **2017**, 53, 252-254.
20. Cassity, C. G.; Mirjafari, A.; Mobarrez, N.; Strickland, K. J.; O'Briena, R. A.; Davis Jr, J. H. Ionic Liquids of Superior Thermal Stability. *Chem. Commun.* **2013**, 49, 7590-7592.
21. Bedford, M. S.; Yang, X.; Jolly, K. M.; Binnicker, R. L.; Cramer, S. B.; Keen, C. E.; Mairena, C. Jwan.; Patel, A. P.; Rivenbark, M. T.; Galbura, Y.; Luzinov, I.;

Smith, R. C. Tetraarylphosphonium Polyelectrolyte Chromophores: Synthesis Stability, Photophysics, Film Morphology and Critical Surface Energy. *Polym. Chem.* **2015**, 6, 900-908.

22. Yang, X.; Smith, R. C. Phosphonium-Based Polyelectrolyte Networks with High Thermal Stability, High Alkaline Stability, and High Surface Areas. *J. Polym. Sci., Part A: Polym. Chem.* **2019**, 57, 598-604.
23. Liu, T.; Wang, Y.; Su, Y.; Yu, H.; Zhao, N.; Yang, Y.; Jiang, Z. Preparation and Properties of Film Materials of Poly(aryl etherketone)–Based Phthalonitrile Resins. *Polym. Eng. Sci.* **2015**, 2313-2321.
24. Machodi, M. J.; Daramola, M. O. Synthesis and Performance Evaluation of PES/Chitosan Membranes Coated with Polyamide for Acid Mine Drainage Treatment. *Sci. Rep*. **2019**, 9, 17657.
25. García-Márquez, A.; Frontera, A.; Roisnel, T.; Gramage-Doria, R. Ultrashort $H^{\delta+}$-$H^{\delta-}$ Intermolecular Distance in a Supramolecular System in the Solid State. *Chem. Commun*. **2021**, 57, 7112-7115.
26. Li, L.; Lin, C. X.; Wang, X. Q.; Yang, Q.; Zhang, Q. G.; Zhu, A. M.; Liu, Q. L. Highly Conductive Anion Exchange Membranes with Long Flexible Multication Spacer. *J. Membr. Sci*. **2018**, 553, 209-217.
27. Banerjee, P.; Pal, P.; Ghosh, A.; Mandal, T. K. Ion Transport and Relaxation in Phosphonium Poly(ionic liquid) Homo- and Co-Polymers. *J. Polym. Sci.* **2021**, 59, 1556-1570.
28. Wan, W.; Yang, X.; Smith, R. C.; Convenient Synthetic Route to Tetraarylphosphonium Polyelectrolytes Via Palladium-Catalyzed P–C Coupling

of Aryl Triflates and Diphenylphosphine. *J. Polym. Sci. A, Polym. Chem.* **2017**, 55, 1984-1990.

29. Tracy, C. A.; Adler, A. M.; Nguyen, A.; Johnson, R. D.; Miller, K. M. Covalently Crosslinked 1,2,3-Triazolium-Containing Polyester Networks: Thermal, Mechanical, and Conductive Properties. *ACS Omega* **2018**, 3, 13442-13453.
30. Scammells, P. J.; Scott, J. L.; Singer, R. D. Ionic Liquids: The Neglected Issues. *Aust. J. Chem*. **2005**, 58, 155-169.
31. Marcoux, D.; Charette, A. B. Palladium-Catalyzed Synthesis of Functionalized Tetraarylphosphonium Salts. *J. Org. Chem*. **2008**, 73, 590-593.
32. Hansch, C.; Leo, A.; Taft, R. W. A Survey of Hammett Substituent Constants and Resonance and Field Parameters. *Chem. Rev*. **1991**, 91, 165-195.
33. Chen, H.; Choi, J.; Salas-de la Cruz, D.; Winey, K. I.; Elabd, Y. A. Polymerized Ionic Liquids: The Effect of Random Copolymer Composition on Ion Conduction. *Macromolecules* **2009**, 42, 4809.
34. Fragidakis, D.; Dou, S.; Colby, R. H.; Runt, J. Molecular Mobility and Li^+ Conduction in Polyester Copolymer Ionomers Based on Poly(ethylene oxide). *J. Chem. Phys*. **2009**, 130, 064907.
35. Bara, J. E.; O'Harra, K. E. Recent Advances in the Design of I0onenes: Towards Convergence with High-Performance Polymers. *Macromol. Chem. Phys*. **2019**, 220, 1900078.

Appendix

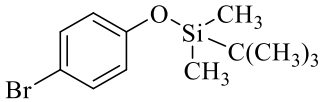

1a

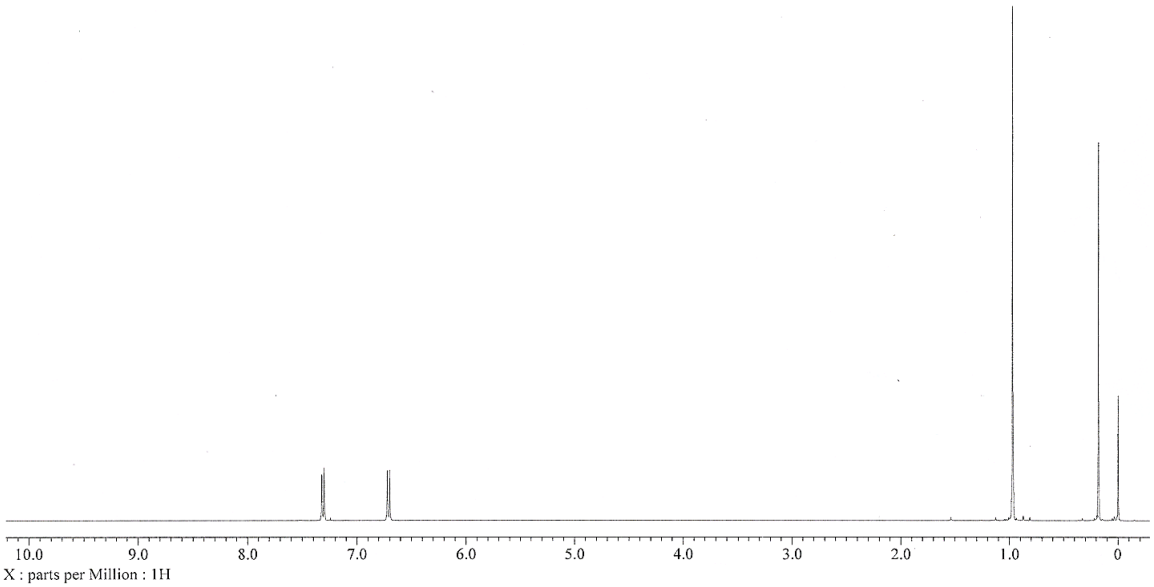

Figure A1: ^{1}H NMR spectrum of TBDMS-protected *p*-bromophenol **1a** ($CDCl_3$ + TMS)

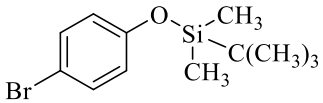

1a

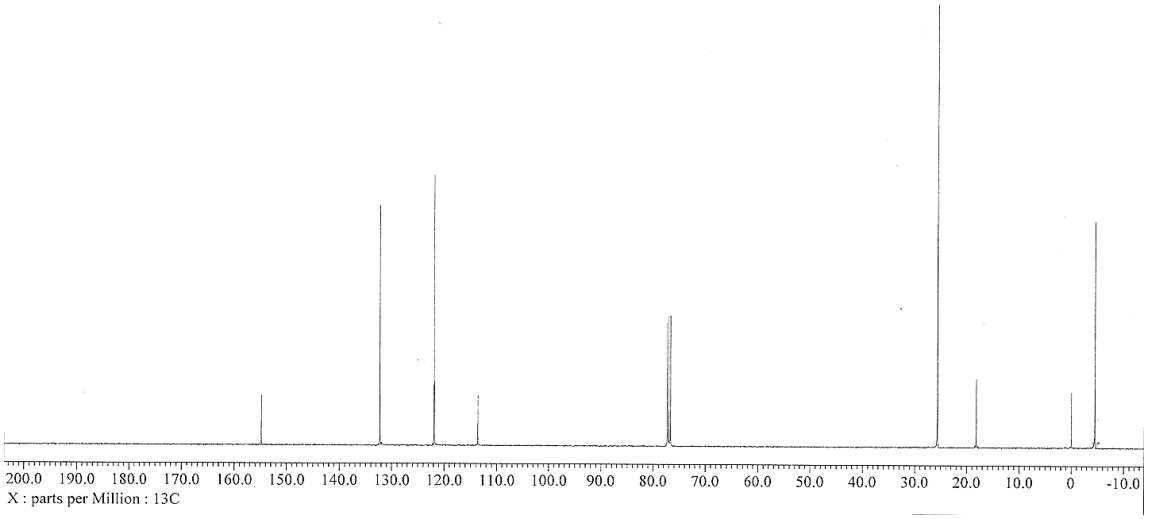

Figure A2: ^{13}C NMR spectrum of TBDMS-protected *p*-bromophenol **1a** ($CDCl_3$ + TMS)

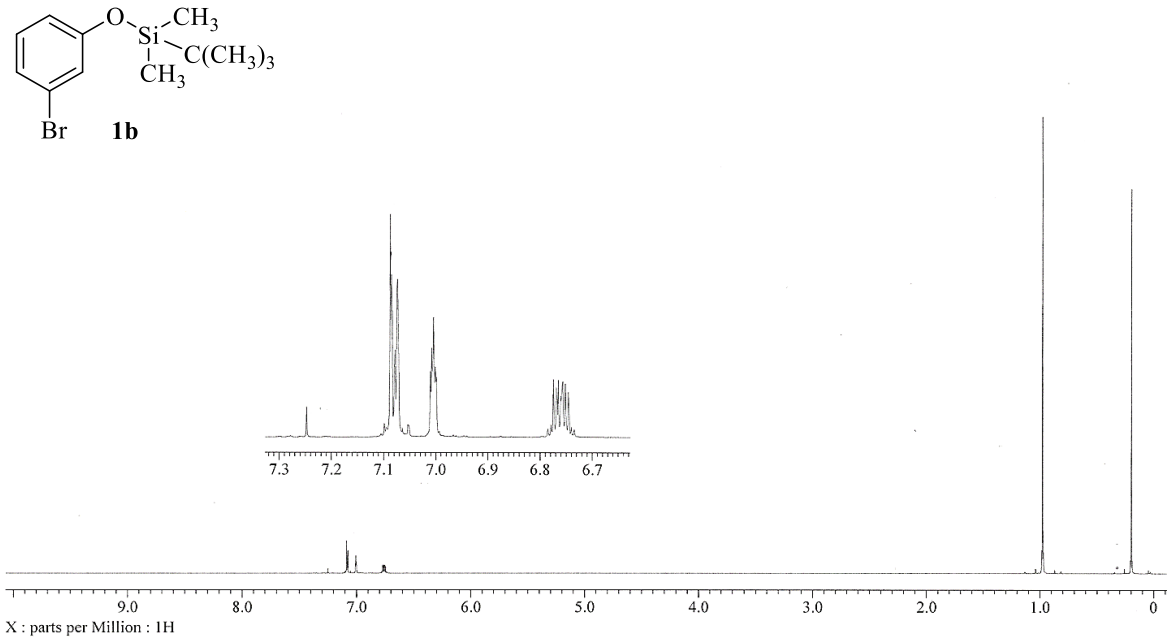

Figure A3: ^{1}H NMR spectrum of TBDMS-protected *m*-bromophenol **1b** ($CDCl_3$)

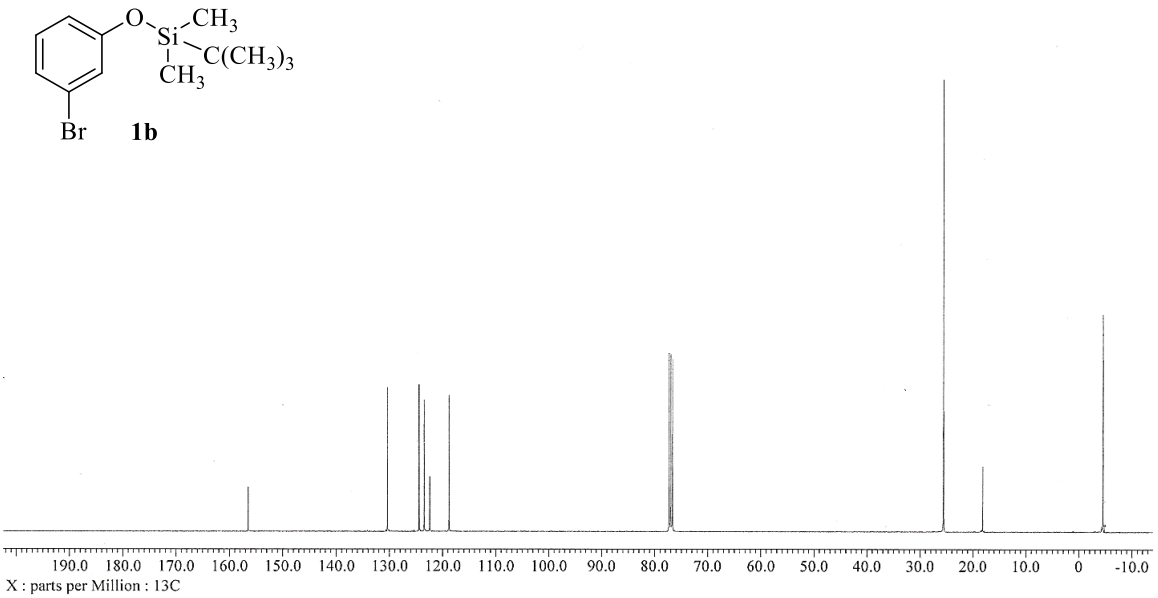

Figure A4: ^{13}C NMR spectrum of TBDMS-protected *m*-bromophenol **1b** ($CDCl_3$)

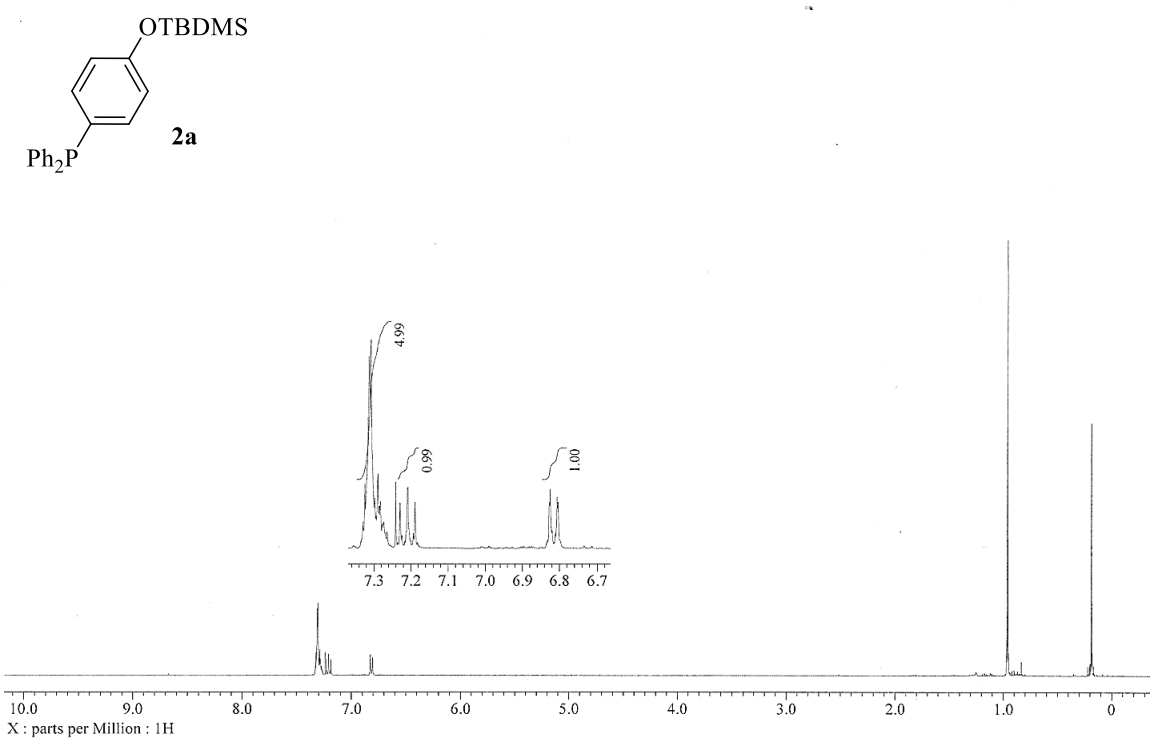

Figure A5: ^{1}H NMR spectrum of TBDMS-protected *p*-hydroxyphenyldiphenylphosphine **2a** ($CDCl_3$)

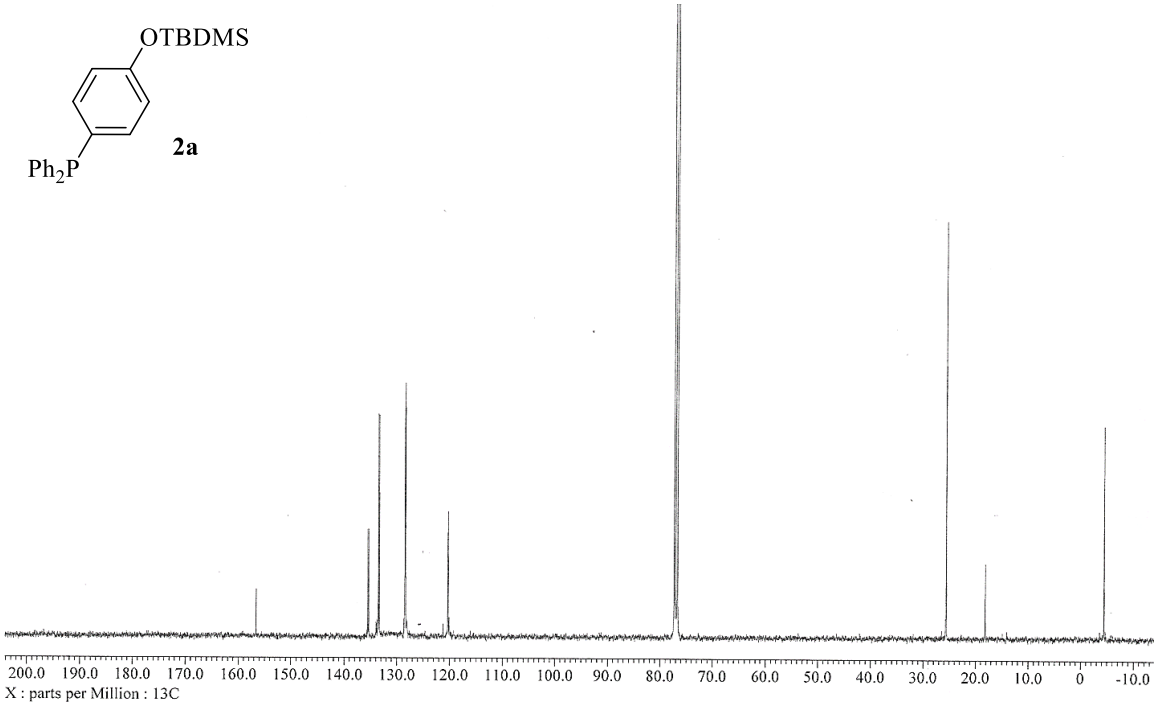

Figure A6: ^{13}C NMR spectrum of TBDMS-protected *p*-hydroxyphenyldiphenylphosphine **2a** ($CDCl_3$)

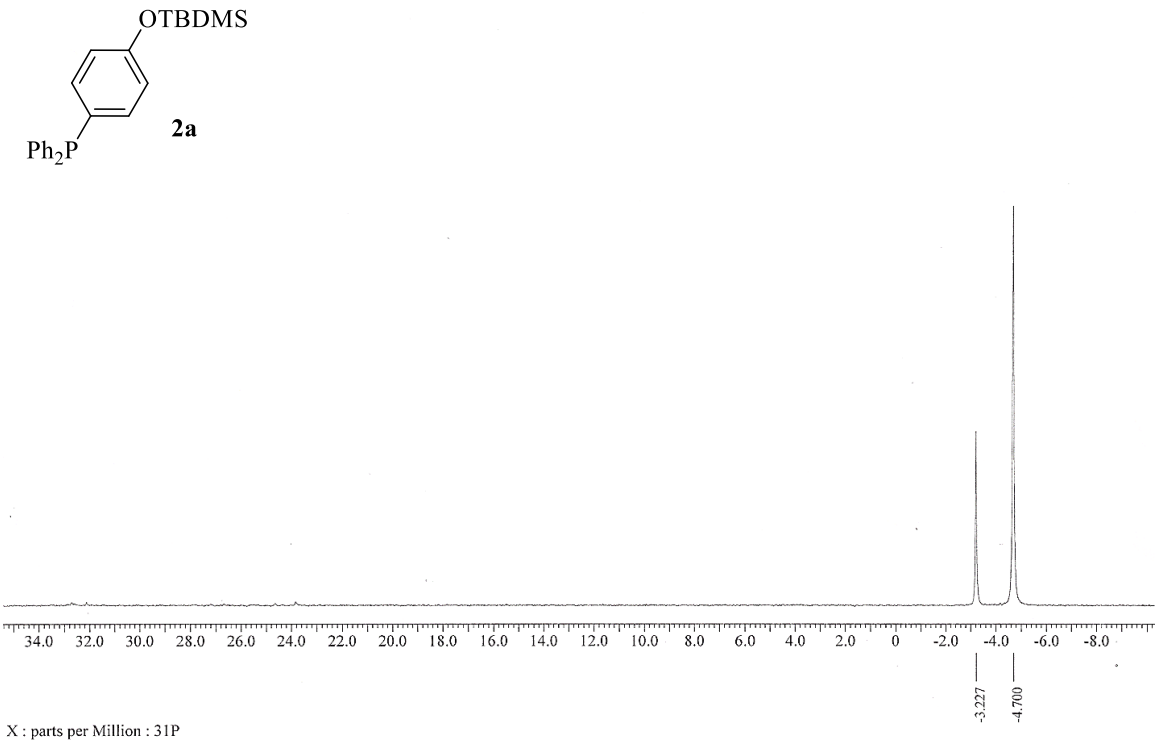

Figure A7: ^{31}P NMR spectrum of TBDMS-protected *p*-hydroxyphenyldiphenylphosphine **2a** ($CDCl_3$ +PPh_3)

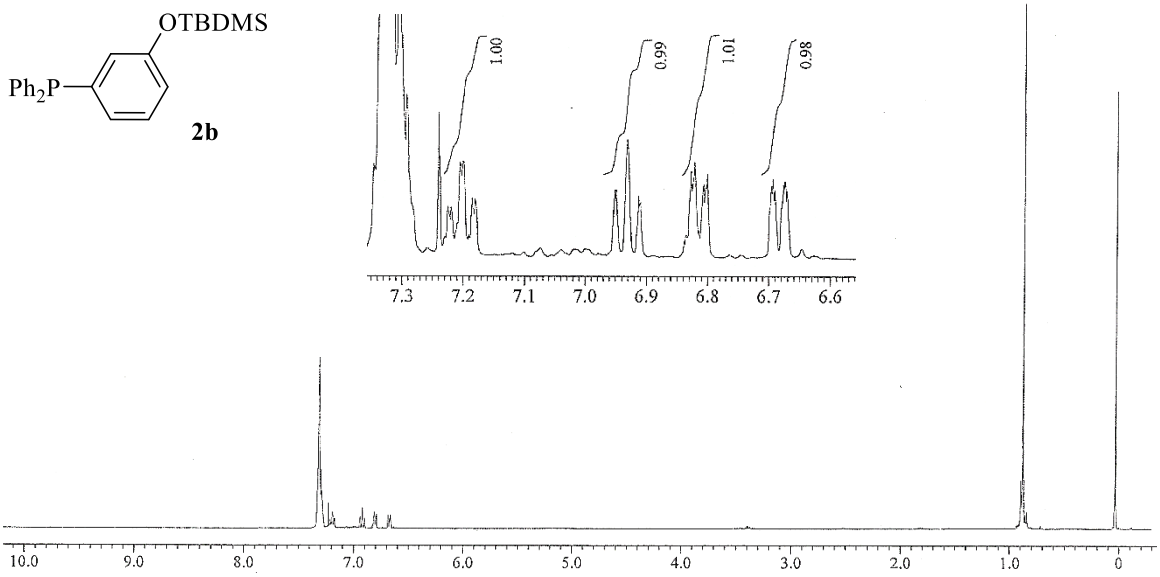

Figure A8: ^{1}H NMR spectrum of TBDMS-protected *m*-hydroxyphenyldiphenylphosphine **2b** ($CDCl_3$)

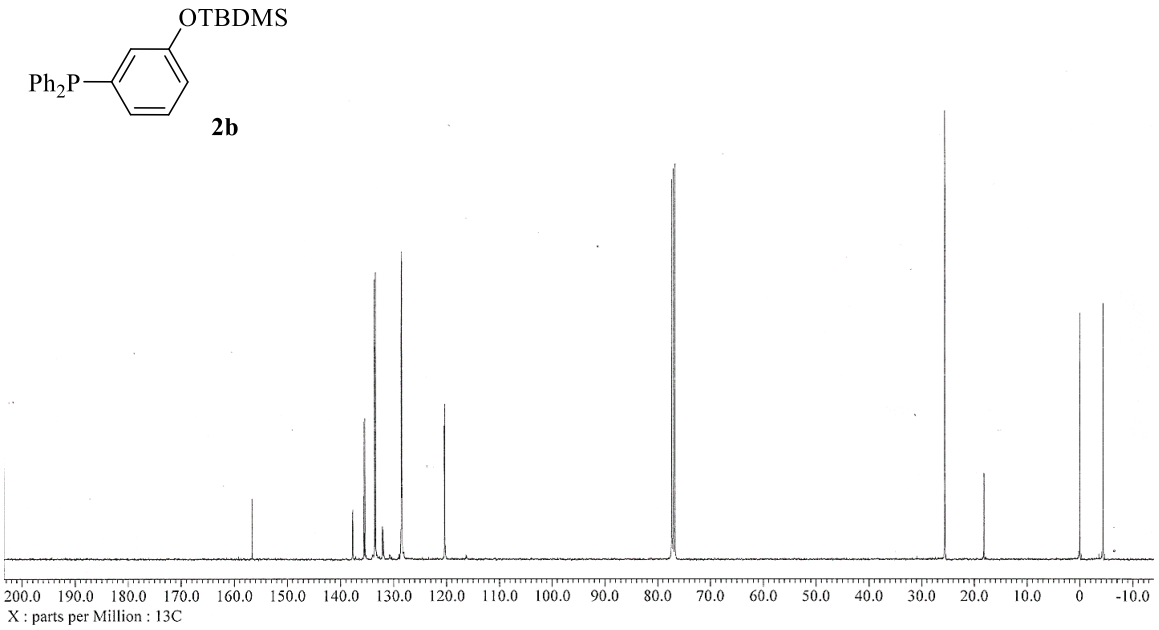

Figure A9: ^{13}C NMR spectrum of TBDMS-protected *m*-hydroxyphenyldiphenylphosphine **2b** ($CDCl_3$)

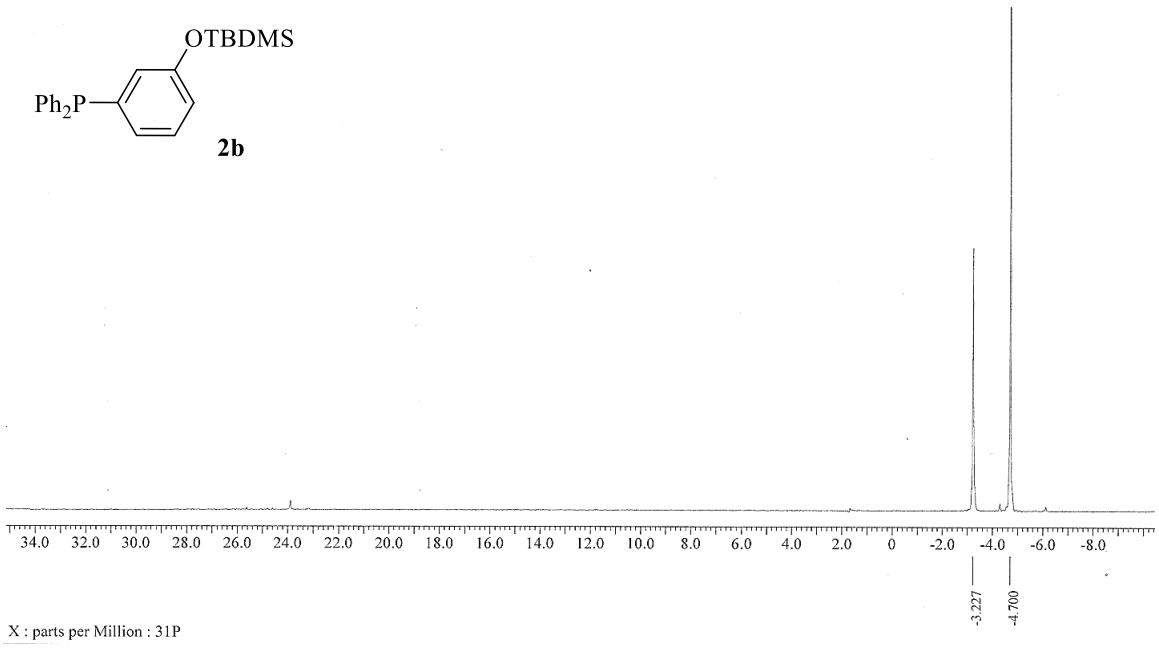

Figure A10: ^{31}P NMR spectrum of TBDMS-protected *m*-hydroxyphenyldiphenylphosphine **2b** ($CDCl_3$ +PPh_3)

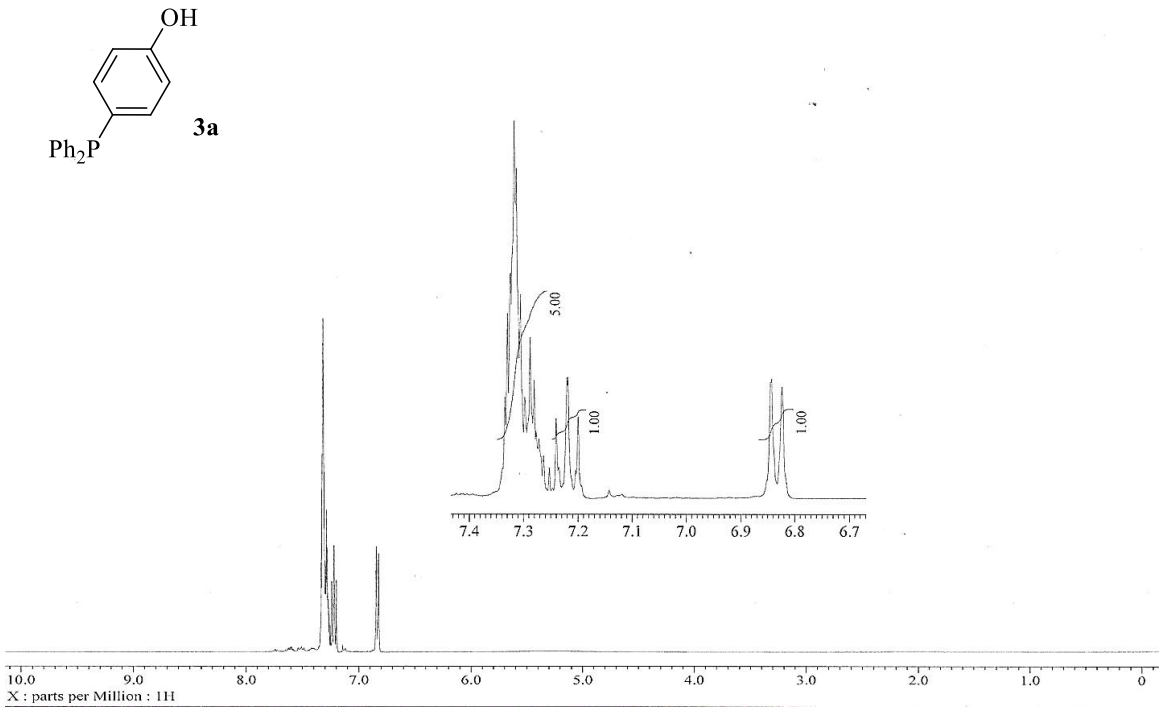

Figure A11: ^{1}H NMR spectrum of *p*-hydroxyphenyldiphenylphosphine **3a** ($CDCl_3$)

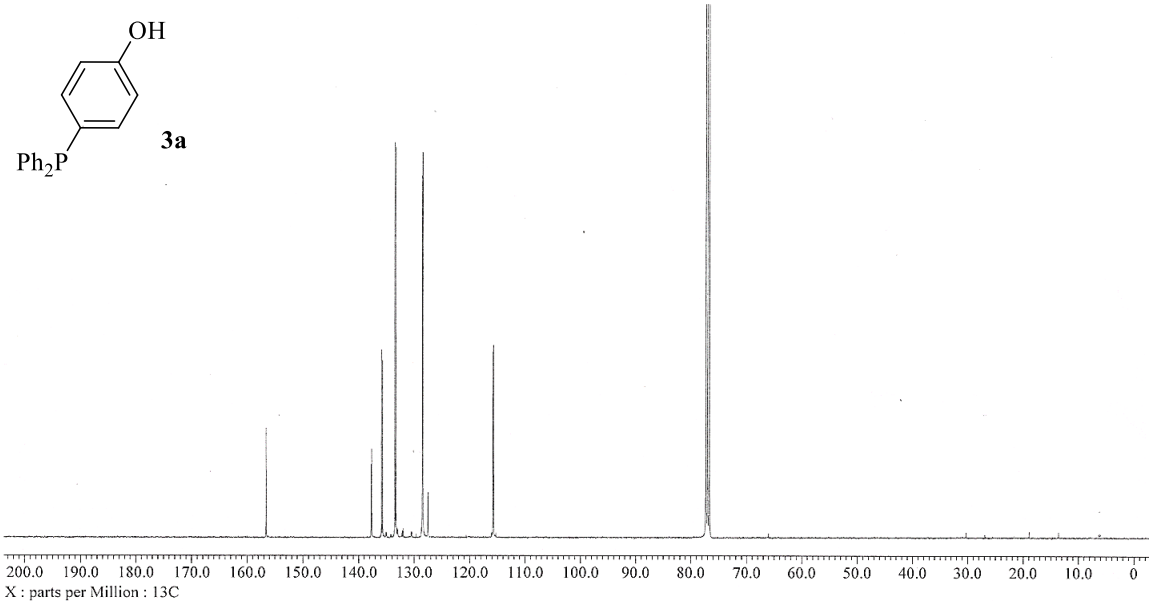

Figure A12: ^{13}C NMR spectrum of *p*-hydroxyphenyldiphenylphosphine **3a** ($CDCl_3$)

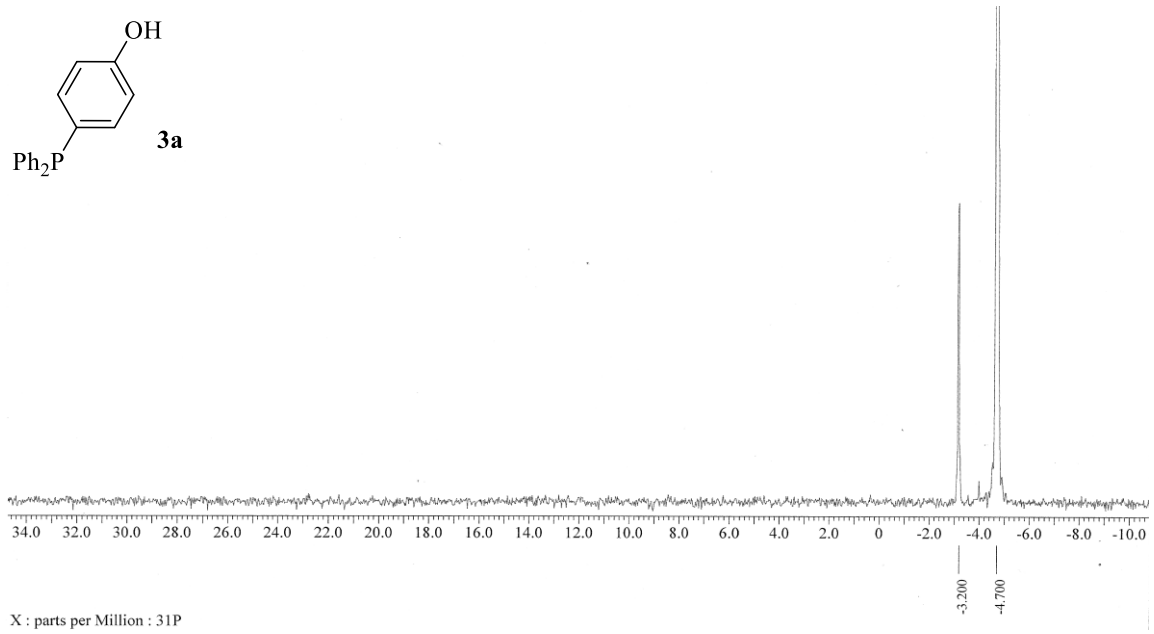

Figure A13: ^{31}P NMR spectrum of *p*-hydroxyphenyldiphenylphosphine **3a** ($CDCl_3$ + PPh_3)

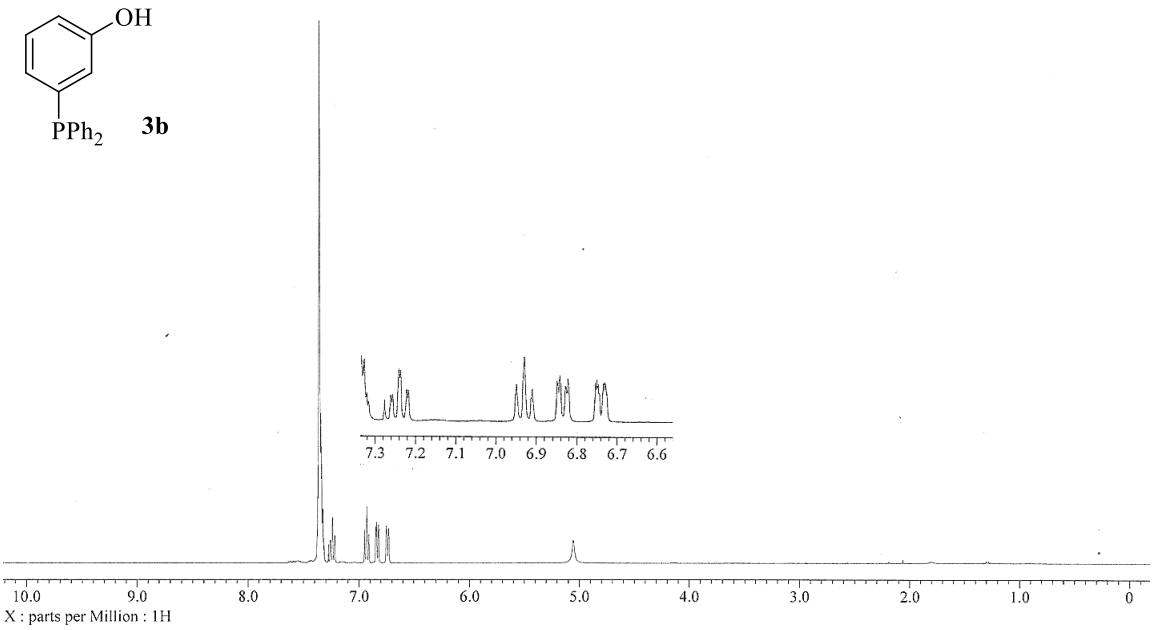

Figure A14: ^{1}H NMR spectrum of *m*-hydroxyphenyldiphenylphosphine **3b** ($CDCl_3$)

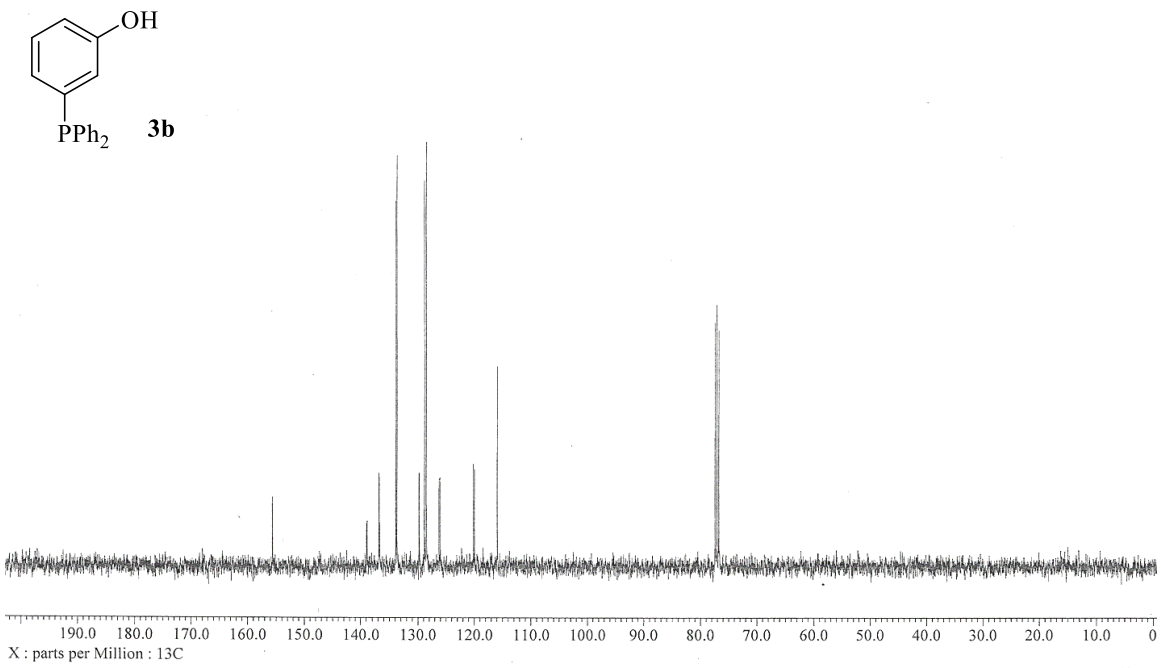

Figure A15: ^{13}C NMR spectrum of *m*-hydroxyphenyldiphenylphosphine **3b** ($CDCl_3$)

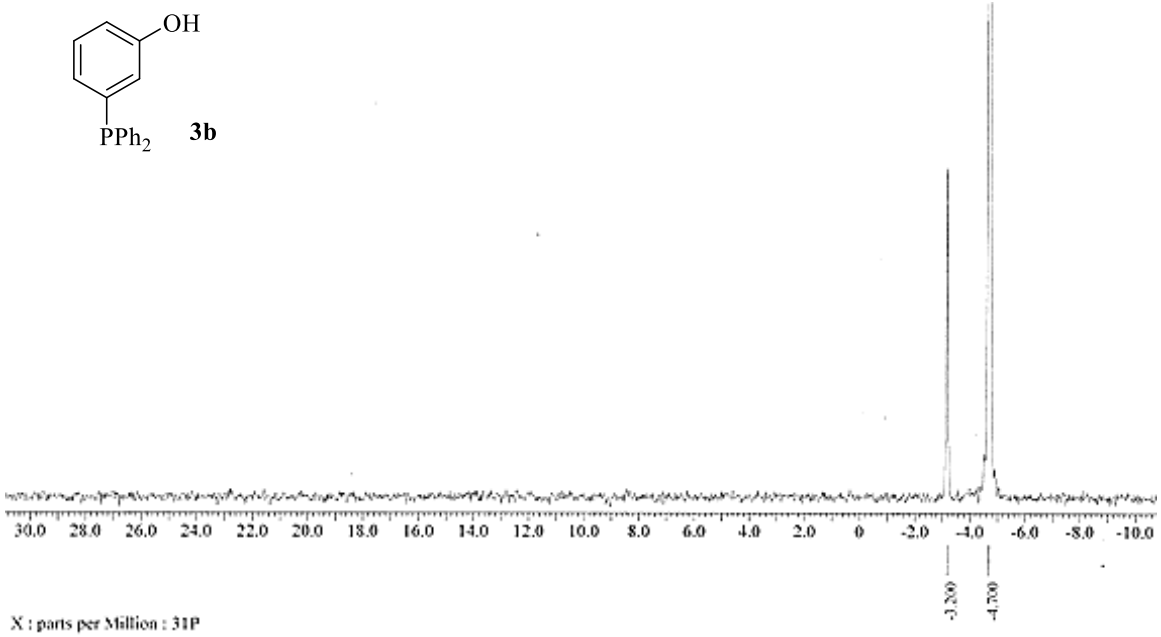

Figure A16: ^{31}P NMR spectrum of *m*-hydroxyphenyldiphenylphosphine **3b** ($CDCl_3$ + PPh_3)

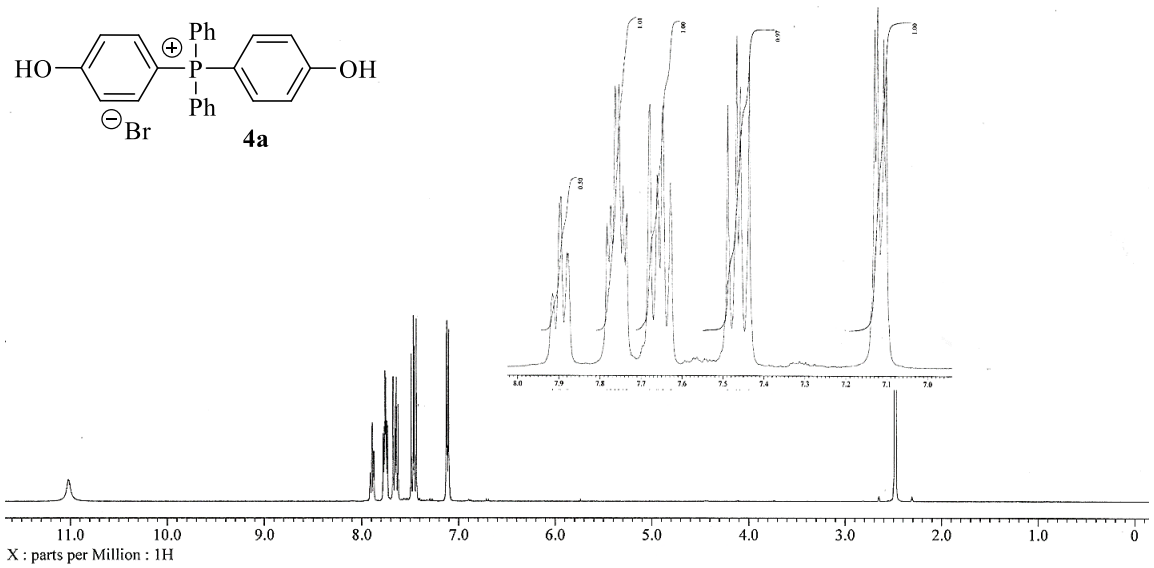

Figure A17: ^{1}H NMR spectrum of *p*-bis(hydroxyphenyl)diphenylphosphine bromide **4a** (DMSO-d_6)

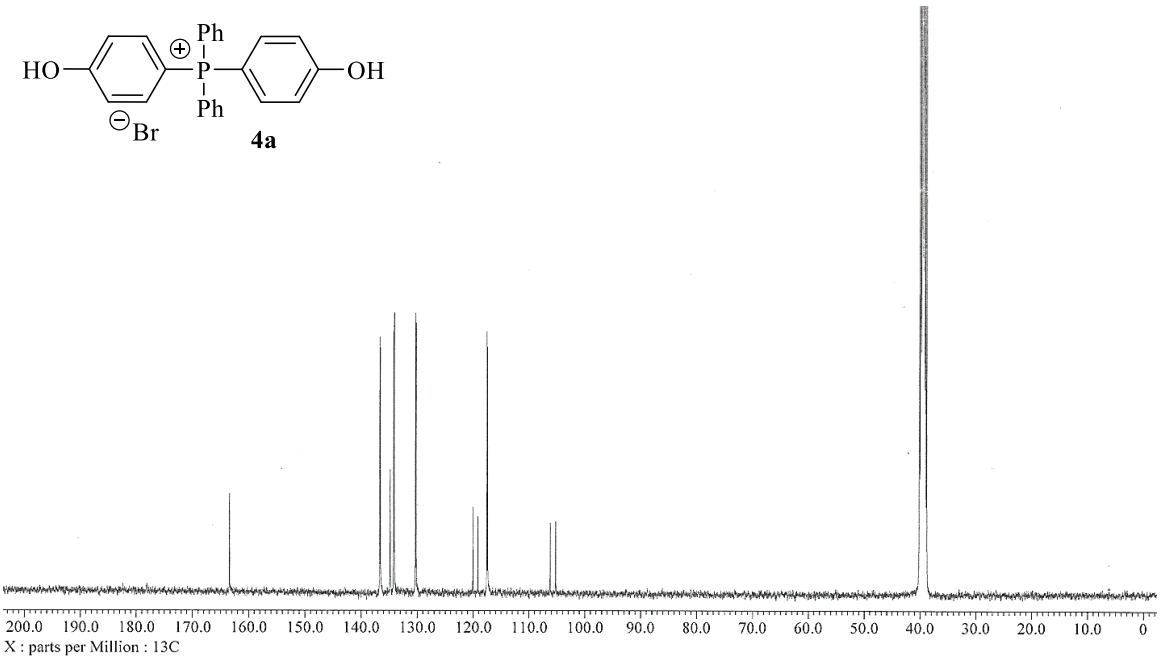

Figure A18: ^{13}C NMR spectrum of *p*-bis(hydroxyphenyl)diphenylphosphine bromide **4a** (DMSO-d_6)

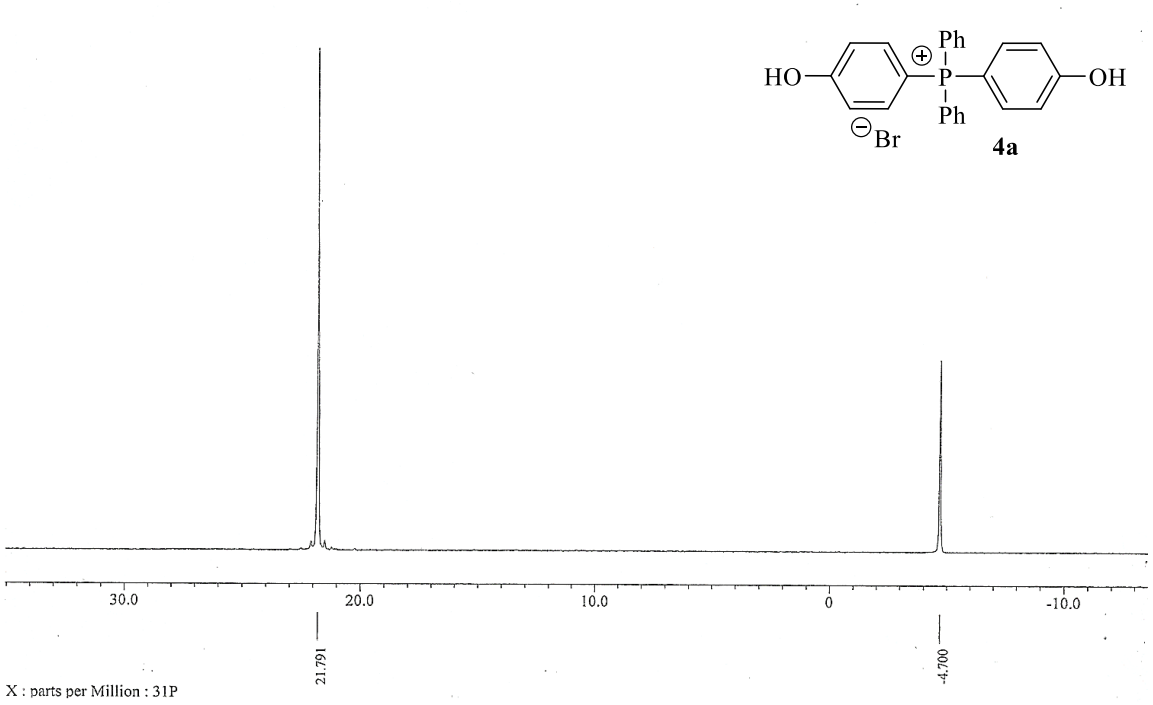

Figure A19: ^{31}P NMR spectrum *p*-bis(hydroxyphenyl)diphenylphosphine bromide **4a** (DMSO-d_6 + PPh_3)

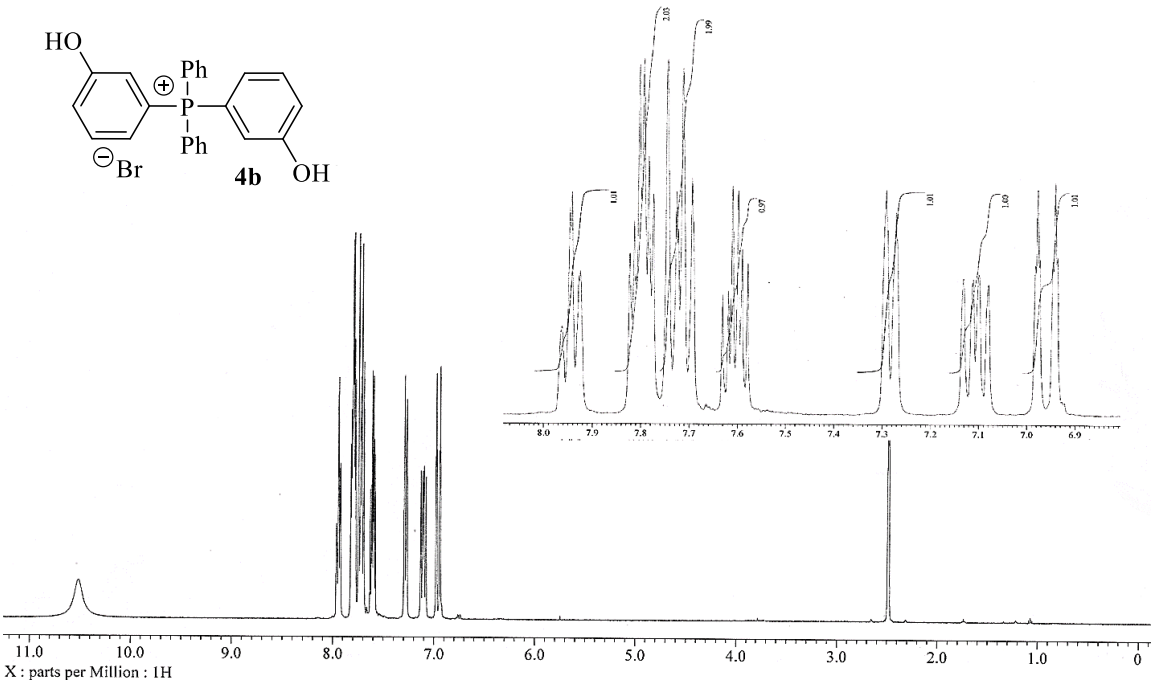

Figure A20: ^{1}H NMR spectrum of *m*-bis(hydroxyphenyl)diphenylphosphine bromide **4b** (DMSO-d_6)

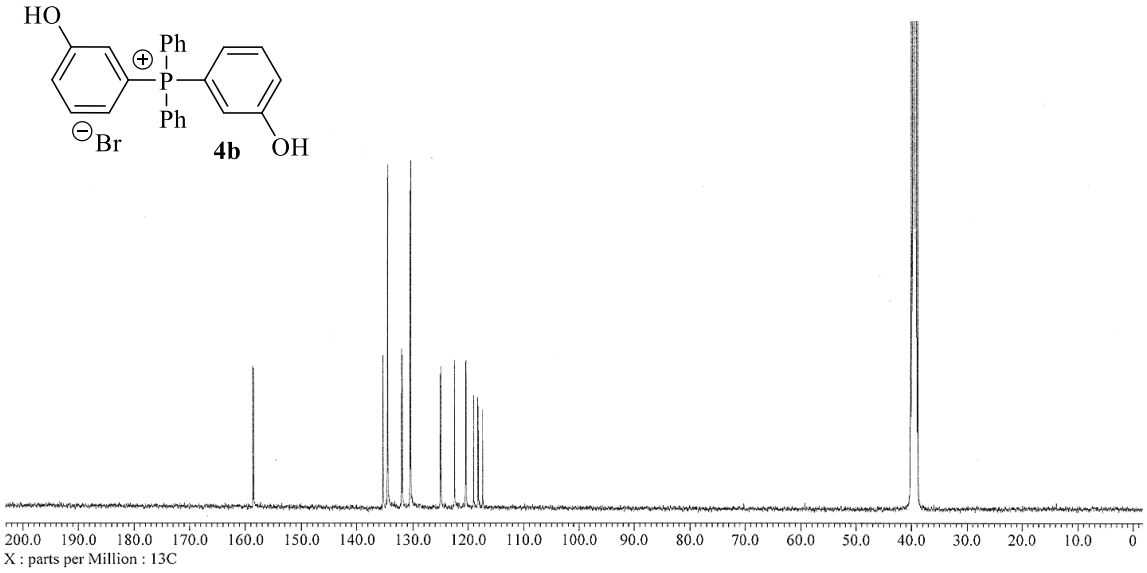

Figure A21: ^{13}C NMR spectrum of *m*-bis(hydroxyphenyl)diphenylphosphine bromide **4b** (DMSO-d_6)

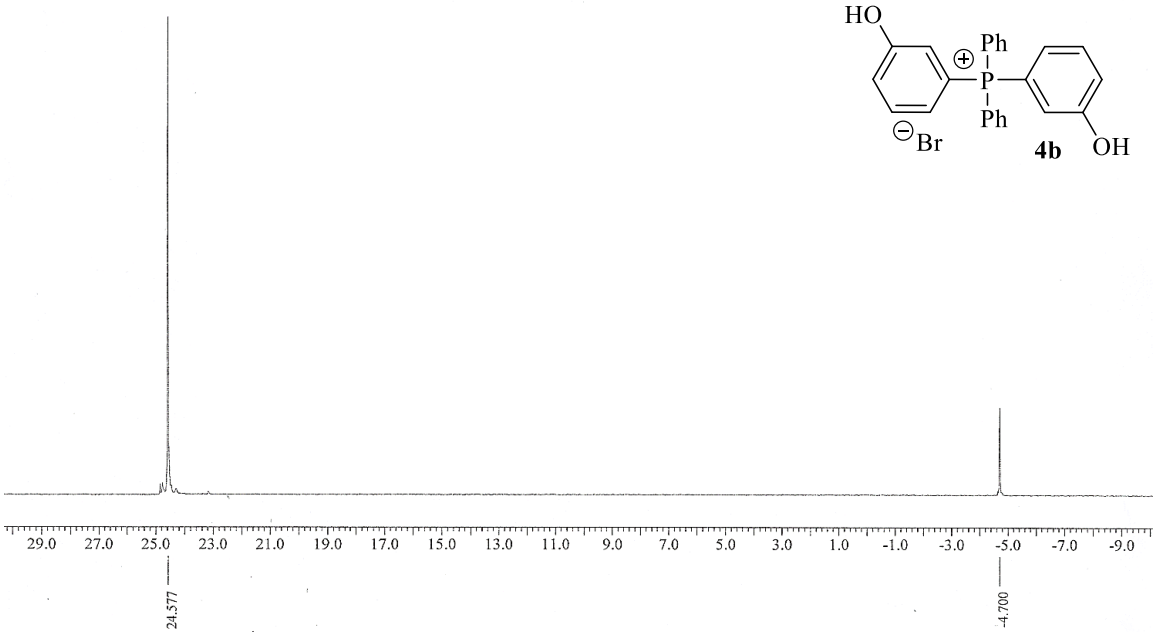

Figure A22: ^{31}P NMR spectrum of *m*-bis(hydroxyphenyl)diphenylphosphine bromide **4b** (DMSO-d_6 + PPh_3)

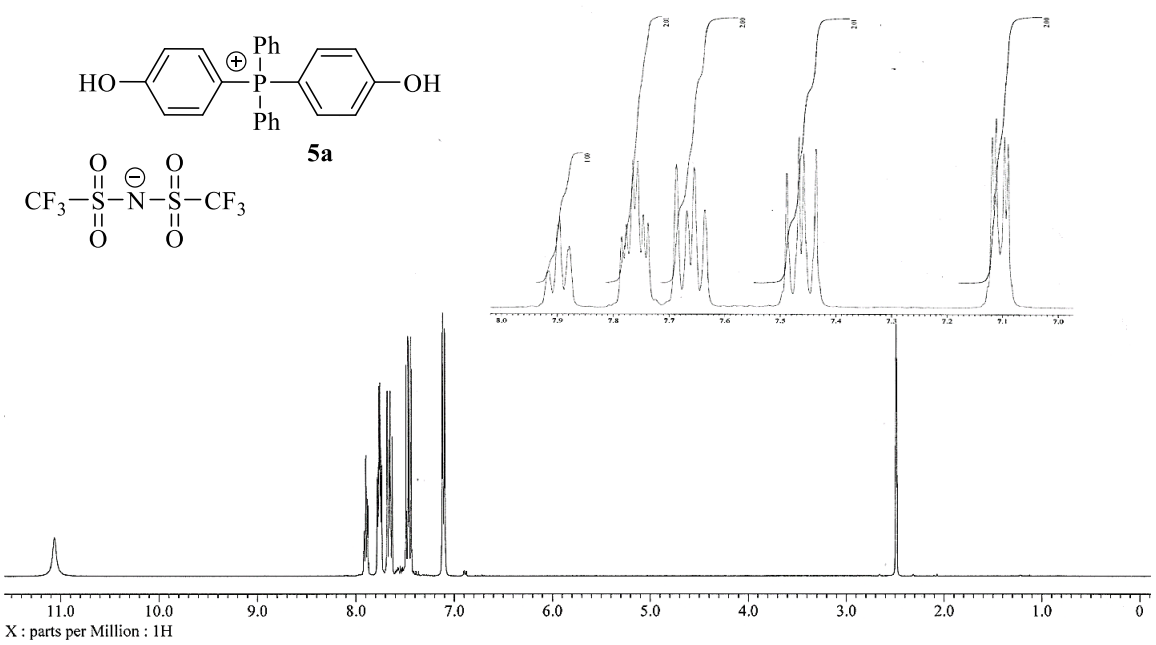

Figure A23: ^{1}H NMR spectrum of *p*-bis(hydroxyphenyl)diphenylphosphine [NTf_2] **5a** (DMSO-d_6)

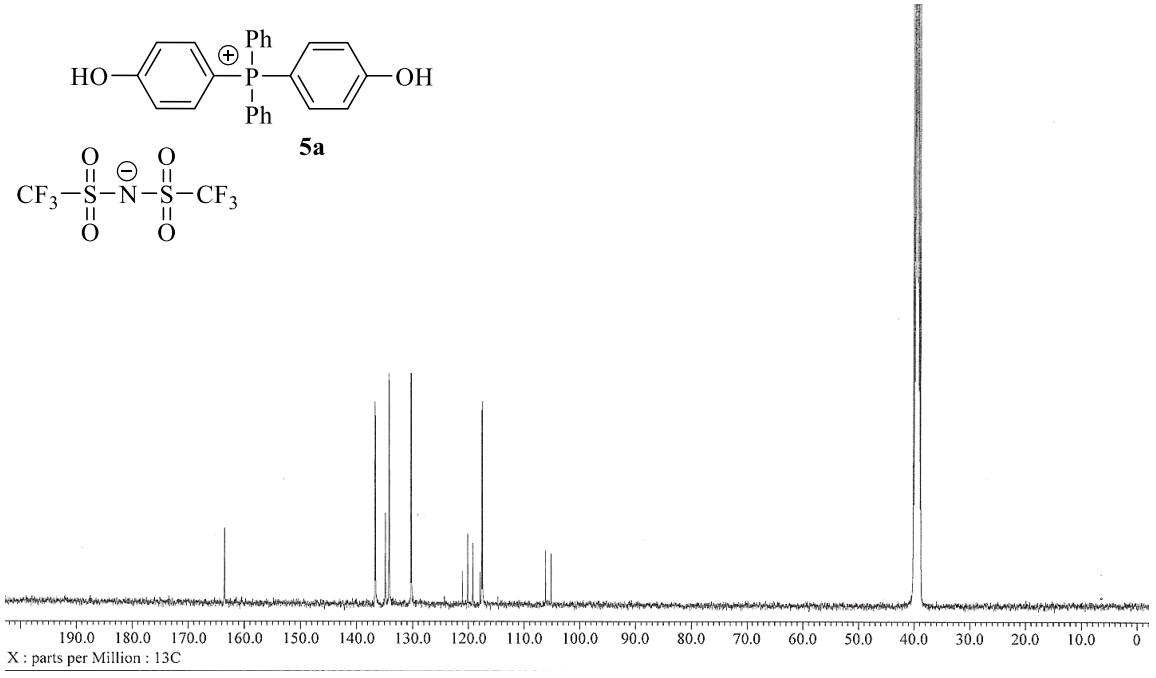

Figure A24: ^{13}C NMR spectrum of *p*-bis(hydroxyphenyl)diphenylphosphine [NTf_2] **5a** (DMSO-d_6)

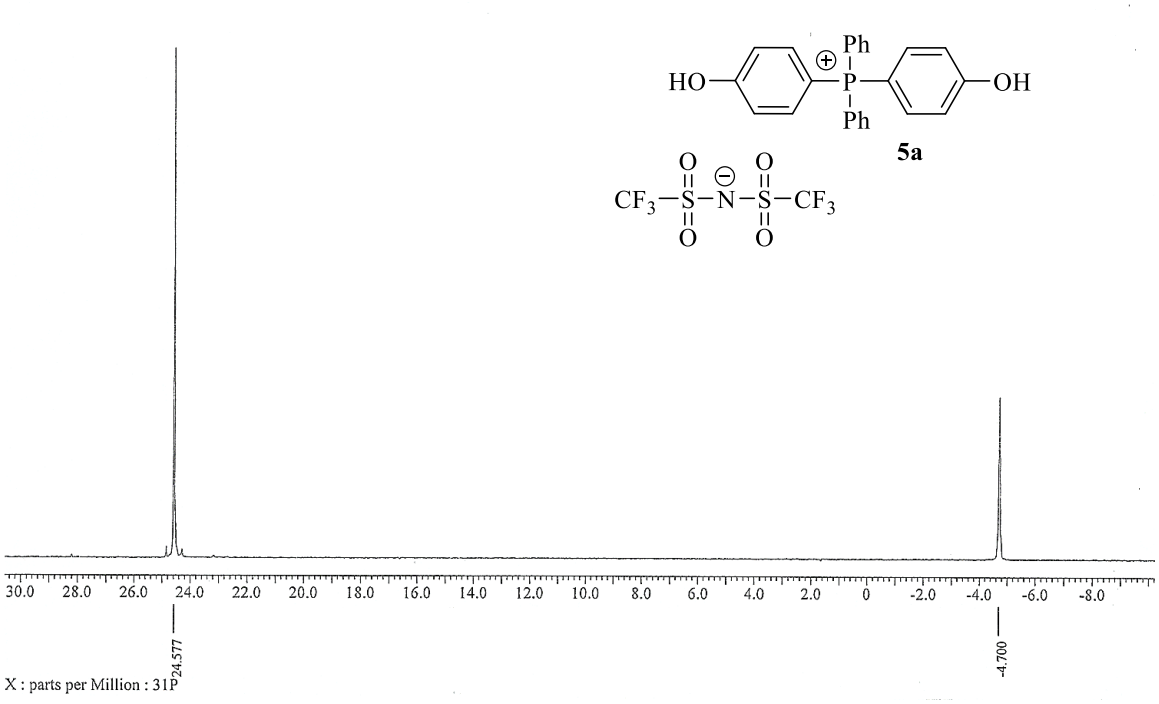

Figure A25: ^{31}P NMR spectrum of *p*-bis(hydroxyphenyl)diphenylphosphine [NTf_2] **5a** (DMSO-d_6 + PPh_3)

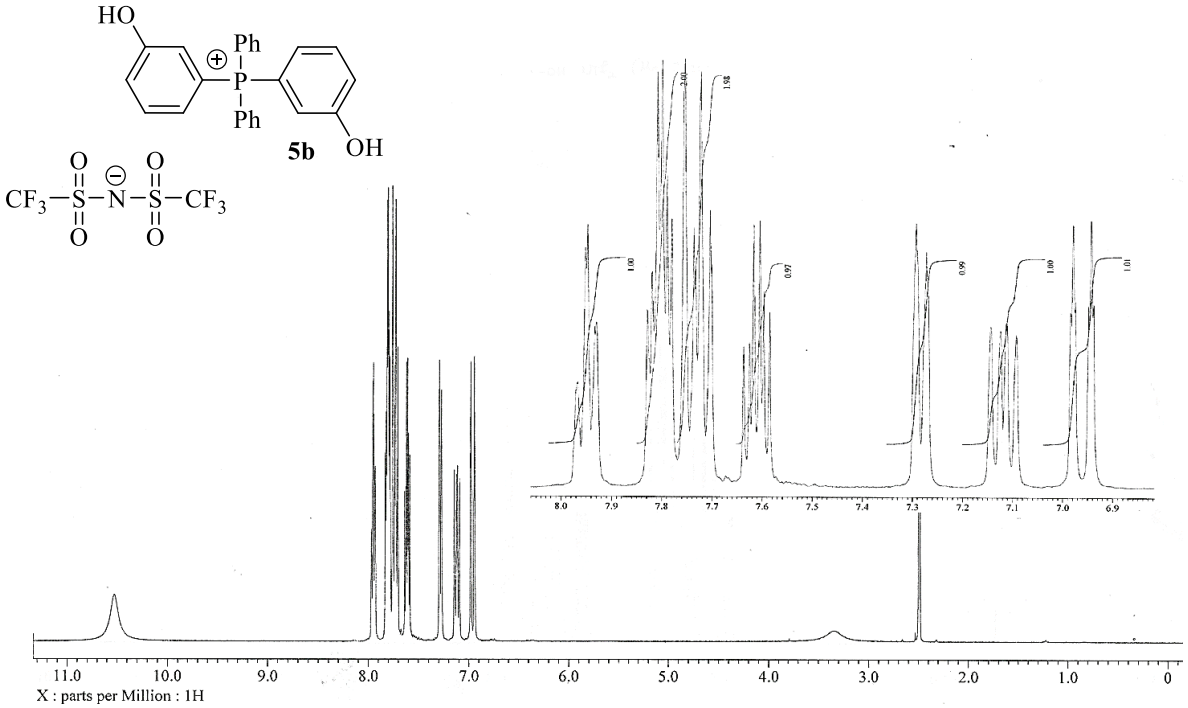

Figure A26: ^{1}H NMR spectrum of *p*-bis(hydroxyphenyl)diphenylphosphine [NTf_2] **5b** (DMSO-d_6)

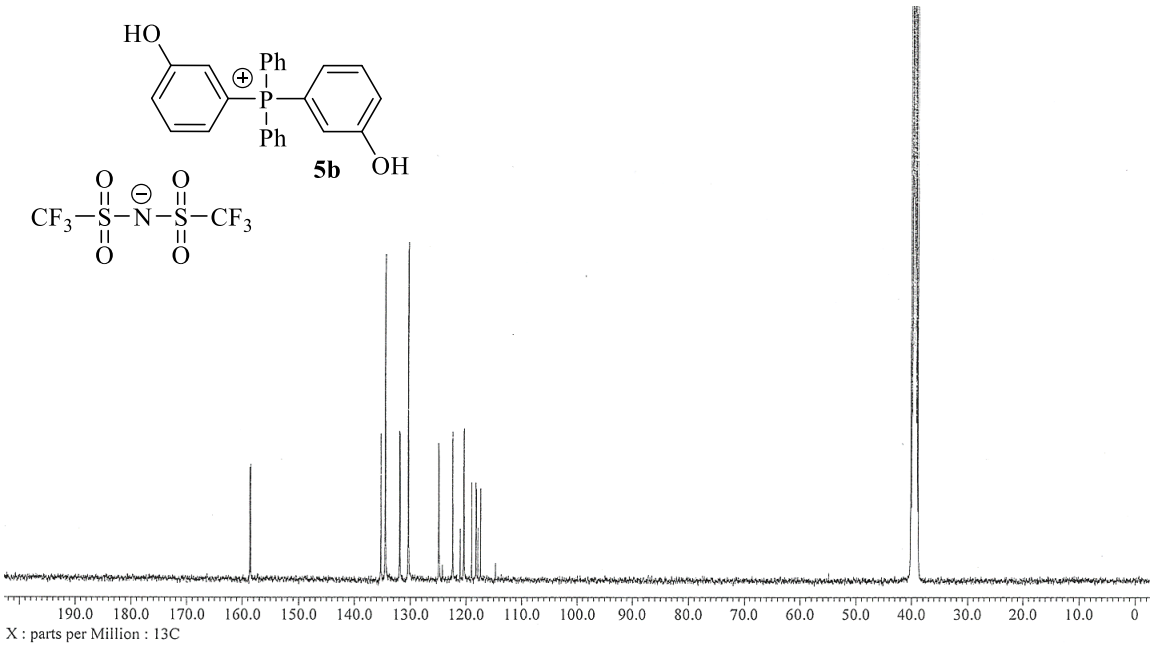

Figure A27: ^{13}C NMR spectrum of *p*-bis(hydroxyphenyl)diphenylphosphine [NTf_2] **5b** (DMSO-d_6)

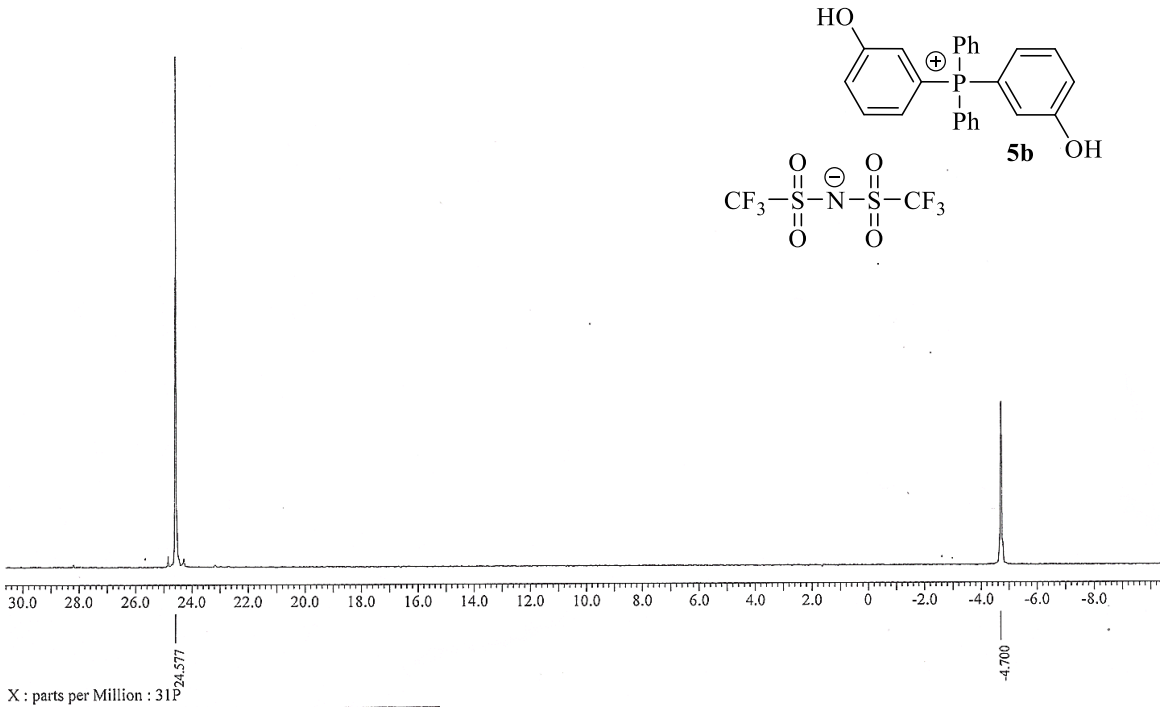

Figure A28: ^{31}P NMR spectrum *p*-bis(hydroxyphenyl)diphenylphosphine [NTf_2] **5b** (DMSO-d_6 + PPh_3)

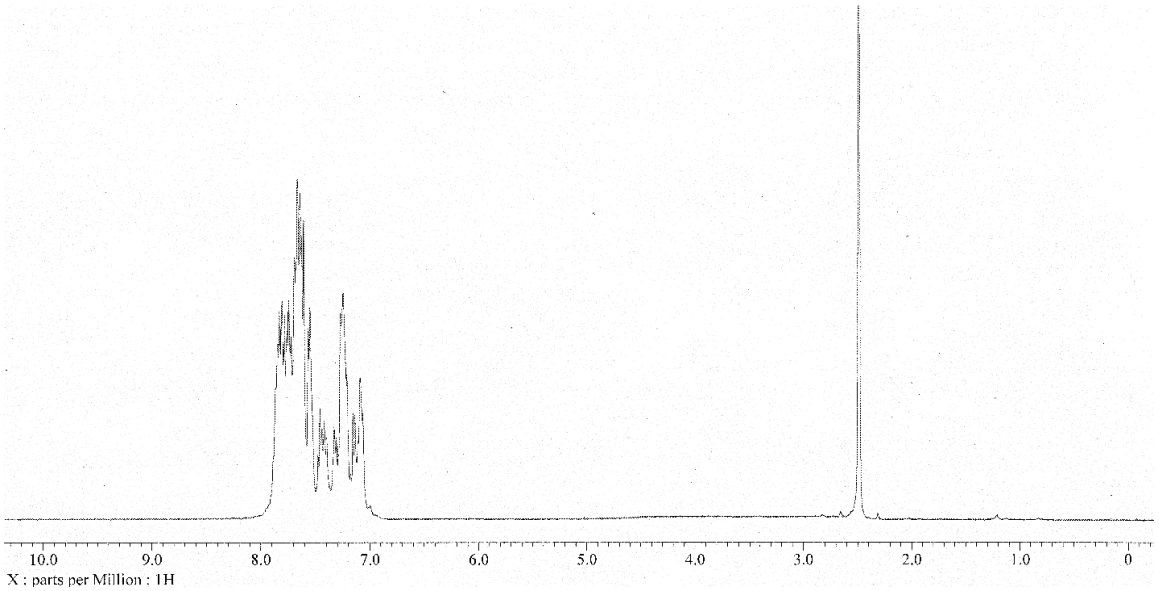

Figure A29: ^{1}H NMR spectrum of *p*-PHOS-CO-NTf$_2$ in DMSO-d_6

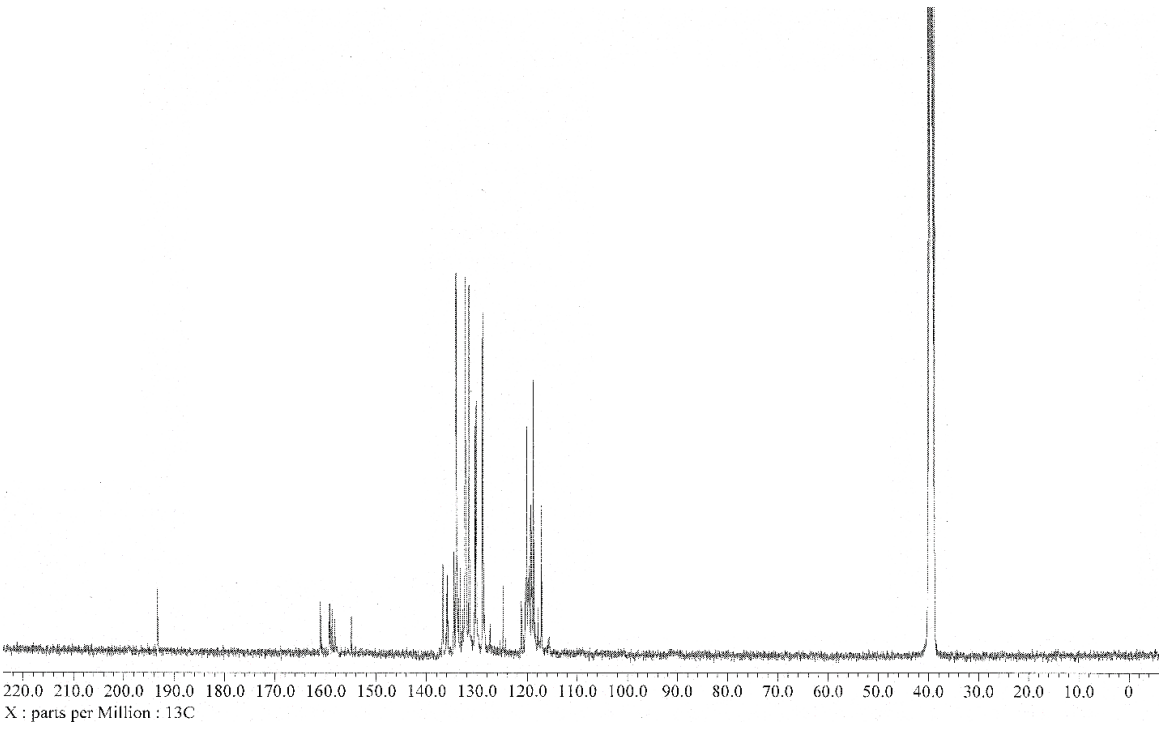

Figure A30: ^{13}C NMR spectrum of *p*-PHOS-CO-NTf$_2$ in DMSO-d_6

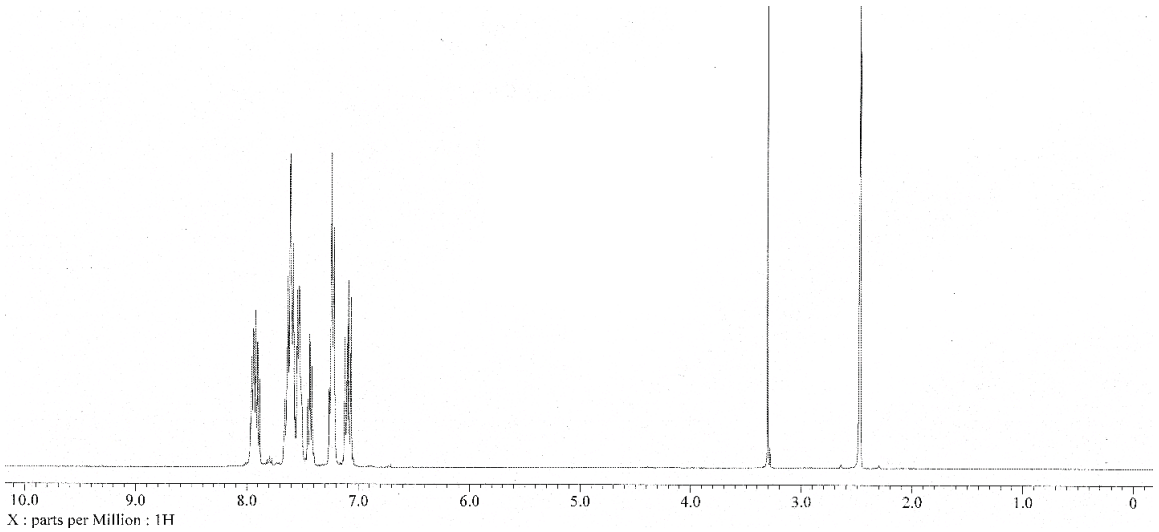

Figure A31: ^{1}H NMR spectrum of *p*-PHOS-S-NTf$_2$ in DMSO-d_6

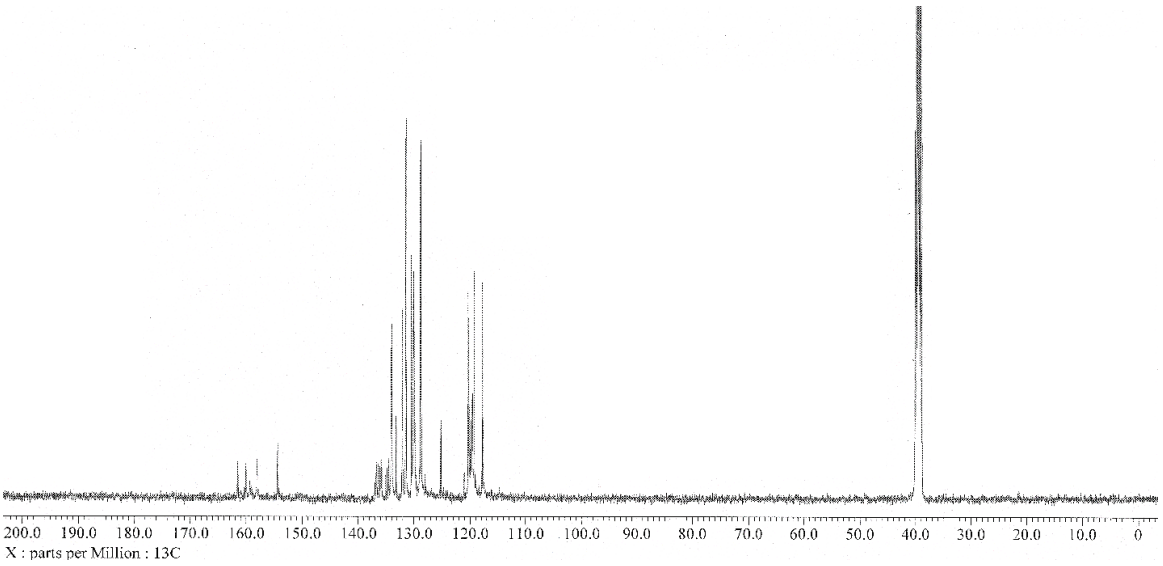

Figure A32: ^{13}C NMR spectrum of *p*-PHOS-S-NTf$_2$ in DMSO-d_6

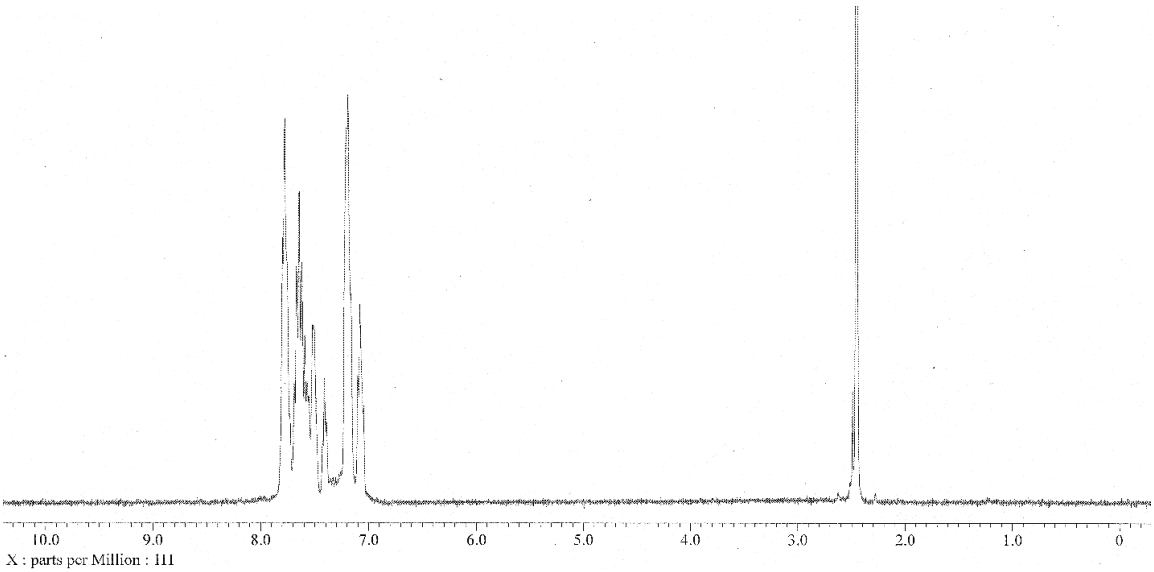

Figure A33: ^{1}H NMR spectrum of *m*-PHOS-CO-NTf$_2$ in DMSO-d_6

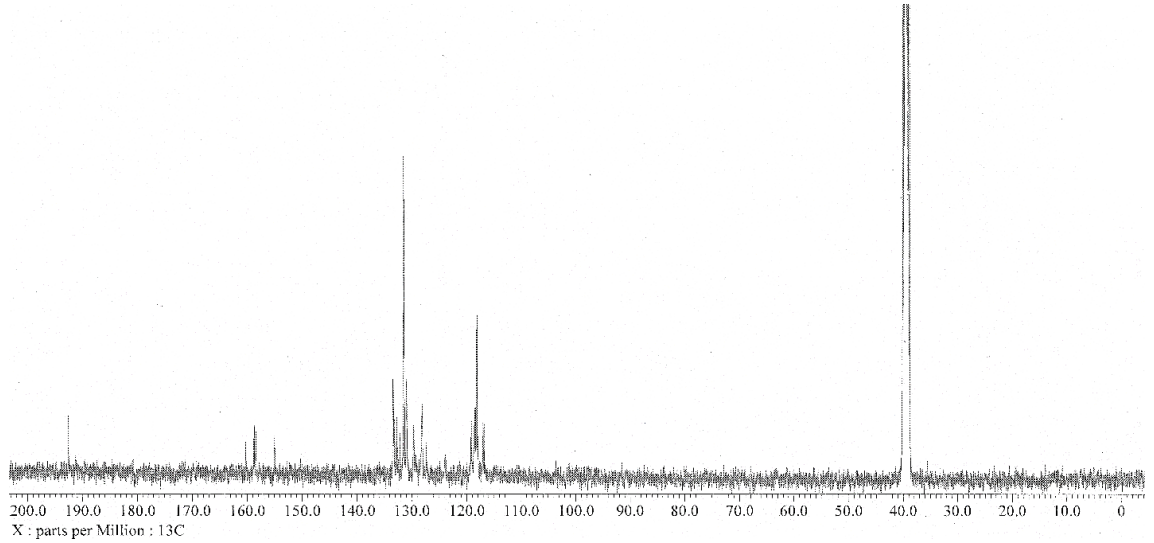

Figure A34: ^{13}C NMR spectrum of *m*-PHOS-CO-NTf$_2$ in DMSO-d_6

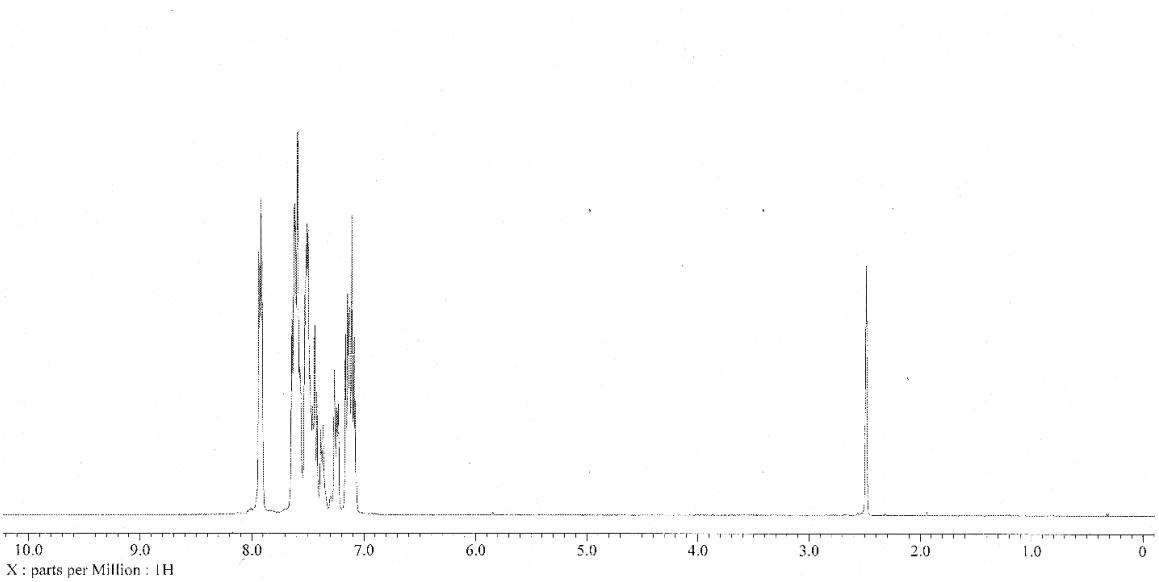

Figure A35: ^{1}H NMR spectrum of *m*-PHOS-S-NTf$_2$ in DMSO-d_6

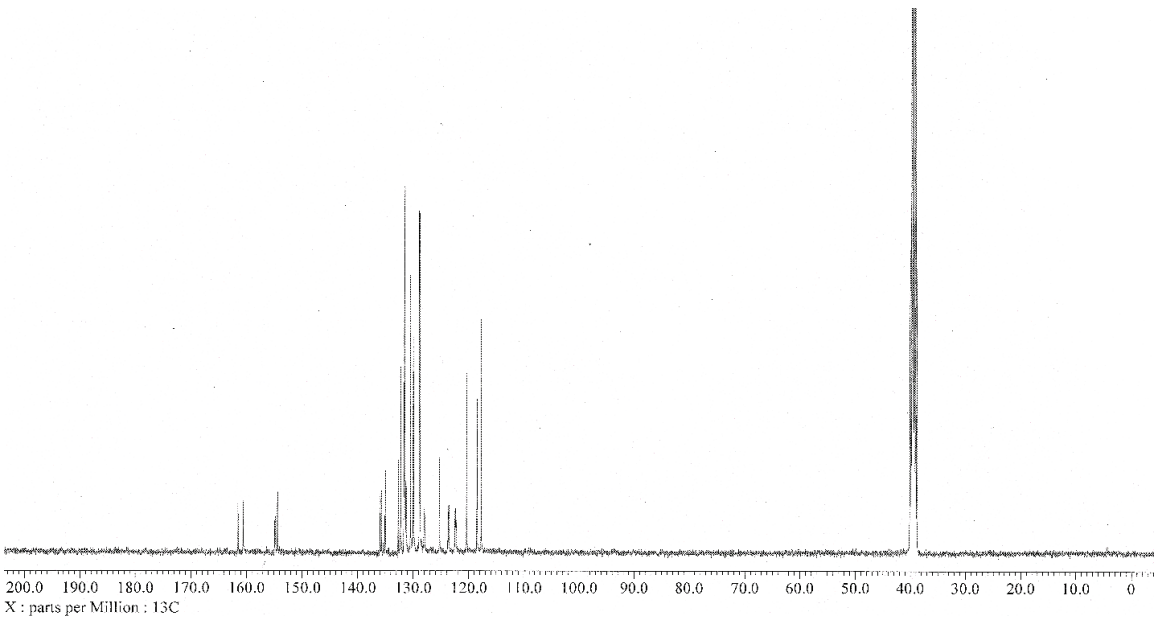

Figure A36: ^{13}C NMR spectrum of *m*-PHOS-S-NTf$_2$ in DMSO-d_6

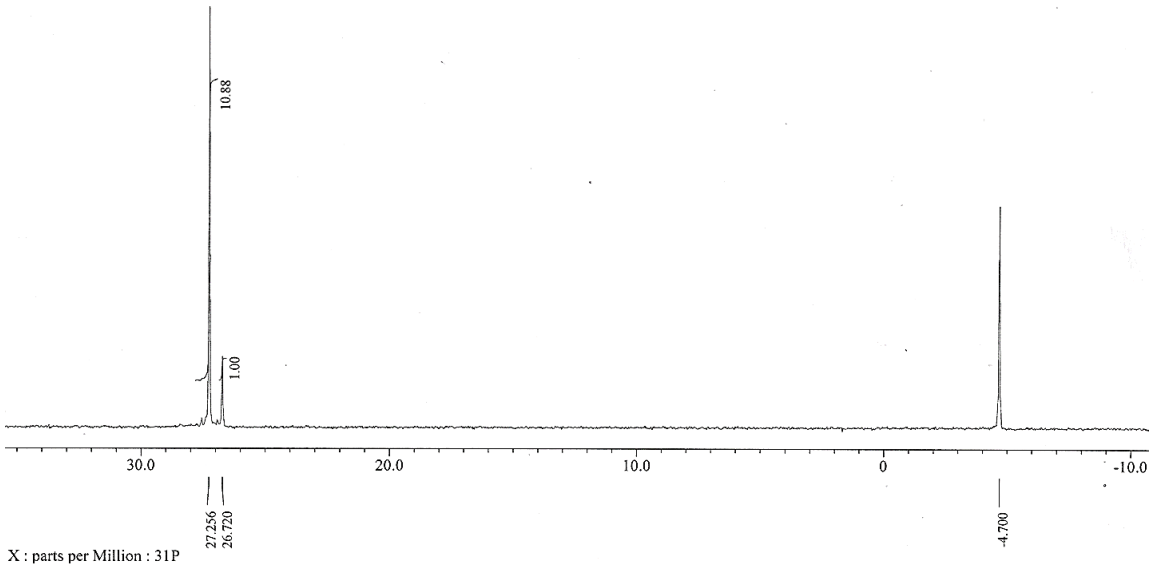

Figure A37: ^{31}P NMR spectrum of *p*-PHOS-CO-NTf$_2$ in DMSO-d_6 (PPh$_3$ standard)

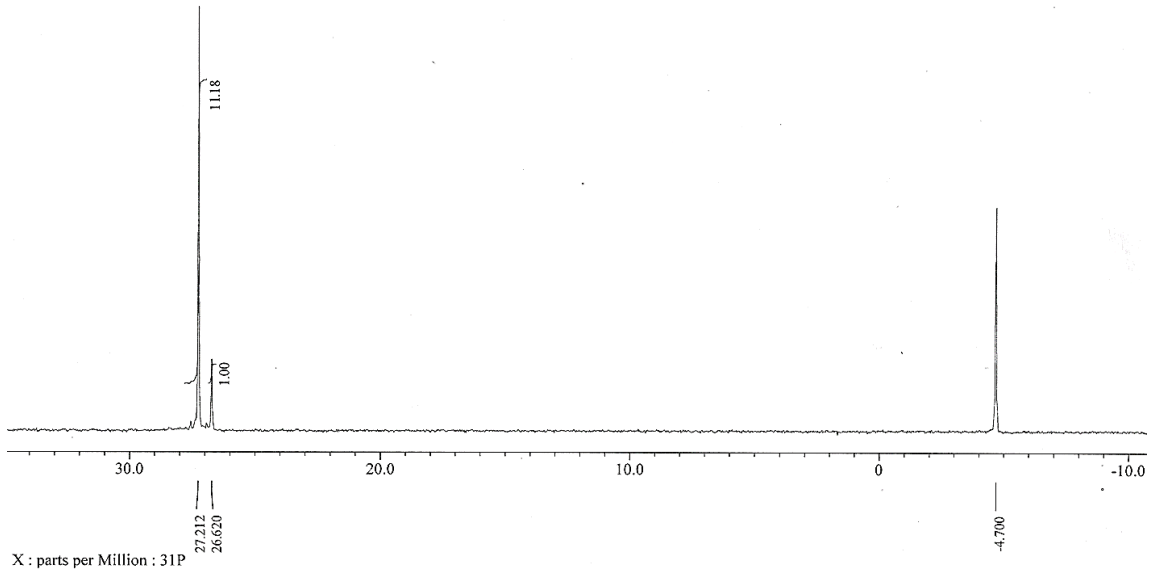

Figure A38: ^{31}P NMR spectrum of *p*-PHOS-S-NTf$_2$ in DMSO-d_6 (PPh$_3$ standard)

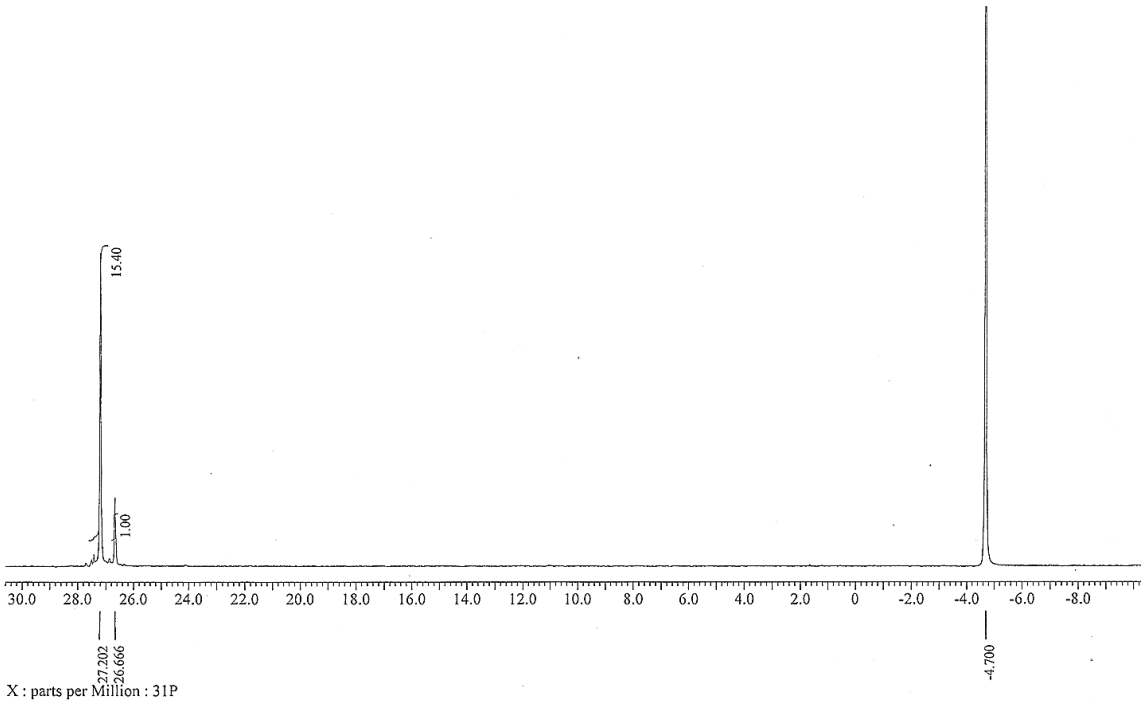

Figure A39: ^{31}P NMR spectrum of *m*-PHOS-CO-NTf$_2$ in DMSO-d_6 (PPh$_3$ standard)

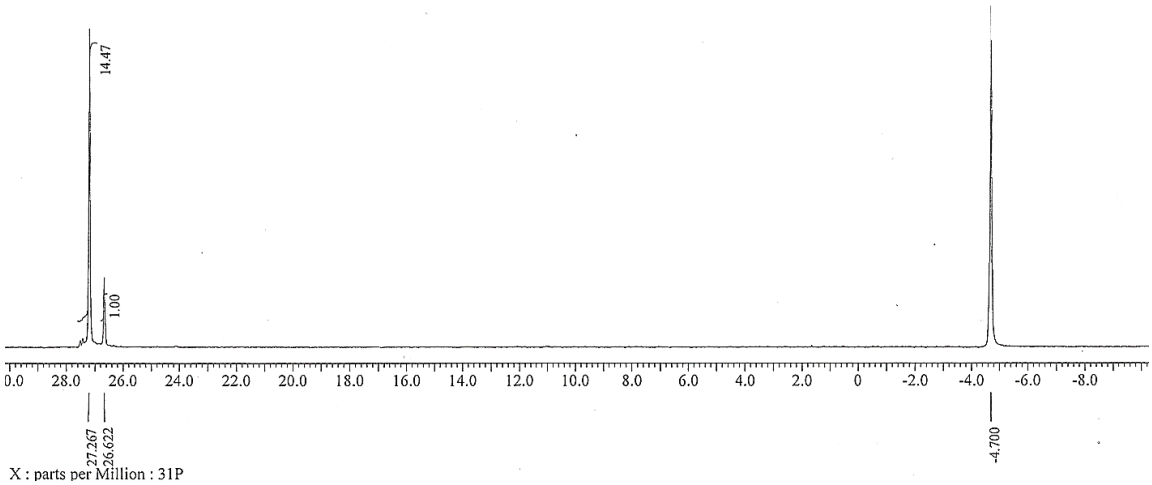

Figure A40: ^{31}P NMR spectrum of *m*-PHOS-S-NTf$_2$ in DMSO-d_6 (PPh$_3$ standard)

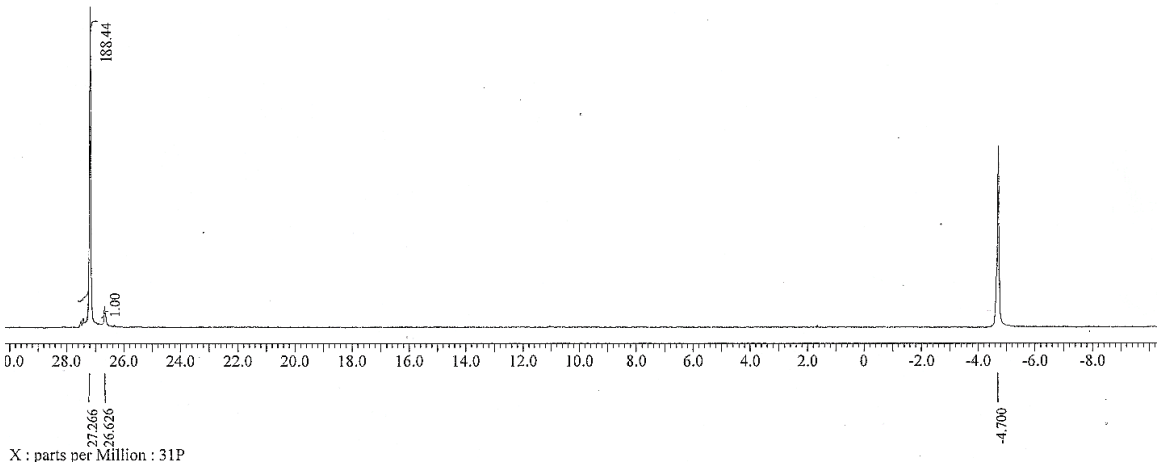

Figure A41: ^{31}P NMR spectrum of the polymerization of *m*-PHOS-S-NTf$_2$ where excess 4,4′-difluorophenylsulfone was added at the end of the reaction. Note that the end-group phosphorus signal at 26.62 ppm (see Figure A40) has been significantly reduced, indicating that this signal is indeed the end group phosphorus atom. Spectrum taken in DMSO-d_6.

Table A1: Elemental analysis data for ionenes.

Polymer	C	H	N	S
m-PHOS-CO-NTf$_2$ (theor)	56.46	3.16	1.69	7.73
(found)	57.36	3.01	1.54	7.55
m-PHOS-S-NTf$_2$ (theor)	52.72	3.03	1.62	11.11
(found)	51.99	3.09	1.56	10.85
p-PHOS-CO-NTf$_2$ (theor)	56.46	3.16	1.69	7.73
(found)	56.01	3.11	1.72	7.80
p-PHOS-S-NTf$_2$ (theor)	52.72	3.03	1.62	11.11
(found)	52.89	2.93	1.59	10.97

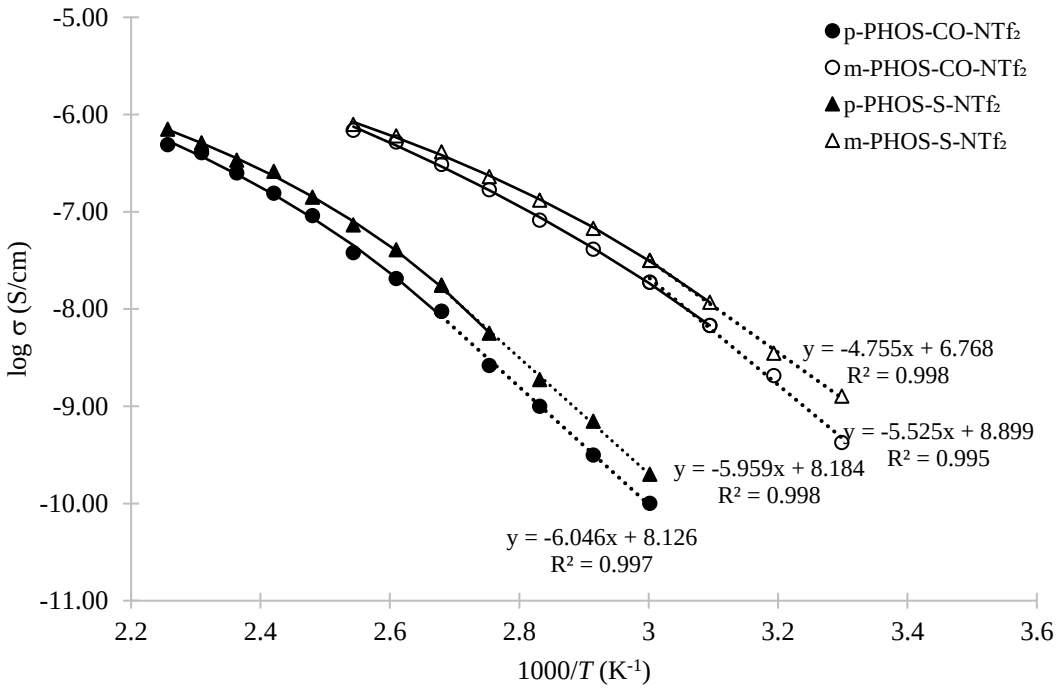

Figure A42: Overlay of log conductivity (S/cm) versus 1000/*T* at 30% RH for the perarylated phosphonium ionenes. Dashed lines are Arrhenius fits (with linear fit data provided) for data at or below the T_g while the solid curves are VFT fits for data at or above the T_g.